The Pennsylvania State University

The Graduate School

College of Agricultural Sciences

# PROPERTIES OF A HYDROPHOBIC SOLUTE IN EMULSIONS: AN EPR STUDY

A Dissertation in

Food Science

by

Umut Yucel



Submitted in Partial Fulfillment
of the Requirements
for the Degree of

Doctor of Philosophy

December 2011

The dissertation of Umut Yucel was reviewed and approved* by the following:

John N. Coupland
Professor of Food Science
Dissertation Co-Advisor
Co-Chair of Committee

Ryan J. Elias
Assistant Professor of Food Science
Dissertation Co-Advisor
Co-Chair of Committee

Gregory R. Ziegler
Professor of Food Science

Darrell Velegol
Professor of Chemical Engineering

John D. Floros
Professor of Food Science
Head of the Department of Food Science

*Signatures are on file in the Graduate School

## ABSTRACT

Small quantities of certain lipophilic molecules (e.g., flavors, colorants, antimicrobials, phytochemicals) are added to food products to produce a desired functionality. These molecules are largely insoluble in aqueous food products and are often chemically labile leading to a broad need for encapsulation methods. Oil-in-water emulsions are attractive candidates as delivery systems for lipophilic ingredients. The lipid phase provides a reservoir of the lipophilic ingredients isolated from aqueous reagents, and it is possible to modify the properties of the delivery system by altering the structure of droplets. Early work on emulsion based delivery systems (EBDS) has expanded to include the use of fine, crystalline emulsion droplets (solid lipid nanoparticles, SLN). Crystalline droplets offer the potential for enhanced retention and chemical stabilization of lipophilic ingredients, as well as for ways to control ingredient release. However there are conflicting reports on the effects of droplet crystallization on distribution and reactivity of lipophilic ingredients. This is partly due to a lack of a suitable technique to characterize EBDS structures *in situ.* EPR spectroscopy offers great potential to characterize the properties of a solute within EBDS directly and non-destructively. However, this technique requires the use of an EPR-active molecule (i.e., spin probe), as a model for the properties of the real ingredient (e.g., bioactive molecules, pharmaceuticals).

My main goal was to show how changes in EBDS structure (i.e., droplet size, crystallinity, surface properties) affect the physical distribution and reactivity of lipophilic ingredients. In this work I developed an EPR method to measure the properties of a small-molecule hydrophobic spin probe (4-phenyl-2,2,5,5-tetramethyl-3-imidazoline-1-oxyl, PTMIO) in different EBDS, and used it to develop a detailed model for the distribution behavior of PTMIO between phases.

The oil-in-water emulsions (10 wt%) were prepared by a hot homogenization technique, where n-tetradecane (C14) or n-eicosane (C20), or their blends, with PTMIO were homogenized into solutions of Na-caseinate (1 wt%, pH 7.0) or lecithin (70% phosphatidylcholine, PC75) + bile salt (taurodeoxycholic acid sodium) blend (2.4 wt% + 0.6

wt%, pH 7.0) to produce controlled size droplets (0.2, 0.6, or 1.3 μm). Then, emulsions containing PTMIO (200 μ*m*) were cooled to, and stored, at 21.5 or 5 °C where C14 is liquid and C20 is crystalline. The measured EPR spectra were deconvoluted into contributions from individual probe populations in different chemical environments by simulation of the spectra. The properties of the spin probe in each environment were evaluated from the parameters of the spectra:the hyperfine splitting constant (sensitive to the polarity of the probe's environment), the rotational correlation times (inversely related to the probe's mobility), and the ratio of the two rotational correlation times (a measure of anisotropic effects). The relationship between the distribution behavior of the probe in EBDS and probe's reactivity was also measured as the rate of reduction of the probe to its EPR-silent form by the addition of iron/ascorbate blend to the aqueous phase.

The changes in the distribution behavior and reactivity of the spin probe were evaluated by systematically changing EBDS structure as three specific objectives: (1) to investigate the effects of droplet size and crystallinity, (2) to investigate the effects of liquid oil fraction and storage, (3) to investigate the effects of surface composition.

In Objective 1, the effects of droplet size and crystallinity on the distribution and reactivity of PTMIO were investigated. C14 and C20 emulsions (0.2, 0.6, and 1.3 μm) were stored at 21.5 °C and 5 °C for 5 h or 24 h, and then analyzed by EPR spectroscopy. The EPR spectra revealed populations of probe in two discrete environments (i.e., aqueous and lipid). PTMIO is largely hydrophobic with 77% and 70% present in the coarse and fine liquid lipid droplets (i.e., tetradecane droplets), respectively. In the solid droplets (i.e., eicosane), all of the probe was excluded from the droplets into the aqueous environment. In all cases, the mobility of the probe in both lipid and aqueous environments was affected by the droplet surface. Moreover, the apparent rate constant for the reduction kinetics of the spin probe was proportional to the fraction of the spin probe in the aqueous phase.

In Objective 2, the effects of mixing liquid lipid (tetradecane) into solid lipid (eicosane) prior to homogenization on the distribution and reactivity of PTMIO as a function of storage time and temperature were investigated. The emulsions of blends of C14:C20, at weight ratios of

100:0 (100%C14), 10:90 (90%C20), and 1:100 (99%C20), and 0:100 (100%C20), stabilized with caseinate were stored at 21.5 or 5 °C for 5 h and 24 h prior to EPR analyses. It was found that even a small fraction of liquid oil can significantly affect the solute properties in SLN. For example, in the SLN where 10% of C20 was replaced with C14 (90%C20), more than half of the PTMIO was still in the droplets even after storage at 5 °C for 24 h, while in pure C20 SLN (100%C20) all the probe was present in the aqueous phase. The liquid lipid fraction is believed to surround the crystalline lipid core and is in close proximity of the immobilized surface layer which hinders the mobility of the spin probe. Moreover, the presence of C14 in C20 containing droplets affected the course of crystallization of C20, and thus the distribution of PTMIO in EBDS. The amount of aqueous probe population followed the sequence 5 h at room temperature < 24 h at room temperature < 24 h at refrigerated temperature. This time-dependency of C20 containing emulsions was attributed to the following mechanisms: (i) difference in nucleation frequency, (ii) the rate of rotator-to-solid transition, and (iii) solvent effects of C14 retarding crystal growth. The results obtained from the analyses of the EPR spectra were consistent with that of the probe reactivity (i.e., $k_{apparent}$ increases with aqueous probe fraction, and so droplet crystallinity). In the next objective the EBDS properties were modified by changing the interfacial region of droplets.

In Objective 3, the effects of surfactant type on the distribution and reactivity PTMIO in C14 and C20 emulsions was investigated. Lipid phase (10 wt% tetradecane or eicosane) was emulsified into caseinate solution (1 wt%, pH 7) or PC75+bile salt dispersion (2.4 wt% + 0.6 wt%, pH7), and samples were stored at 5 °C prior to EPR measurements. In C14 emulsions stabilized with PC75+bile salt, three populations of PTMIO were observed: lipid core (~60%, $a_N$ ~13.9 G) and aqueous phase (~20%, $a_N$ ~15.4 G) with high mobility, and immobilized surface layer (~20%, $a_N$ ~14.2 G) with low mobility. However, in C14 emulsions stabilized by caseinate, two distinct populations of PTMIO were seen: lipid phase (~70%, $a_N$ ~13.8 G) and aqueous phase (~30%, $a_N$ ~15.5 G) with high mobility. In both C20 emulsions stabilized either with PC75+bile salt or caseinate, crystallization excluded PTMIO from the droplets. In PC75+bile salt-stabilized SLN the majority of the probe (~77%) was in the interfacial layer, while in caseinate-stabilized SLN all of the probe was in the aqueous phase. For both surfactant systems $k_{apparent}$ was greater for C20 emulsions than C14 emulsions.

# TABLE OF CONTENTS

# LIST OF FIGURES

# LIST OF TABLES

# ACKNOWLEDGMENTS

Completion of this work could not be accomplished without the help and support of many people. I would like to mention those who deserve my sincere acknowledgment.

First of all, I would like express my deepest gratitude for my major advisor Dr. John N. Coupland. Although I have his signature on formal documents as my advisor, he was more a mentor to me from a much wider perspective during my life at Penn State. I regard myself very fortunate for not only having the privilege of working in Dr. Coupland's group but also having acquaintance of him personally. His patience throughout our collaboration and invaluable support during the difficult times have essential impacts on the quality if the present work.

I would like express my sincerest thanks to my co-advisor Dr. Ryan J. Elias. His encouragement and support for any problem I experienced ensured the completion of this work. Besides his invaluable intellectual input for the present work, having the liberty of calling upon his office any time and talking with him freely was really important and greatly appreciated. Moreover, his enthusiasm and great energy provided remarkable improvement for the quality of the present work.

I would like to thank the members of my Ph.D. committee, Dr. Gregory R. Ziegler and Dr. Darrell Velegol, for all their kind support, time and valuable input improving the quality of this work.

I would like to thank former and prior members of my lab, with whom I had the chance to share good times and laugh as well as intellectual acquaintance, for being there when needed. I would like to thank all of the Food Science Department family for creating this positive atmosphere and their kind help whenever needed, and ensuring my time here a great experience. I would also like to thank all my friends at State College for making it bigger than physically it is, and my friends in Turkey for being next to me regardless of the ocean in between.

I would also like to acknowledge USDA-AFRI program (Award number 2009-65503-05960, Program code 93430) for supporting the present work.

Finally, and maybe the most importantly, I would like to thank my family in Turkey for their support and love. I cannot express my thanks for my family thoroughly by merely using words, but only I can say that much that I would like to thank for everything sincere I would not be in my current position without them. My special thanks are for Valentina Trinetta for her unceasing support, love, and heartiest company whenever I need it…

# Chapter 1

## 1. Introduction and a Review of Related Literature

### 1.1. Delivery Systems in Foods

Certain functional properties of foods depend to a great extent on the presence of relatively low concentrations of certain endogenous or exogenous small molecules. These molecules may be classified by their function, such as flavors (e.g., limonene, citral), colorants (e.g., β-carotene), and increasingly phytochemicals (e.g., tea catechins, β-carotene, highly polyunsaturated fats), but many of them share the common property of producing a biological reaction in the consumer (i.e., are bioactive). Most of these molecules are lipophilic and often chemically labile under oxidizing conditions, at elevated temperatures or in highly acidic environments. They are amongst the most expensive ingredients in the food and their addition is critical to the economics of the product formulation and their loss can limit shelf-life. There is therefore a broad need for methods to allow these bioactive lipophilic ingredients (BLI) to be used effectively in aqueous foods. There is an obvious parallel between the need to encapsulate BLI in foods with the need to incorporate poorly-soluble drugs in a form that can be ingested, injected or applied topically. Indeed, in the pharmaceutical industry lipophilic drugs are delivered parenterally as commercial products in the form of emulsions (Muller et al., 2000; Mehnert and Mader, 2001). Most of these approaches involve some form of encapsulation.

McClements et al. (2007) provided some useful guidelines for the characteristics of an effective delivery system for BLI. An effective delivery system should:

(i) be easy and economical to manufacture. Ideally using process equipment currently available either to the food manufacturer or ingredient supplier.

(ii) be physically stable over the intended time of use. The encapsulation system must maintain its integrity both before it is applied in the food and then throughout manufacture and on the shelf during storage.

(iii) bind and retain large quantities of the BLI of interest. If the ratio of encapsulating material to BLI becomes too large, the effectiveness of the ingredient is diluted.

(iv) protect the BLI from (bio) chemical degradation. Usually this involves sequestering the ingredient away from the reagents that would otherwise degrade it (e.g., protons, free radicals).

(v) improve the bioavailability of the BLI. Bioavailability is defined as the amount of bioactive ingredient to be metabolizable at the corresponding part of the living body (Acosta, 2009).

(vi) control the release and delivery of the BLI. An encapsulation system that binds and does not release the ingredient would not allow it to be functional. Some level of binding is essential to provide protection but the binding must be weak enough to release when the ingredient is required. Moreover, the encapsulation system should provide some flexibility to modify the release rate of BLI depending on the intended use.

(vii) be compatible with the food matrix. Most foods are largely aqueous so the encapsulation system must be dispersable and stable in water. This recommendation can be extended to note that the encapsulation system must not provide any unwanted sensory properties to the food (i.e., unwanted cloudiness, taste, phase separation).

Based on these recommendations and on the nature of BLI molecules, some inferences on the nature of suitable delivery systems can be made. First, the encapsulation should be supported by non-covalent interactions and/or physical entrapment; covalent bonds are too strong to allow release of the ingredient and would render it non-functional. As BLI ingredients are non-polar, hydrophobic interactions will likely provide the basis for at least some of the binding necessary; the encapsulation system must provide a hydrophobic domain in a hydrophilic media. If the hydrophobic domain is to be dispersed in an aqueous food then the encapsulation system must allow bulk physical stability (e.g., have some hydrophilic regions). The encapsulation system must also be small enough or share sensory properties common to the native product so as not to be perceived in the food. Given these constraints, the number

of delivery systems available for use with BLI in food is relatively limited and, in practice, can be classified into three main groups.

In the first group of delivery systems, the BLI is bound or encapsulated by a food polymer (polysaccharide or protein) and then dispersed within the food. For example, lycopene entrapped within whey proteins (Richelle et al., 2002), Vitamin D2 in casein micelles (Semo et al., 2007) and carotenoids in starch-based materials (Wagner and Warthesen, 1995). In the second group of delivery systems, the BLI is incorporated into a thermodynamically stable surfactant self-association structure (e.g., a microemulsion). For example, Amar et al. (2003) used microemulsions of different surfactant types to improve the solubilization of lutein and lutein esters, which are otherwise insoluble in water and have limited solubility in food-grade oils. In the final group of delivery systems, the BLI is dissolved in a lipid carrier and subsequently homogenized to form fine emulsion droplets. This final group is known as emulsion-based delivery systems (EBDS) and is the focus of my research.

Emulsions are attractive candidates for delivery systems as they are already widespread in foods and utilize commonly available ingredients and process technologies. The lipid phase provides a reservoir for the BLI which can then be uniformly dispersed in an aqueous food by homogenization and stabilized with emulsifiers. It is possible to modify the performance of the delivery system by altering the size or number of the lipid droplets, or by altering the interfacial and/or lipid composition. Recently work in pharmaceutical EBDS has pioneered the use fully or partially crystalline droplets as delivery systems (i.e., solid lipid nanoparticles, SLN or and nano-structured lipid carriers, NLC), (Muller et al., 2000; Mehnert and Mader, 2001; Bonacucina et al., 2009). Several researchers have considered parallel applications in foods (McClements et al., 2007, 2009; Velikov and Pelan, 2008; Weiss et al., 2008). In the next sections, I will introduce the relationships between structure of emulsions and crystalline emulsions, both micro- and nano-scale, and their functionality as delivery systems in foods.

## 1.2. Structure of Emulsions

An emulsion is a mixture of two immiscible liquids, one of which is uniformly dispersed within the other as small droplets (i.e., droplet diameter in the range of 0.1 and 100 $\mu$m)(McClements 2005). In my research, I am concerned exclusively with dispersions of oil in water (i.e., oil in water emulsions) and the term emulsion is referred to these systems unless otherwise indicated.

Emulsions are formed either by using mechanical energy to reduce the particle size of a coarse mixture or, less frequently, by a controlled phase separation (e.g., spinodal phase separation on dilution of raki). Although chemical methods, such as solvent evaporation or phase inversion, were introduced in literature to manufacture sub-micron size droplets, they require the use of certain chemical formulations, which are not usually food grade. Various technologies are used for particle size reduction in emulsions; the most common are high-pressure valve homogenizers, although other devices including high intensity ultrasound, membrane homogenizers, and microfluidic devices are also capable of generating very fine particles with uniform droplet size distributions (Solans et al., 2005). Although the efficiency of droplet formation (i.e., size and uniformity of the droplets) depends on many factors, in general there is an approximately linear inverse relationship between the homogenization pressure and particle size (McClements, 2005). Recent advances in homogenizer technology have allowed the development of nanoemulsions with droplets far smaller and with more uniform size distributions than commonly seen in manufactured foods (Weiss et al., 2008). There is not a commonly accepted size cut-off for nanoemulsions and different researchers have used different definitions: below 1000 nm (Muller et al., 2000), 500 nm (Anton et al., 2008), 200 nm (Higami et al., 2003; Solans et al., 2005), and 100 nm (Luykx et al., 2008).Emulsions with nano-scale crystalline droplets are sometimes referred to as solid lipid nanoparticles (SLN).

Emulsions are thermodynamically unstable structures given a degree of kinetic stability by an adsorbed interfacial layer of amphiphilic emulsifiers (see Figure 1.1). The thermodynamic driving force for the phase separation of lipid and aqueous phases can mainly be attributed to the mismatch between the internal energies of two phases, and thus the excess surface free energy. When the lipid phase is dispersed throughout the aqueous environment as colloidal-size droplets, the contact area between lipid and aqueous phases is increased, and lipid molecules organize into a spherical shape to minimize the contact area with the aqueous phase, and so the excess surface energy. This curvature at the interface results in an increase of the internal pressure of the droplets, known as the Laplace pressure ($P_{L)}$, and thus a pressure gradient between inside a droplet and its surroundings (Walstra, 1993):

$$P_L = \frac{4\gamma}{d} \qquad [1.1]$$

where d is the droplet diameter and γ is the surface tension at the interface of the lipid and aqueous phases.

Emulsifiers can increase the physical stability by two modes of action. Firstly, they can serve to lower the interfacial tension, and to decrease the excess surface free energy, and thus the thermodynamic driving force for the phase separation. Secondly, they can provide a kinetic barrier to droplet fusion via some interdroplet repulsive forces to stabilize the dispersions (e.g., steric and electrostatic). Some other surfactant-specific processes, such as Gibbs-Marangoni effect seen in small-molecule surfactants, can also contribute to the kinetic stabilization properties of the emulsifiers. The interfacial layer is typically between about 1 and 10 nm thick for food grade emulsifiers, such as surfactants, phospholipids, proteins, or polysaccharides, and the interfacial concentration is in the order of a few mg per square meter of surface.

The various mechanisms for emulsion destabilization include flocculation, coalescence (in fluid particles), partial coalescence (in semi-crystalline particles), Ostwald ripening and gravitational separation (creaming or sedimentation) (Claesson et al., 2004; Dickinson, 1992;

McClements, 2005; Vanapalli and Coupland, 2004). In general, except for Ostwald ripening, the instability processes are slower for fine particles (e.g., the rate of creaming by Stokes Law is inversely proportional to the square of particle diameter). The rate of Ostwald ripening (i.e., the growth of large particles at the expense of fine particles) and the associated phenomenon of compositional ripening (i.e., diffusion of molecules from droplet to another to minimize differences in composition) depends on the degree of surface curvature (i.e., solubility increases with pressure) and is therefore faster in very fine particles. Ripening processes are particularly important when molecules in the lipid phase have some solubility in the aqueous phase so while triacylglycerols (TAG) typically ripen slowly, the transport of more polar emulsified BLI may be faster. Aqueous surfactant micelles can increase the solubility of lipids in the aqueous phase and thus increase the rate of ripening (Weiss et al. 1996).

### 1.3. Localization of BLI in Emulsions

An emulsion can be envisaged as consisting of at least three distinct microenvironments for added BLI molecules (Figure 1.1): the continuous aqueous phase, the lipid core of the droplets, and surface of the droplets as the amphiphilic region. The relative volume of the aqueous and lipid phases can be altered by changing the formulation of the emulsion while the surface to lipid volume ratios can be altered by changing the particle size (Figure 1.2). BLI localized in the lipid core or aqueous phases will be predominantly surrounded by TAG and water molecules respectively while BLI molecules in the interfacial region will interact with both to some extent as well as with the high concentration of emulsifiers on the surface.

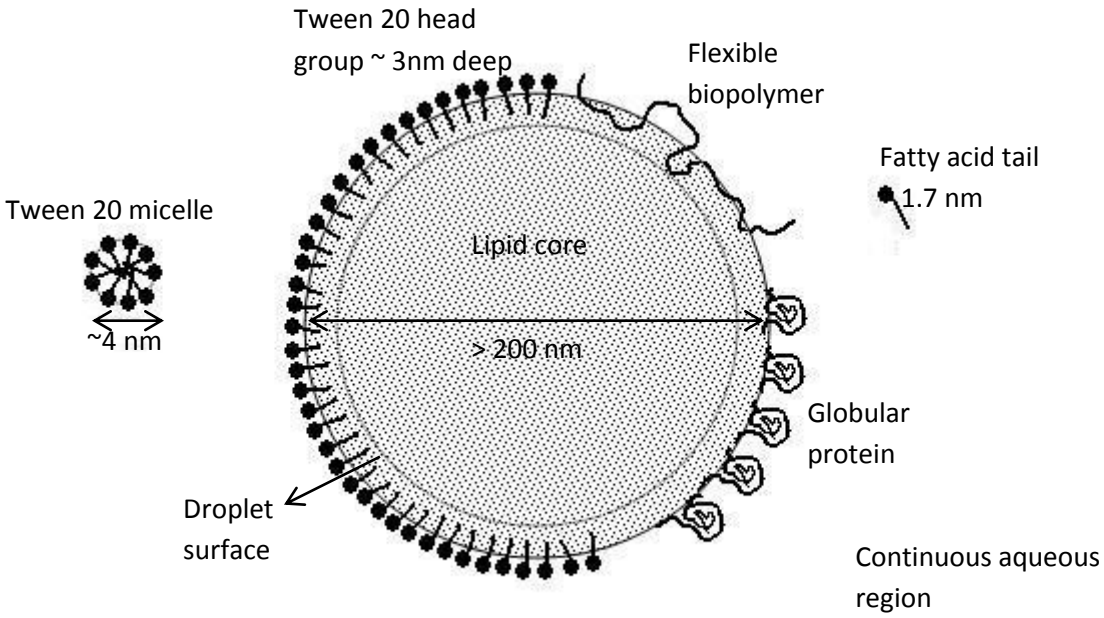


Figure 1.1. Regions in a conventional emulsion stabilized by different emulsifiers, i.e., Tween 20, a flexible biopolymer, and a globular protein, (not to scale, adapted from Povey, 2001).

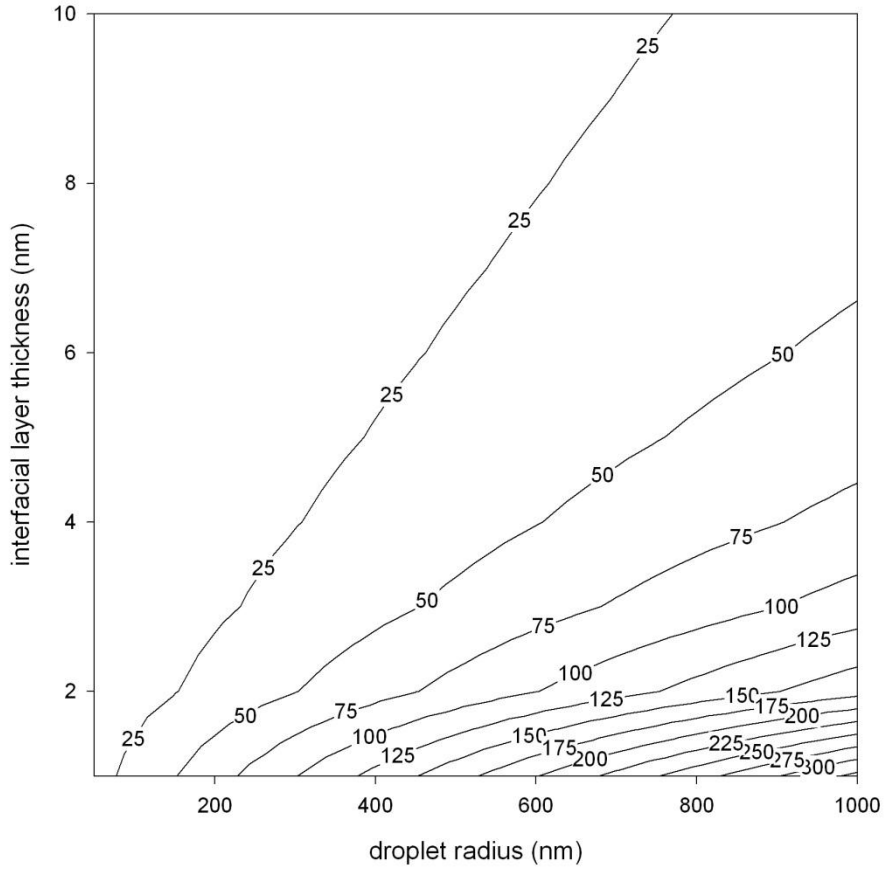


Figure 1.2. Ratio of the internal phase volume to interfacial phase volume as a function of droplet size and the thickness of the interfacial layer.

BLI molecules will partition between the different microenvironments depending on their chemical structure and intermolecular interactions. However, as these are lipophilic molecules, the aqueous concentration will typically be very low. Molecular lipophilicity is most commonly expressed in terms of the log P value, where P is the ratio of equilibrium concentrations in octanol and water. Large log P values suggest the molecule will exist predominantly inside the emulsion droplets (see examples in Table 1.1). One weakness of the log P approach is that it neglects the presence of the surface region which, as I have noted, enjoys properties distinct from the lipid core and aqueous phase. Many BLI have at least some amphiphilic character with a few polar groups located on an otherwise non-polar structure. Such molecules will have a tendency to align at interfaces, losing some rotational and translational entropy to optimize the chemical environments of its parts. A second weakness in applying log P values to predict distributions in very fine droplets is that the BLI solubility around the droplets tends to increase as particle size decreases due to the Laplace pressure effects. Finally, many of the log P values reported in the literature are values calculated from the chemical structure rather than experimentally measured numbers. These calculations can be highly unreliable (Table 1.2).

Table 1.1. Calculated log P values for selected BLI molecules (taken from Yannai, 2004; except otherwise indicated).

| **Compound** | **Functional role** | **log P** |
|---|---|---|
| Benzaldehyde | flavor, antioxidant | 1.5 |
| Hexanal | flavor, antioxidant | 1.8 (Reineccius, 2006) |
| Benzoic acid | Antimicrobial | 1.88 |
| Curcumin | flavor, antioxidant | 2.05 |
| Eugenol | flavor, antioxidant | 2.4 |
| | | 2.73 (Reineccius, 2006) |
| Apiole | flavor, antioxidant | 2.5 |
| Quinine | flavor, antioxidant | 2.93 |
| Octanoic acid | antimicrobial | 2.94 |
| Anethole | flavor, antioxidant | 3.31 |
| | | 3.39(Reineccius, 2006) |
| Thymol | flavor, antioxidant | 3.4 |
| Capsaicin | flavor, antioxidant | 3.5 |
| Hexyresorcinol | flavor, antioxidant | 3.95 |
| Valerenic acid | flavor, antioxidant | 4.74 |
| limonene | flavor, antioxidant | 4.83 (Reineccius, 2006) |
| narasin A | flavor, antioxidant | 5.54 |
| bullatacinone | flavor, antioxidant | 8 |
| vitamin D2 | vitamin | 9.39 |
| vitamin D3 | vitamin | 9.48 |
| vitamin K | vitamin | 11.76 |
| α-tocopherol; acetate | vitamin | 12.15 |
| β-carotene | colourant, antioxidant | 15.23 |

Table 1.2. Experimental (taken from Rothwell et al., 2005) vs. calculated log P (taken from Yannai, 2004) values for selected flavor molecules.

| **Compound** | **log P** | |
|---|---|---|
| | **experimental** | **calculated** |
| genistein | 2.51 + 0.06 | 0.98 |
| kaempferol | 3.11 + 0.54 | 0.31 |
| luteolin | 3.22 + 0.08 | 0.38 |
| naringenin | 2.60 + 0.03 | 1.8 |
| quercetin | 1.82 + 0.32 | 0.29 |

Measurement of the distribution of molecules between microenvironments in an emulsion is challenging. The three main groups of approaches are:

(i) Separation and direct analysis of one of the phases. If the aqueous phase can be separated and analyzed it is possible to measure the proportion of BLI associated with the droplets (surface and core) by difference. Unfortunately, fine particles are hard to filter or separate by sedimentation. More aggressive separation procedures (e.g., solvent extraction) often destroy the equilibrium under investigation (especially surface and Laplace pressure effects).

Alternatively, a volatile BLI can be determined in the headspace allowing its activity coefficient in the emulsion to be determined non-destructively. The measured partition coefficient of volatile molecules with the headspace ($K_{ge}$) depends on the oil-water, and air-water partition coefficients ($K_{ow}$ and $K_{aw}$ respectively) and the volume fraction ($\varphi$) of lipid (Ghosh et al., 2006):

$$\frac{C_g}{C_e} = \frac{K_{gw}}{1+(K_{ow}-1)\phi} \qquad [1.2]$$

As $K_{gw}$ can be measured independently, changes in headspace concentration can be related to the partitioning of the BLI with the droplet.

(ii) Chemical Degradation Kinetics. An indirect method to determine the distribution of BLI is to measure their chemical degradation kinetics in response to an aqueous oxidizing agent, radical source, or acid. The assumption in these studies is usually that BLI at the interface will degrade faster than those in bulk. Studies of BLI stability are obviously valuable in their own right. However care must be taken in inferring distribution between microenvironments as the assumption that molecules at surface are most vulnerable to degradation is rarely confirmed by other methods. For example, Boon et al. (2008) compared lycopene oxidation kinetics in SLN and lipid nanoemulsions and argued that the lycopene in the SLN was concentrated at the surface. However, Helgason et al. (2009) used this approach to argue that surfactant type can affect the oxidation rate of β-carotene in SLNs of same solid fat.

(iii) Spectroscopic Methods. The spectroscopic signal of many molecules is sensitive to their immediate chemical environment. If the spectroscopic method is capable of analyzing the BLI (or more likely a labeled analog) in situ in the emulsion then there will be distinguishable signals for the proportion in each microenvironment. For example, Arboleya et al. (2005) prepared a palm oil-in-water emulsion containing a stable free radical spin probe in the lipid phase. The probes were monitored using electron paramagnetic resonance (EPR) spectroscopy and the investigators were able to deconvolute the spectra and determine the proportion in the lipid and aqueous phases. The molecular mobility of the probe as a function of lipid crystallization was also determined. Nuclear magnetic resonance (NMR) spectroscopy is a similar technique to EPR, and can similarly be used to probe the properties of different compartments. For example, proton NMR ($H^1$-NMR) was used to investigate the mobility and distribution of a liquid lipid (medium chain TAG) loaded into solid lipid droplets (long chain TAG) (Jenning et al., 2000a, b).

### 1.4. Emulsions as Delivery Systems

Emulsion based delivery systems (EBDS) has been introduced as successful carrier systems for BLI. For example, $\omega$-3 fatty acid-rich TAGs were incorporated as emulsions into different food products, such as milk, yogurts, ice cream, and meat patties (Chee et al., 2005, 2007; Lee et al., 2005, 2006a, 2006b; McClements and Decker 2000; Sharma, 2005). Other BLI have been dissolved in carrier lipids prior to emulsification, for example lycopene (Ribeiro et al., 2006; Tyssandier et al., 2001), astaxanthin (Ribeiro et al., 2005, 2006), lutein (Losso et al., 2005; Santipanichwong and Suphantharika, 2007), $\beta$-carotene (Santipanichwong and Suphantharika, 2007), and plant sterols (Sharma, 2005). As I noted above, the delivery system must chemically stabilize the BLI without impairing bioavailability.

Many emulsified lipids and encapsulated BLI are vulnerable to chemical destruction; most commonly via oxidative reactions or acid hydrolysis. The structure of the emulsion and the microlocalization of the BLI can affect the rate of chemical degradation. It is also important to consider the relative localization of any other reagents (e.g., oxygen, protons), catalysts (e.g., transition metals), and inhibitors of oxidation reactions (e.g., antioxidants) involved in the BLI degradation reaction. The presence of an emulsifier layer at the oil water interface can affect the distribution of small molecules in the emulsion. It has been demonstrated that the electrostatic properties of emulsion droplets can be modified in order to repel prooxidative metals for the purpose of inhibiting lipid oxidation (McClements and Decker 2000). Emulsifiers can modify the electrical charge on the droplet surface which can affect the rate of exchange of ions between the aqueous phase and the droplet surface. For example, the degradation of an omega-3 enriched oil-in-water emulsion by oxidation reactions can be inhibited by conferring cationic properties to emulsion droplets (Donnelly, Decker et al. 1998). This was accomplished by lowering the pH of the aqueous continuous phase below that of the emulsifying protein's isoelectric point (pI), thereby establishing a net positive charge on the droplet interface. Under such conditions, positively charged transition metals are electrostatically repelled from the emulsified lipid, and oxidation reactions are inhibited. An opposite trend can be seen at pH values above the pI of the emulsifier, in which case the droplets carry a net negative charge that attracts transition metal catalysts to emulsion

interfaces, accelerating lipid oxidation reactions. Other studies have demonstrated the importance that droplet charge has on lipid oxidation kinetics in oil-in-water emulsions (McClements and Decker 2000; Hu, McClements et al. 2003;Klinkesorn, Sophanodora et al. 2005; Mei et al., 1998a, 1998b). In a similar study, Boon et al. (2008) showed that the oxidative stability of lycopene emulsions is higher when stabilized with cationic and non-ionic surfactants than in emulsions stabilized with anionic surfactants.

The thickness of the interfacial layer is an important parameter affecting droplet lipid oxidation reaction rates. Increasing interfacial membrane thickness can conceivably hinder the physical interaction between aqueous phase prooxidants (e.g., transition metals) and emulsified lipids (Chaiyasit et al. 2000; Silvestre et al. 2000). For example, Silvestre et al. (2000) showed that iron-catalyzed cumene hydroperoxide reduction, as well as salmon oil-in-water emulsion oxidation, was slower when Brij 700 was used in place of Brij 76. Brij 700 and 76 are small molecule surfactants with identical hydrophobic tail group lengths ($CH_3(CH_2)_{17}-$), but vary only with respect to the size of their polar head groups: Brij 700 and 76 consist of 100 and 10 oxyethylene head groups, respectively. Lower hydroperoxide decomposition and lipid oxidation rates in Brij 700-stabilized emulsions suggest that a thicker interfacial layer was able to act as a physical barrier to decrease lipid-prooxidant interactions (Silvestre et al., 2000). The same effect can be seen in protein-stabilized oil-in-water emulsions. For example, casein is known to form a thicker interfacial layer (10 nm) than whey proteins (1-2 nm) (Dalgleish et al., 1995), which may explain, at least in part, why emulsions stabilized with casein tend to have greater oxidative stability than those prepared with whey protein. This is despite the fact that whey protein-stabilized emulsions droplets are more positively charged (+ 55.9 mV) than their casein counterparts (+29.9 mV) at acidic pH values.

Smaller droplets (larger interfacial area) increase the exposure of the encapsulated BLI to reactive molecules so would be expected to reduce their chemical stability. Despite this, comparisons of BLI degradation rates at different particle sizes are relatively few and the postulated relationship is not always seen. For example, Kiokias et al. (2007) did not report any effects of droplet size (0.5-2 μm) on the rate of lipid oxidation in model food emulsions

as a function of temperature, while Let et al. (2007) and Nakazawa et al. (2008) showed fine ω3 fatty acid-rich oil and methyl linolenate emulsions oxidized more slowly than coarse ones (0.5-1.5 μm and 0.017-8 μm, respectively). Droplet size distribution affects not only the chemical stability of BLI and the physical stability of the EBDS but also the bioavailability of BLI within the EBDS.

Bioavailability, the amount of bioactive ingredient metabolized at the appropriate part of the living body, is believed to increase with decreasing particle size in the EBDS. Acosta (2009) reviewed various bioavailability studies and showed that in general there was an increased bioavailability in emulsions with droplets smaller than 500 nm, and even greater for droplets less than 100 nm. Various mechanisms have been suggested to explain this effect and perhaps the most universal is the increased solubility of BLI associated with very small particles (i.e., Laplace pressure effects). However, it has also been shown that residence time of the carrier particles in the intestine increases with decreasing particle size, which in turn increases the amount absorbed (Kreuter, 1991). The shorter diffusion paths in fine particles have been suggested as an alternative reason for increased bioavailability (Acosta, 2009; McClements et al., 2007). However, while the diffusion paths in the lipid phase are certainly reduced it is unclear if they are rate limiting in the overall process of absorption. Finally Jani et al. (1990) proposed that very fine particles ($d < 100$ nm) could themselves be adsorbed whole by living cells.

### 1.5. Crystallization in Emulsions

The equilibrium solid fat content (SFC) of a lipid is determined by the temperature and the type of molecules present (e.g., longer saturated or trans-unsaturated fats have higher melting points). The vegetable oils most commonly used in conventional food emulsion preparation are liquid at both storage and use temperatures. Other food lipids, notably milk fat, partially hydrogenated vegetable oil and some tropical fats are semi-crystalline at room temperature and below. Finally, hard fats (e.g., stearin fractions from tropical oils and animal fats, fully hydrogenated vegetable oils, certain waxes) are (almost) completely crystalline at room temperatures. The physical properties of lipids can be manipulated by changing the TAG

composition by either chemical (e.g., hydrogenation or interesterification) or physical means (e.g., fractionation or blending) (Haumann, 1994). In all cases, commercial food lipids are a complex mixture of different TAG molecules.

TAG molecules can crystallize typically as one of three polymorphic crystal structures, α, β' and β, each with different subcell structures (i.e., hexagonal, orthorhombic-perpendicular, and triclinic-parallel respectively) and with increasing melting points and enthalpies of fusion (Sato, 1999). If a liquid-oil is cooled quickly, it will tend to nucleate into a less stable polymorphic form and then possibly transform into a more stable polymorphic form with time, particularly if stored at higher temperatures (Himawan et al., 2006). In some cases, different yet physically similar TAG molecules can co-crystallize to form a compound crystal (Sato, 2001). If a lipid is processed into colloidal size droplets, the crystallization process is considerably different, affecting both the kinetics of crystallization, crystalline microstructure, and the structure of the fat crystal matrix.

**Kinetics of Crystallization in Fine Droplets.** The process of crystallization proceeds via two distinct processes: crystal nucleation and growth (Garside, 1985). The nucleation kinetics in fine droplets is often different from nucleation in the same liquid in bulk. In a fine emulsion, the number of droplets exceeds the number of potential nucleation catalysts (impurities) present in the liquid oil. Thus, a proportion of the lipid is effectively catalyst-free and must nucleate by other mechanisms. This may either be completely spontaneous homogeneous nucleation, or more probably some catalytic effect of the droplet surface (Coupland, 2002). In either case, the crystallization temperature is greatly reduced below the melting point and depends both on particle size and on the nature of the emulsifier selected. For example, Higami et al. (2003) showed that the crystallization temperature of trilaurin molecules was decreased from 18.9°C, the crystallization temperature of the bulk lipid, to -9.5°C when emulsified into droplets smaller than 100 nm.

In a fine droplet (i.e., heterogeneous nucleation is unimportant) crystallization is often governed by surface effects, i.e., surface heterogeneous nucleation. The most generally accepted model for surface heterogeneous nucleation is based on an ordering of lipid

molecules by the hydrophobic portion of the emulsifier at the interface. If the hydrophobic tail of the surfactant molecule has a similar molecular structure to the lipid, it may catalyze the surface nucleation event (Coupland, 2002). A good example of surfactant-directed interfacial heterogeneous nucleation is provided by Awad and Sato (2002) and Kaneko et al. (1999) who showed that hydrophobic sucrose oligoesters of stearic acid and palmitic acid accelerated the crystallization rate in emulsified palm kernel oil and hexadecane respectively. They argue the hydrophobic surfactant absorbs to the interior surface of the droplet where it provides a template for crystal formation.

The ordering effect preceding surface heterogeneous nucleation is believed to take place via the formation of rotator phase; a transient structure corresponding to TAG molecules orientated along their long axis but retaining some rotational mobility (Sirota, 1998). This phase is believed to act as an interfacial frozen monolayer, which in turn acts as a template for crystallization of the remainder of the lipid droplet (Wu et al., 1993; Sirota, 1998). However, Gulseren and Coupland (2008) argue that the region of lipid affected by the surfactant is much greater than a monolayer. Some recent and elegant support for this mechanism is provided by Shinohara et al. (2008) who used a focused X-ray beam to study hexadecane emulsions stabilized with different polysorbate surfactants. They showed that when the size and shape of the hydrophobic tail of the surfactant is similar to hexadecane, then the rotator of the lipid was detectable before crystallization and produces a radial distribution of crystals after crystallization is complete (Figure 1.3).

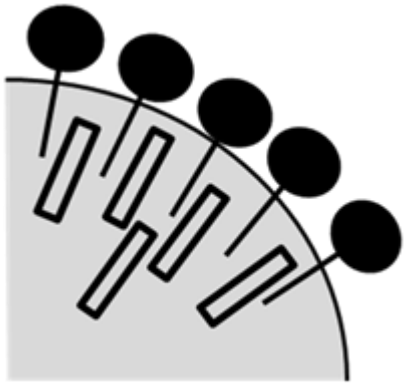

Figure 1.3. Alkane molecules (open rectangles) align with surfactant at the interface and produce a template for crystal nucleation (adapted from Awad and Sato, 2002).

The second effect of emulsification on fat crystallization is thermodynamic in origin and arises from the elevation in internal droplet pressure due to the curvature of the surface. The lipid is pressurized by the interfacial tension and thus the formation of the more dense crystal phase is favored. This effect is only really important for very small particles (<100 nm). For example, Higami et al. (2003) showed that the melting temperature of very fine trilaurin droplets (β-polymorph, bulk melting point 46.7°C) was reduced to as low as 26.5°C. In some very fine particles, the different lamellae of the lipid may have distinct melting points. For example, Bunjes et al. (2000) showed that as the particle size of TAG droplets was decreased the melting range broadened (especially for particle sizes smaller than 300 nm) and in DSC showed a number of distinct peaks, which were attributed to the melting of distinct layers of the crystal.

The high Laplace pressure created by curvature of the surface of small droplets is largely responsible for the melting point lowering effect (Montenegro et al., 2003) and can be explained by the Gibbs-Thompson equation (Bunjes and Unruh, 2007):

$$\ln \frac{T}{T_0} = -\frac{2\gamma_{sl} V_s}{r \Delta H_{fus}} \qquad [1.3]$$

where T is the melting temperature of the particle with radius r, $T_0$ is the melting temperature of the bulk material at the same external temperature, $\gamma_{sl}$ is the interfacial tension at the solid-liquid interface, $V_s$ is the specific volume of the solid, and $\Delta H_{fus}$ is the specific heat of fusion.

**Structure of Crystalline Fat Droplets.** The type of TAG polymorph is determined by many factors and affects the crystalline structure within a droplet. Emulsions prepared from pure TAG usually nucleate into the α-polymorph upon cooling followed by a solid-solid transformation into a β` or β polymorph on storage, or reheating (Awad et al., 2008; Bunjes and Unruh, 2007; Higami et al., 2003; Weiss et al., 2008). Bunjes et al. (2003) reported an unusual polymorphic form in rapidly cooled SLN corresponding to α-polymorph without any apparent long range order (i.e., no SAXS pattern, Bunjes et al., 2003). Moreover the α-crystals are aligned with the surface (Figure 1.4) in a similar manner seen in X-ray microbeam measurements on larger droplets (Shinohara et al., 2008) suggesting a potential role of the surface emulsifier in directing crystallization.

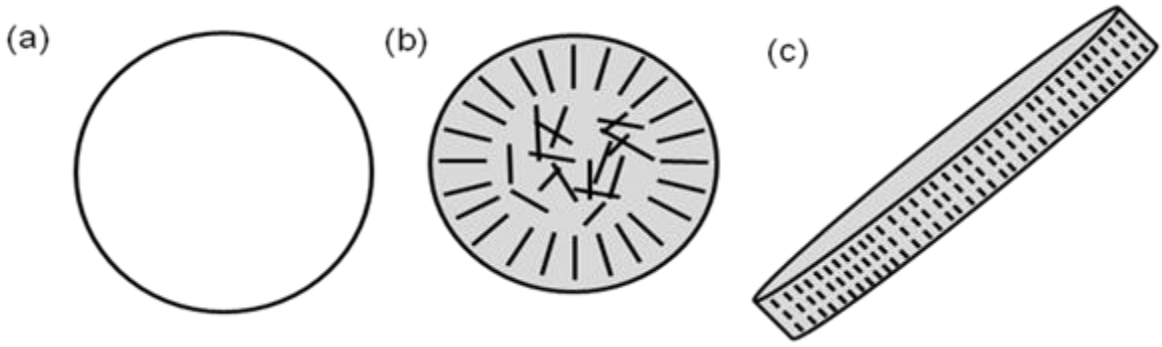


Figure 1.4. Proposed structures of (a) liquid nanoemulsions and SLN from TAG in the (b) α and (c) β crystal form (adapted from Bunjes et al., 2007). Straight lines show the alignment of selected molecular backbones in the crystal lattice. The α crystals are aligned near the droplet surface and the more disordered structure in the core. The β crystals are aligned in lamellae as shown. Highly schematic and not to scale.

In general, the α-form is preferred over β-form for SLN as firstly because BLI can be more readily incorporated in the less-dense crystals and secondly because the formation of the β-form is associated with a change in droplet shape and subsequent gelation of the suspension (see below). The rate of polymorphic transformation in fine particles is:

- greater for fine droplets and becomes especially significant at nano-scale (Awad et al., 2008; Bunjes et al., 2003, 2007; Bunjes and Koch, 2005; Helgason et al., 2008; Higami et al., 2003; Illing et al., 2004; Unruh et al., 2002; Westesen and Siekmann, 1997). The increased α to β transformation tendency in SLN can be attributed to "the relaxation of lattice strain developing during the transition is facilitated in smaller crystalline domains due to the high surface-to-volume ratio, as suggested for bulk material by Dafler (1977)" (Bunjes and Westesen, 2001).
- greater for shorter chain TAG than longer ones as the molecular mobility of small molecules is greater (Bunjes et al., 1996).
- lower at lower temperatures. Helgason et al. (2008) showed that the polymorphic transformation rates of tripalmitin nanoparticles (r ~150 nm) increased by increasing the temperature from 1 °C to 10 °C. Similarly, Awad et al. (2008) showed that faster cooling rates retard the polymorphic transition.
- dependant on the surfactant selected (Awad and Sato, 2002; Bunjes et al., 2002, 2003). Although the mechanism of surfactant action is not understood thoroughly, Bunjes et al., (2002, 2003) suggested that since the selection of hydrophilic surfactants can significantly alter the transformation kinetics, the polymorphic transition starts at the surface rather than the lipid core. This observation is reasonable assuming that TAG molecules in the surface region interacting with surfactant molecules have higher free energy and mobility. The capacity of different surfactants to stabilize the α-form varies considerably. For example, Bunjes and Koch (2005) showed that saturated long-chain phospholipids decreased the rate of polymorphic transitions compared to unsaturated soy bean phospholipids. Awad and Sato (2002) saw similar results in larger droplets with other hydrophobic emulsifiers. Bunjes et al. (2003) found that combining bile salts with saturated long chain phospholipids stabilized the α-form during recrystallization. One of the most striking examples published to date is a 9

month shelf life in refrigerated saturated TAG nanoparticles stabilized solely with polyvinyl alcohol (Rosenblatt and Bunjes, 2009).

In very fine droplets, the recrystallization event from less stable to more stable polymorphic form is often associated with a change in droplet shape from spherical to plate-like (Bunjes et al., 2007) (Figure 1.4), and subsequent gelation of the dispersion. For example, tristearin droplets with particle sizes around 100-200 nm crystallized in the α-form were spheroidal in shape with some possible elongation and also with concentric layers of TAG molecules. When these droplets converted to the β-modification they were plate-like nano-crystals with a planar layered internal structure (Figure 1.5). One reason for this change in shape is that a-nucleation occurs quickly at multiple locations throughout the droplet to form a polycrystalline particle. The α to β transition is slower and perhaps one β-crystal forms initially which grows at the expense of existing α-crystals within the droplet yielding a single monocrystalline particle. For the larger droplet sizes (i.e., >1 μm) shape change and stack formation were not observed on crystallization (Bunjes et al., 2003). This may be because there are a greater number of β-nucleation events within the larger droplets yielding a grained structure, with approximately the same shape as the starting droplet.

The β-form plates can pack together in stacks. The interpolate distance has been measured by small angle X-ray scattering (SAXS) and transmission electron microscopy (TEM), to be in the order of 20 nm (Illing et al., 2004; Unruh et al., 2002). It may be possible in some cases to reduce the tendency of plate-like particles to associate by adding more surfactant to cover the increased interfacial area (Westesen and Siekmann, 1997; Helgason et al., 2008). Presumably, there is an attractive force between fat crystals suspended in water but the effective magnitude of the force is greater between flat plates than between spheres as it acts over a larger area.

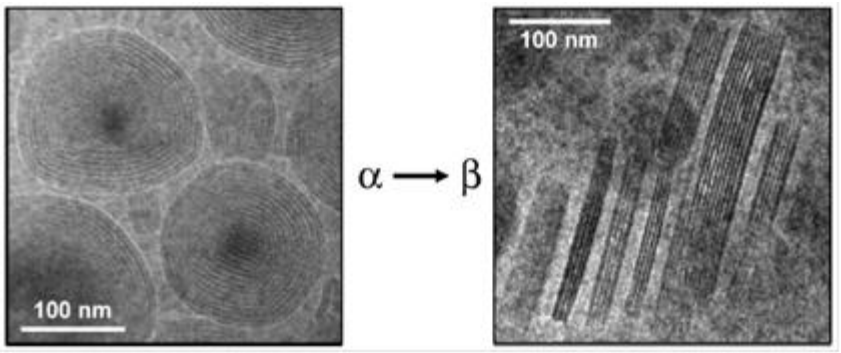


Figure 1.5. Cryo-TEM micrograph of tristearinnano-particles (~ 150 nm) showing the microstructural change upon polymorphic transition (taken from Bunjes et al., 2007).

### 1.6. Localization of BLI in Solid Lipid Nanoparticles

BLI dissolved in liquid oil nanoemulsions will redistribute on crystallization of the fat (Figure 1.6). Even if the BLI is soluble in the liquid oil (i.e., forms a one-phase solution), crystallization of the carrier lipid will likely cause a phase separation. Figure 1.6a shows the unlikely event where phase separation does not follow lipid crystallization, i.e., the BLI can form a single solid phase with the carrier lipid. Co-crystallization would presumably be detectable as large shifts in the XRD but unsurprisingly, considering the wide disparity in molecular shapes of solute and solvent, co-crystallization appears to be uncommon. For example, Bunjes et al. (2001) found no evidence that ubidecarenone was incorporated into the lattice of SLN although the kinetics of polymorphic transition in the lipid increased in the presence of the drug. It may however be possible to form compound crystals if the BLI of interest is itself a TAG (Takeuchi et al., 2002a, 2002b). Presuming co-crystallization is the exception rather than the rule then some level of phase separation must occur and the question becomes where are the separate phases localized?

Figures 1.6b, c and d show a phase separation of the BLI as either a solid precipitate or as a solution with residual liquid lipid. In Figure 1.6b, the BLI is entrapped within the solid droplet; in Figures 1.6c and d the BLI is excluded from the crystalline lipid core and either adsorbed at the surface or dispersed in the aqueous phase respectively. The major thermodynamic difference between the models is that the surface bound model (Figure 1.6c) has more crystalline lipid-BLI interactions and fewer water-BLI and water-crystalline lipid interactions than the BLI-excluded model (Figure 1.6d). While there may be some exceptions, the surface-bound model is probably energetically preferable in most cases. In conclusion, amongst the models presented for BLI encapsulation in Figure 6 the core-trapped (Figure 1.6b) and surface-bound (Figure 1.6c) seem the most probable. The most likely suitable location for entrapment in the solid droplet core (i.e., Figure 1.6b) is the grain boundaries between TAG crystals or simply dissolved in any residual liquid oil.

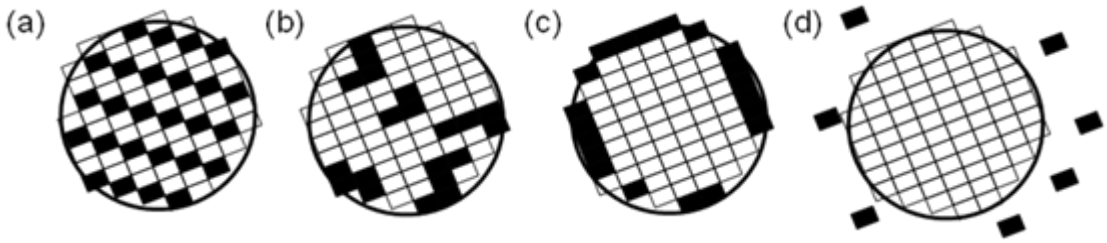


Figure 1.6. Possible effects of droplet crystallization on solute distribution. Solute is shown schematically as filled rectangles and crystalline carrier lipid as open rectangles. (a) The solute is incorporated directly into the crystal lattice and protected from oxidation, the solute is excluded from the lattice and either (b) accumulates at grain boundaries inside the droplet either as dissolved or precipitated or (c) at the surface of the droplets or even (d) partitions into the aqueous phase, or physical adsorption of precipitates on the surface. Note the droplets are drawn as spheres although different shapes are possible as discussed previously. Highly schematic and not to scale.

The imperfection density in the crystalline matrix is equal to the number of nucleation events so it may be possible to modify the internal structure of the droplet by using surfactants or alterations in cooling rate to change the rate of nucleation. If a droplet crystallizes as a single crystal, then there is no phase volume available in the droplet core so the surface-bound model is the only one available. For example, Ghosh et al. (2006, 2007) used headspace measurements to show that the crystallization of eicosane droplets forced an encapsulated BLI out of the droplet core. In SLN from polymorphic TAGs, the α-β transition is associated with the rapid release of encapsulated molecules (i.e., "burst release") (Muhlen et al., 1998; Muller et al., 2000) presumably because the β-crystalline particle is a single crystal. Structuring the SLN as a mixture of different types of crystals may allow the development of more internal structures to entrap BLI in the core of the droplet. For example, TAGs with different fatty acid composition can crystallize into double or triple chain length structures, which are immiscible, and a mixture of them may provide desired crystalline lipid network characteristics (Muller et al., 2000).

Finally, a small fraction of non-crystallizing lipid may provide superior performance to a purely solid SLN. These semicrystalline particles are sometimes known as nanoscale lipid carriers (NLC). Ideally, the small fraction of liquid oil would provide a reservoir for the BLI and hence slower release while the crystalline fat provides some physical protection from chemical degradation (Jenning et al., 2000a, b). The solid fat content of the droplets can be modified by mixing solid fats with compatible or partially compatible liquid oils. Jenning et al. (2000a, b) manufactured NLCs by replacing solid lipid with medium chain and showed that liquid lipid phase at low concentrations (8-16%) was evenly distributed within the crystal matrix. In contrast, Jores et al. (2004) produced similar NLC particles from similar lipids and observed irregular shapes and uneven distribution of the oil, i.e. on the surface or edge of the solid portion. At high oil concentrations, liquid oil attached as distinct droplet on platelet solid lipid, a so called "nano-spoon". Similar conclusions were reached by Ahlin et al. (2003) who showed that the affinity of BLI for the lipid core increases with the lipophilicity, while amphiphilic molecules tend to be carried in the amphiphilic surface region.

# Chapter 2

## 2. Significance and Hypotheses

Oil-in-water emulsions and related systems are often used to deliver hydrophobic solutes in foods, personal care products and pharmaceuticals. Recent work has considered the use of crystalline lipid carrier particles (SLN) to control the availability of the solute; however there is little direct evidence for the localization of small molecules in these systems. Although various formulations were proposed by different groups to improve the efficiency and effectiveness of SLN, the results and proposed mechanisms were often inconsistent (e.g., the extent of retention of hydrophobic solutes within SLN). This is partly due to the lack of a suitable technique which can determine the distribution and reactivity of a solute *in situ,* and thus there is no systematic approach has been done to quantify and evaluate the effect of different formulations in these variables. EPR spectroscopy offers great potential to characterize the properties of solutes within EBDS.It is a non-destructive technique so the results are measurements of the structure and properties of the intact emulsions. A disadvantage of this technique is that it requires the use of EPR-active molecules (i.e., spin probes), and in the present study a hydrophobic small molecule spin probe (PTMIO) was used.

My main goal is to show how changes in EBDS structure (i.e., droplet size, crystallinity, surface properties) affect the physical distribution and reactivity of lipophilic ingredients. In this work, I will develop an EPR method to measure the properties of the spin probe in different EBDS. Based on these findings I will develop a detailed model for the distribution behavior of the selected hydrophobic compound between phases in an EBDS.Within this framework, I will systematically approach the research questions via three specific objectives:

1. **Effects of droplet size and crystallinity:** The effects of droplet size and crystallinity in model lipid (tetradecane and eicosane) EBDS on the distribution and subsequent chemical stability of a model lipophilic ingredient (free radical PTMIO) will be evaluated. While there have been some studies concerning the entrapment efficiency of SLNs for selected solutes, none have directly compared solid vs. liquid and coarse vs. fine droplets. I hypothesize that the selected lipophilic ingredient will mostly be located in the lipid droplet than the aqueous phase, and the crystallization of droplets is expected to exclude the solute into the aqueous phase. Moreover, I also hypothesize that decreasing droplet size will increase surface effects (which can be seen as changes in probe mobility and anisotropy), and increase aqueous solubility due to an increase in Laplace pressure.

2. **Effects of liquid oil fraction and storage:** The effect of blending small amounts of liquid lipid (tetradecane) with solid lipid (eicosane) on crystallinity of droplets, and consequently distribution and reactivity of the lipophilic ingredient (PTMIO) will be studied. It is believed that because tetradecane is a smaller molecule than eicosane, it is unlikely that it will co-crystallize with eicosane but can dissolve. Although some researchers studied nanostructured lipid carriers (NLC) formed from mixtures of liquid and solid lipids, there are conflicting reports on the distribution of a hydrophobic solute or liquid lipid fraction. Moreover, the effects of small amounts of liquid lipid on solute distribution characteristics and its functionality have not been evaluated quantitatively, probably because conventional NMR techniques are insufficiently sensitive. I hypothesize that the presence of liquid lipid will limit lipid crystallization and thus improve the retention of the spin probe within the droplet. I will also consider the effects of sample storage on the properties of NLC. I hypothesize that tetradecane will slow down the crystallization rate of droplets, and thus the kinetics of redistribution of the spin probe.

3. **Effects of surface composition:** The effect of emulsifier (i.e., either soy bean lecithin with 70% phosphatidylcholine plus bile salts or caseinate) on distribution and reactivity PTMIO in C14 and C20 emulsions. Some early work suggested that entrapment efficiency for a solute within SLN can be improved via modification of the interfacial properties. Most of the successful formulations have used lecithins, which can modify the crystalline microstructure of SLN via their hydrocarbon chains. Although the general trend of results reported by different research groups are mostly in agreement, the effects of the lecithin interfacial layer itself on the distribution and functionality of probe is not understood thoroughly. I hypothesize that the hydrophobic nature and long hydrocarbon chains of lecithin can serve as a medium to increase the retention of hydrophobic solute within the droplets as compared to caseinate, and can also alter the crystallization behavior of C20 droplets.

# Chapter 3

## 3. Distribution and Chemical Stability of a Hydrophobic Solute in Liquid and Solid Lipid Emulsion Droplets as a Function of Droplet Size

### 3.1 Introduction

Certain lipophilic molecules, such as flavors, colorants, pharmaceuticals and phytochemicals, are added to food, pharmaceutical and personal care products to give desired functionality. These molecules are often chemically labile so there is demand for encapsulation methods to allow their effective use in aqueous systems. Oil-in-water emulsions are attractive candidates as delivery systems for lipophilic ingredients as they can be readily diluted in aqueous media and because the localization of the non-polar solute within emulsion droplets can provide some level of protection from reaction with aqueous phase compounds (e.g., transition metal ions, acids). This approach is common in pharmaceutical applications, where lipophilic drugs can be delivered parenterally as commercial emulsion products (Muller et al., 2000; Mehnert and Mader, 2001). Similarly, in the food industry, $\omega$-3 fatty acid-rich triglycerides can be incorporated as oxidatively stable emulsions into various food products, such as milk, yogurts, ice cream, and meat patties (Chee et al., 2005, 2007; Lee et al., 2005, 2006a, 2006b; McClements and Decker 2000; Sharma, 2005). Bioactive lipophilic small molecules can also be incorporated into foods in the form of oil-in-water emulsions. Typically, these ingredients are first dissolved in carrier lipids prior to emulsification, as has been demonstrated with lycopene (Ribeiro et al., 2006; Tyssandier et al., 2001), astaxanthin (Ribeiro et al., 2005, 2006), lutein (Losso et al., 2005; Santipanichwong and Suphantharika, 2007), $\beta$-carotene (Santipanichwong and Suphantharika, 2007), and plant sterols (Sharma, 2005).

In the last decade or so, work on emulsion based delivery systems (EBDS) has expanded to include the use of fine, crystalline emulsion droplets (i.e., solid lipid nanoparticles, SLN) (Acosta, 2009; McClements et al., 2007; Weiss et al., 2008). SLN are typically made by heating a high melting lipid above its melting point prior to homogenization, followed by cooling to initiate droplet crystallization. SLN have been used for drug delivery (Bonacucina

et al., 2009; Bunjes et al., 2001; Jenning and Gohla, 2001; Muller et al., 2000; Mehnert and Mader, 2001) although several researchers have considered parallel applications in foods (Ghosh et al., 2006, 2007; McClements et al., 2007, 2009; Velikov and Pelan, 2008; Weiss et al., 2008). Some early studies have shown that solute molecules can be encapsulated within the lipid crystal matrix, thereby protecting them from chemical degradation (Bunjes et al., 2001; Muhlen et al., 1998; Muller et al., 2000). However more recent work has concluded that droplet crystallization results in the release and eventual expulsion of entrapped molecules, either into the aqueous phase or to the droplet surface. For example, Ghosh et al. (2006, 2007) showed that crystallization of alkane droplets triggered the release of volatile molecules into the headspace. One exception seems to be SLN systems that utilize polymorphic fats, where droplets in the less perfect α-form can entrap a fraction of the solute (presumably in the intercrystalline spaces of a polycrystalline droplet), while an α to β transition causes "burst release" of the encapsulated molecule (Muhlen et al., 1998; Muller et al., 2000), presumably because the β-crystalline particle is a single crystal that cannot entrap the solute. Bunjes et al. (2003) proposed the existence of an unusual α-form, unique to lecithin stabilized fine droplets, that offers enhanced retention of lipophilic molecules.

However, most of our current understanding of the distribution of small molecules in EBDS is based on indirect techniques. For example Ghosh et al. (2006, 2007) used headspace measurements to infer the distribution of volatile molecules between phases in an oil-in-water emulsion. Another approach assumes a direct correlation between the distribution of the lipophilic ingredient and its chemical reactivity (Helgason et al., 2009). A spectroscopic method that could accurately determine the distribution of small molecules within an EBDS, preferably *in situ*, would enable the design of structures to optimize functionality. Electron paramagnetic resonance (EPR) spectroscopy is based on the interaction of unpaired electrons of paramagnetic species (i.e., free-radicals) with the magnetic component of microwave radiation. An EPR spectrum is a function of the chemical structure of the free radical molecules, their mobility and the polarity of their environments as well as being affected by the presence of paramagnetic impurities (e.g., $O_2$). EPR requires the use of a stable free radical as a probe molecule but can make measurements in opaque media without any sample disruption.

Ahlin et al. (2000a, 2003) measured the EPR spectra of spin probes in a phospholipid stabilized glycerol tripalmitate emulsion above and below the melting point of the fat. Line broadening increased on lipid crystallization consistent with the immobilization of the probes. However the probes used were aliphatic, and the changes may be associated with a phase change in the phospholipid membrane. Arboleya et al. (2005) measured the EPR spectra of lipophilic spin probes in a caseinate-stabilized palm kernel oil-in-water emulsion as a function of temperature and showed that probe mobility decreased at lower temperatures. They argued that the microviscosity of the lipid phase increased as the fat crystallized, although no data is presented on how the amphipillic probe might partition between phases as a result of crystallization.

As well as spectroscopic analysis, EPR can be used to obtain a measure of the total residual probe concentration following reaction with an aqueous compound, for example ascorbate (Ahlin 2000a, 2003; Jores et al., 2003; Mikhalev et al., 1989). Fast degradation kinetics are used to infer the presence of the probe in the aqueous phase or interface.

In summary, EPR offers great potential to characterize the properties of EBDS. While there have been some studies in this area, none have directly compared solid vs. liquid and coarse vs. fine droplets. Furthermore, inferences drawn from analysis of spectra have never been quantitatively compared to measurements of probe stability. In this work, I use EPR to develop a detailed model for the distribution of a model hydrophobic compound between phases in an EBDS.

## 3.2 Materials and Methods

### 3.2.1 Materials

The free radical spin probe 4-phenyl-2,2,5,5-tetramethyl-3-imidazoline-1-oxyl nitroxide (PTMIO, Figure 3.1) was used as a model lipophilic ingredient (Enzo Life Sciences, Plymouth Meeting, PA, USA). Sodium caseinate (from bovine milk), n-eicosane, sodium L-ascorbate were obtained from the Sigma Chemical Company (St. Louis, MO, USA), n-

tetradecane was obtained from Fisher Scientific (Pittsburgh, PA, USA), and ferric chloride 6-hydrate was obtained from Mallinckrodt Chemicals (Phillipsburg, NJ, USA). All other materials were reagent grade and were used as received.

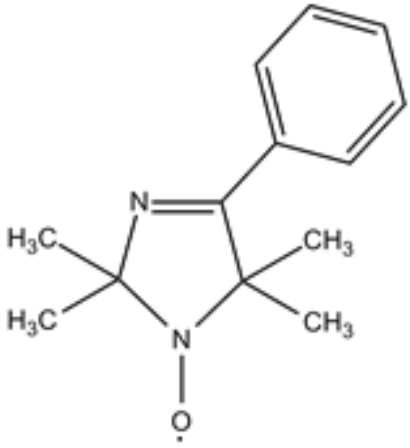


Figure 3.1. PTMIO, the model EPR-active lipophilic compound studied.

3.2.2 Preparation of EBDS containing the lipophilic ingredient.

Emulsions (10 wt% lipid) were prepared using a hot-homogenization technique. In brief, a known amount of PTMIO was dissolved in the lipid phase at 50°C for 1h. An emulsion premix ($d_{32}$ ~40-50 μm) was prepared by mixing the PTMIO-containing lipid with 1 wt% Na-caseinate solution (in pH 7, 100 mM (milli-molar) phosphate buffer) using a high-speed blender (Brinkmann Polytron, Brinkmann Instruments Inc., Westbury, NY). The emulsion premix was then passed through a microfluidizer (M-110Y Microfluidizer, Microfluidics, Newton, MA). Coarse ($d_{32}$ = 1.3 μm) emulsions were prepared by passing the premix through the microfluidizer configured with a 400 μm interaction chamber at 200 bar (one pass), Fine ($d_{32}$ = 0.2 μm) emulsions were prepared by passing the premix through the microfluidizer configured with 75 and 200 μm interaction chambers in series at 1200 bar (5 passes). All equipment and reagents were pre-heated to 65-70 °C to ensure the lipids were liquid for effective homogenization. The particle size distribution of the emulsions was measured by

static light scattering (Horiba LA-920, Irvine, CA). Emulsion samples (40 g) were transferred to 50 mL glass flasks, sealed under rubber stoppers, and allowed to stand at room temperature (21.5 ± 0.5 ºC) to allow the eicosane droplets to solidify. The final emulsions contained 200 μ*m* (micromolal) PTMIO. All samples were prepared in triplicate.

3.2.3 EPR analysis.

EPR spectra of emulsions were measured using a Bruker eScanR spectrometer (Bruker-Biospin, Billerica, MA) operating in X-band. The EPR parameters were as follows: microwave frequency, 9.775 GHz; modulation frequency, 86.0 kHz; microwave power, 18.97 mW; scan range, 50 G; modulation amplitude, 0.98; sweep time, 2.62 sec; time constant, 5.12 msec; conversion time, 5.12 msec. Measurements were made at 21.5 ± 0.5 °C.

Prior to EPR analyses, samples were deoxygenated by passing humidified $N_2$ gas (3 sL/min) through the headspace of the flasks for about 90 min while the samples were mixed using a magnetic stirrer (Figure 3.2). Preliminary experiments showed this treatment was sufficient to deoxygenate the samples. Aliquots of the deoxygenated emulsions were loaded into close-packed 19-bore quartz capillaries (AquaX, Bruker-Biospin, Billerica, MA) which had been previously flushed with $N_2$ gas and the spectra were recorded. To study the chemical reduction of PTMIO, small volumes of sodium ascorbate solution and ferric chloride solution (final concentration 1 m*m* and 10 μ*m*, respectively) were added to the samples under a $N_2$ blanket and EPR spectra were recorded at intervals.

EPR measurements in bulk lipids were carried out in a similar manner, except for the following modifications: the nitrogen gas used to deoxygenate bulk lipid samples was not humidified, and samples were loaded into borosilicate glass capillary tubes (VWR, Cat. No. 53432-783) instead of a 19-bore quartz measurement cell.

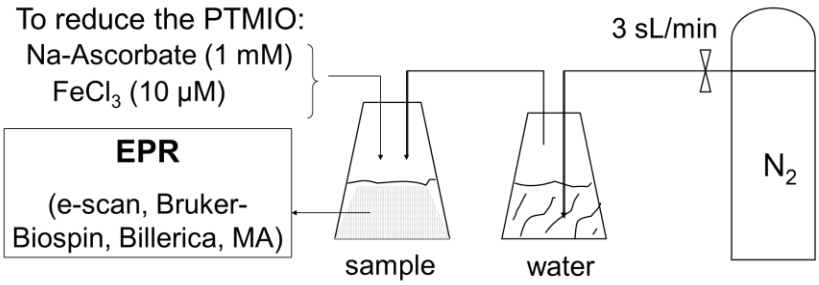


Figure 3.2. Experimental setup for the analysis of PTMIO in EBDS.

3.2.4 Spectral deconvolution and line-width analysis.

The shape of the absorption line (*i.e.*, by convention the first derivative of the bell-shaped absorption curve) is determined by the relaxation behavior of the free electrons. The total line width can be expressed in terms of two relaxation times, $T_1$ (the spin-lattice relaxation, or longitudinal relaxation time), and $T_2$ (spin-spin relaxation, transverse relaxation time) as: $LW = 1/T_1 + 1/T_2$ (Nordio, 1976; Gerson and Huber, 2003). In the rapid motion regime and low microwave power $T_1 >> T_2$, thus $T_2$ determines the line shape.

In the fast motion regime (i.e., rotational correlation time < 1 ns), the Lorentzian line-width can be described in terms of a spin-spin relaxation time $T_2$ as:

$$\left[T_2(M_I)\right]^{-1} = A + BM_I + CM_I^{\,2} \qquad [3.1]$$

where $M_I$ is the nuclear magnetic quantum number and the constants A, B and C are terms describing the magnetic anisotropy of the unpaired electron, and are functions of g- and hyperfine-tensors and molecular relaxation times in liquids (Nordio, 1976; Fairhurst et al., 1983). The low- and high-field lines are designated as +1 and -1 nuclear spin states, respectively. In the fast motion regime, the anisotropy is averaged out and line-shape parameters can be calculated from the widths of the individual hyperfine lines as (Fairhurst et al., 1983; Edgcomb et al., 2000; Arboleya et al., 2005):

$$-B = \frac{\left[T_2(-1)\right]^{-1} - \left[T_2(+1)\right]^{-1}}{2} \qquad [3.2]$$

$$[T_2(0)]^{-1}\left[\frac{T_2(0)}{T_2(\pm 1)} - 1\right] = C \pm B \qquad [3.3]$$

$$C = \frac{\left[T_2(-1)\right]^{-1} + \left[T_2(+1)\right]^{-1}}{2} - \left[T_2(0)\right]^{-1} \qquad [3.4]$$

Therefore, two rotational correlation times $\tau_c$(B) and $\tau_c$(C) can be calculated as (Nordio, 1976; Fairhurst et al. 1983; Nakagawa, 2009):

$$B = \frac{4}{15} b(\Delta\gamma) H_0 \tau_C(B) \qquad [3.5]$$

$$C = \frac{1}{8} \frac{h}{\beta_e g_{iso}} b^2 \tau_C(C) \qquad [3.6]$$

where

$$b = \frac{4\pi}{3}\left[ A_{zz} - \frac{(A_{xx} + A_{yy})}{2} \right] \qquad [3.7]$$

$$\Delta\gamma = \beta_e h^{-1}\left[ g_{zz} - \left( \frac{g_{xx} + g_{yy}}{2} \right) \right] \qquad [3.8]$$

$$g_{iso} = \frac{1}{3}(g_{xx} + g_{yy} + g_{zz}) \qquad [3.9]$$

and $H_0$ is the center field of the spectrum, $\beta_e$ is the Bohr magneton, and h is the reduced Plank's constant. The values for g- and hyperfine-tensors (g(xx), g(yy), g(zz) in equations 3.8 and 3.9, and A(zz), A(xx), A(yy) in equation 3.7, respectively) were taken from Berliner (1976), and the values for B and C were calculated from the simulated spectra.

The EPR spectrum of the spin probe in an emulsion represents the superimposed spectra of radicals that have partitioned into different environments. The experimental spectra were first simulated, and then the individual centers were deconvoluted into contributions from probe in polar and non-polar environments (with different hyperfine splitting constants). The experimental spectra were simulated using the WinSim2002 software (version 0.98, National Institute of Environmental Health Sciences, National Institutes of Health, USA). The

WinSim2002 Software can simulate motion of a nitroxide radical by using independent line widths at the -1, 0, +1 positions (i.e., nuclear spin states; see above). A spectral titration protocol was developed to determine the parameters describing the spectra (i.e., line widths, hyperfine splitting constants, g-values and shifts, and relative intensities, and Lorentzian-Gaussian line width ratio) of the probe in each phase (i.e., polar and non-polar phases in an emulsion). The initial parameters for each population of PTMIO in an emulsion were taken from the EPR spectra of PTMIO in respective phases as bulk, and then actual parameters were determined using a Simplex algorithm to provide a best fit. The iterations were restarted 10 times, and a fractional tolerance of 0.001 was used. In all iterations, the fractional tolerance was satisfied, and the final correlation coefficient was greater than 0.995 for all simulations. In order to check for the local minima, after 10 iterations were completed a new optimization protocol was run, and finally for each sample the results of the best three simulations were averaged.

The rotational correlation times (i.e., measurements of the inverse of probe mobility, see above) and signal intensities (i.e., measurement if the amount of spin probe in a given environment) from each phase were calculated from line widths (i.e., the distance between the maxima and minima of the first derivative absorption curve) and from a double integration of the single signal (i.e., see Appendix A.2) from the corresponding phase, respectively. Hyperfine splitting constants (and also g-shifts) are affected from the polarity of the probe's environment (i.e., due to different electron density on Nitrogen), and hyperfine splitting constants were used to characterize the polar and non-polar spin-probe populations. Unresolved broadening due to unresolved hyperfine couplings (i.e., isotopes and proton effects), the presence of paramagnetic impurities such as dissolved molecular oxygen, and magnetic field inhomogenities were taken into consideration by the Gaussian line-width parameter. Although two rotational correlation times were calculated, $\tau_c(B)$ (Equation 3.5) is more reliable than $\tau_c(C)$ (Equation 3.6) (Arboleya et al., 2005), as well as being more sensitive to any changes probe anisotropy, $\tau_c(B)/\tau_c(C)$ (Fairhurst et al., 1983). The ratio $\tau_c(B)/\tau_c(C)$ is unity for isotropic motion and can be used as a measure of probe anisotropy (Edgcomb et al., 2000; Freed, 1976). The parameters used for analyses of the EPR spectra were summarized in Appendix A.2.

3.2.5 DSC analysis.

The crystallization behavior of emulsion droplets was investigated by differential scanning calorimetry (VP-DSC, Microcal, Northampton, MA). The emulsion was diluted in phosphate buffer to 0.1 wt% lipid prior to analysis. Aliquots (0.513 mL) were loaded into the instrument and cooled from 40 to 10°C at 12 °C/h. Heat flux was measured relative to water.

3.2.6 Statistics

The significance of difference between samples were evaluated using t-test for a pair-wise comparison of two samples at $\alpha = 0.05$.

**3.3 Results and Discussion**

3.3.1 Probe behavior in bulk phases

PTMIO (0.2 m*m*) was dissolved in tetradecane and then added to sodium caseinate solution (1 wt%) to a final lipid content of 10 wt%. The mixture was sealed and gently agitated for 24 h at room temperature on a platform shaker, taking care not to form an emulsion. Aliquots were taken from each phase and EPR spectra were recorded in air. The shapes of the first derivative absorption curves (i.e., the EPR spectra) were characteristic of a nitroxide radical (Figure 3.3). The position and width of the peaks depends mainly on the polarity of the environment and mobility of the probe molecules, respectively, while the total signal intensity (i.e., calculated by the double integration of the first derivative absorption spectra, see Appendix A.2) is determined by probe concentration in a given environment, and has a linear dependence on peak height and on the square of line-width. The peak-to-peak height (i.e., the vertical distance between the minima and the maxima of the first derivative absorption spectra) of the signal from PTMIO in the tetradecane phase in air was ~5 fold greater than that the signal from PTMIO in the aqueous phase; however, the peak width in tetradecane was also considerably greater than in the aqueous phase which decreased the peak-to-peak height (Figure 3.3). The presence of triplet oxygen (a biradical) is known to affect EPR patterns due

to Heisenberg spin exchange (i.e., can result in signal intensity losses and Gaussian-type line broadening) (Weil and Bolton, 2007). Consequently, the presence of oxygen, especially in the lipid phase, can cause underestimation of intensities and larger rotational correlation times (i.e., line broadening) as seen in several studies (Arboleya et al., 2005). Nakagawa (2009) was able to obtain precise characterization of the EPR spectra from deoxygenated oil-water mixtures; however it is unclear how other workers dealt with the important effects of oxygen on their results (Ahlin et al., 2000a, 2003; Arboleya et al., 2005). Therefore, the effect of dissolved oxygen on EPR spectra was determined after first deoxygenating the samples by exhaustively exchanging with headspace nitrogen (Figure 3.3).

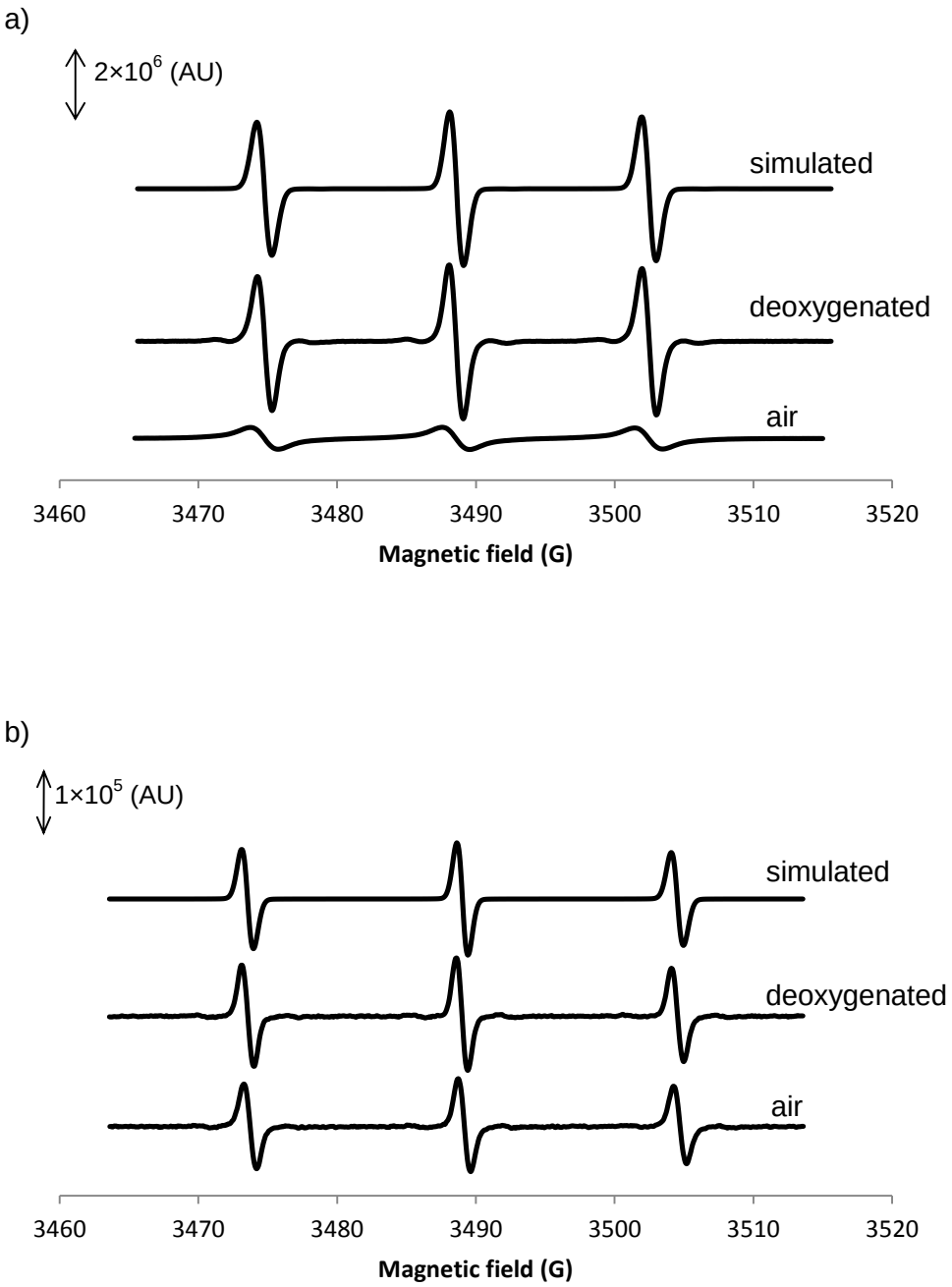


Figure 3.3. EPR spectra of PTMIO in (a) tetradecane, and (b) aqueous sodium caseinate solution (1 wt%) after storing the phases together on a rocking tray for 24 h. EPR measurements are shown both in air and after deoxygenation under nitrogen. Simulated spectra of the deoxygenated samples are also shown.

The g-factor (i.e., center peak position) and hyperfine splitting constants (i.e., positions of the hyperfine peaks) of PTMIO in either phase were not affected by deoxygenation; suggesting the chemical nature of the radical and the polarity of its environment were unchanged. However, deoxygenation of the tetradecane phase greatly reduced line-broadening and consequently increased the signal peak-to-peak height by approximately one order of magnitude (Figure 3.3a). In contrast, deoxygenation of the aqueous phase had much lesser effect (Figure 3.3b). The different effects of deoxygenation in the two environments can be attributed to the fact that the solubility of oxygen in lipids is about three fold higher than that in water, as well as to differences in the dielectric properties and polarities of the two phases (Diakova and Bryant, 2006; Popp and Hyde, 1981; Swartz and Clarkson, 1998; Weil and Bolton, 2007). Regardless of the actual mechanism, deoxygenation removed a quenching agent and allows a direct comparison of the signal from the two phases. All subsequent comparison and evaluation of the partitioning behavior of PTMIO in emulsion systems were carried out for deoxygenated samples only. I will later exploit the different effects of deoxygenation on probe signal in lipid and aqueous phases to characterize the spectra from emulsions.

The parameters describing the properties PTMIO in bulk aqueous and lipid phases were evaluated from the simulated spectra (Table 3.1). After 24 h of contact with sodium caseinate solution, the signal intensity of the lipid phase was similar ($1.0\times10^7$ AU) to the control sample (i.e., not in contact with sodium caseinate solution), while the signal intensity in the aqueous solution increased from zero to $1.7\times10^5$ AU. This finding shows that only a very small fraction of the PTMIO (~1.7%) partitioned from the bulk lipid to the bulk aqueous sodium caseinate solution phase. The corresponding loss of probe from the lipid phase was too small (i.e., about 2 orders of magnitude smaller than the original amount) to be measured. The properties of the probe in each bulk phase were investigated by line shape analysis of the simulated spectra (Table 3.1).

The hyperfine splitting constant of PTMIO in the aqueous phase ($a_N$ = 15.46 G) is higher than that in the lipid phase ($a_N$ =13.83 G). These hyperfine splitting constants are in agreement with values reported for similar molecules in the literature (Arboleya et al., 2005; Owenius et

al., 2001). The difference between the hyperfine splitting constants in lipid and aqueous environments can be attributed to the difference in the polarity of these phases, which affects the local distribution density of the unpaired electron (Deo & Somasundaran, 2002; Nordio, 1976).

Line shape analysis showed that the probe is highly mobile and isotropic in both bulk phases (Table 3.1). The mobility of PTMIO in the aqueous phase is lower than in the lipid phase despite the fact that tetradecane is approximately twice as viscous as water. Similar measurements of PTMIO in phosphate buffer showed the spin probe was much more mobile than in Na-caseinate solution ($\tau_c(B) < 0.01$ ns). The lower mobility in the Na-caseinate solution is probably due to association between the probe and protein molecules. Moreover, the diameter of an equivalent sphere for PTMIO can be calculated as (Freed, 1976; Nordio, 1976):

$$\tau_r = \left(6D_r\right)^{-1} \qquad [3.10]$$

where $\tau_r$ is rotational correlation time, and $D_r$ is the rotational diffusion coefficient. In the bulk C14, $D_r$ was calculated as $1\times10^{10}$ ($s^{-1}$). This approximation is valid for complete isotropic motion. By assuming the spin-probe as a sphere, the rotational correlation time can be calculated in a isotropic liquid (i.e., in this study, tetradecane) from rotational Stokes-Einstein relationship as (Nordio, 1976):

$$D_r = \frac{kT}{8\pi\eta R^3} \qquad [3.11]$$

where k is Boltzmann constant, η is viscosity of the isotropic liquid, and R is radius of the characteristic sphere. The viscosity of tetradecane at 21.5 °C was calculated to be 2.237 (mPa.s) from Dymond and Oye (1994). Thus, the diameter of the characteristic sphere was calculated using equation 3.11 as about 0.4 nm. This value is in agreement with molecular size of the PTMIO molecule. Indeed, the longest dimension of PTMIO is along the N-O bond and is approximately 0.7 nm, while its perpendicular axis is shorter (i.e., C-C length in the

benzene ring is 0.14 nm). Thus, PTMIO is not spherical and geometrical averaging of different dimensions is equivalent to the diameter of the characteristic sphere, as also suggested in Freed (1976).

Based on my measurements in bulk solutions I conclude that PTMIO is predominantly lipid soluble but may partition to some extent into an aqueous phase where it apparently interacts with caseinate molecules. It should be noted however that the partitioning behavior in an emulsion may differ from the behavior in bulk phases due to the presence of a larger interfacial area as well as Laplace pressure effects. In the next section, I report the properties of the probe in a liquid oil emulsion.

Table 3.1. Parameters describing the simulated EPR spectra of PTMIO in bulk solutions. The different letters show significant difference in a column ($\alpha = 0.05$).

| Environment | $\tau_c(B) \times 10^{11}$ (sec) | $\tau_c(B)/\tau_c(C)$ | $a_N$ (G) |
|---|---|---|---|
| Aqueous (1% Na-caseinate solution) | $1.85 \pm 0.12^a$ | $1.23 \pm 0.11^a$ | $15.461 \pm 0.002^a$ |
| Lipid (C14) | $1.42 \pm 0.19^b$ | $1.10 \pm 0.18^a$ | $13.829 \pm 0.002^b$ |

### 3.3.2 Probe behavior in liquid lipid emulsions

The EPR spectra of PTMIO in deoxygenated emulsions can be interpreted as superimposed EPR patterns of the spin probe in aqueous and in lipid environments (Figure 3.4). Similar spectra have been reported for EPR probes in oil-water mixtures (Nakagawa, 2009). The difference in the hyperfine splitting peaks for polar and non-polar phases is more clearly distinguishable in the high-field peak compared to the low-field peak due to zero-field splitting.

The first (~3502.3 G) and the second (~3504.5 G) hyperfine peaks (i.e., separation at the high-field peak) corresponded to the signals from PTMIO in the non-polar (lipid phase) and polar (aqueous phase) environments respectively (Figures 3.3 and 3.4a). When the same emulsion was examined under air instead of nitrogen, the line-width of the peak attributed to PTMIO in a lipid environment increased significantly, with a corresponding decrease in peak-to-peak height, while the peak attributed to PTMIO in an aqueous environment did not appreciably change (Figure 3.4b). These changes mirror the relative effects of deoxygenation on the separate bulk phases (Figure 3.3) and support our attribution of the peaks. Peak assignments were also confirmed by physically separating the lipid droplets from the aqueous phase via centrifugal filtration and subsequent analysis of the filtrate. Aliquots (15 mL) of emulsions were sampled into centrifugal filters (Amicon ultra, ultracel, 100 kDa, Carrigtwohill, Co. Cork, Ireland) and centrifuged at 14,000 × $g$ for 30 min at room temperature. Preliminary measurements showed the membrane was permeable to caseinate. The EPR spectrum of the filtrate was recorded and compared to that of unfiltered emulsion (Figure 3.5). The spectrum of the filtrate was similar to that of the probe in bulk aqueous caseinate solution, and the intensity and hyperfine splitting constants were in agreement with the second hyperfine peak of the unfiltered emulsion. Consequently, the second hyperfine peak in the high-field region was confidently associated with PTMIO molecules in a polar environment (i.e., aqueous phase) (Figure 3.4).

a)

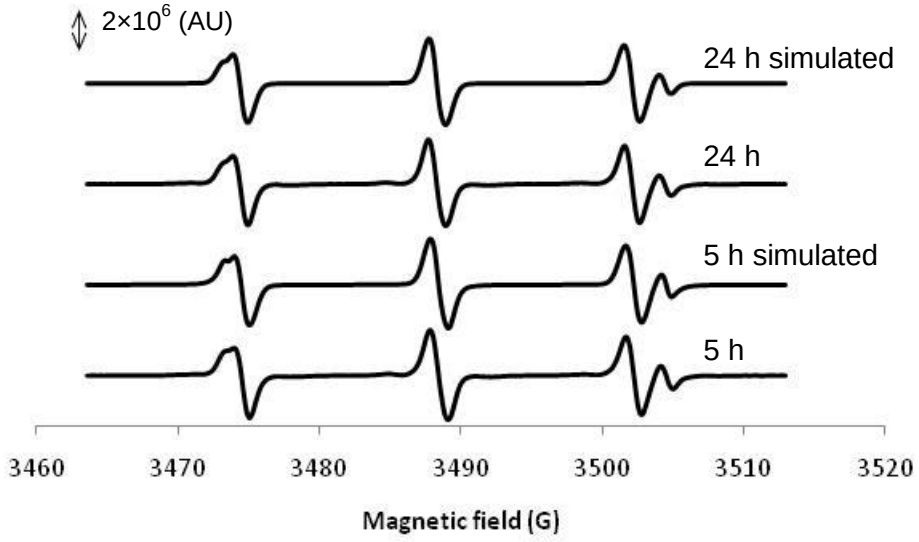


b)

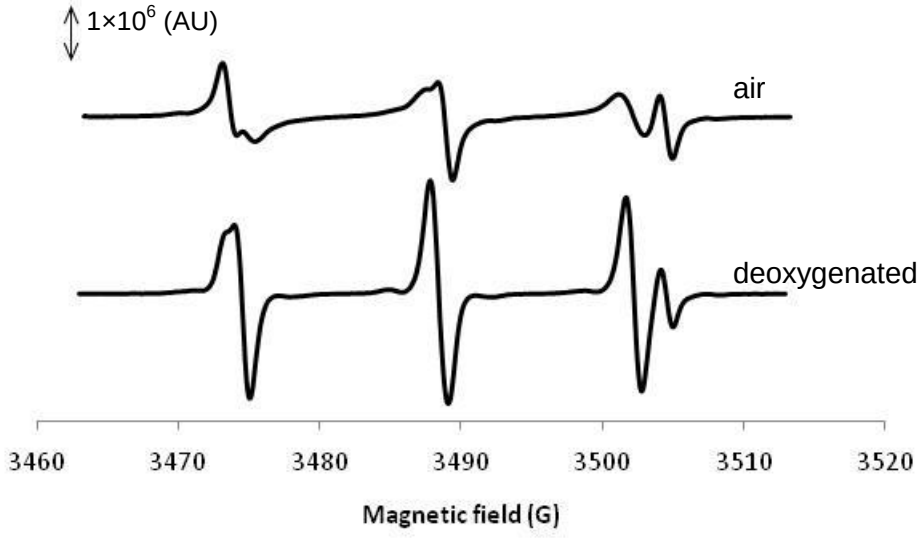


Figure 3.4. EPR spectra of PTMIO (200 μ*m*) in a 10 wt% tetradecane emulsion ($d_{32}$ = 1.3 μm). (a) After 5 h and 24 h of storage at room temperature along with simulated spectra, and (b) before and after deoxygenation of the 5 h stored sample.

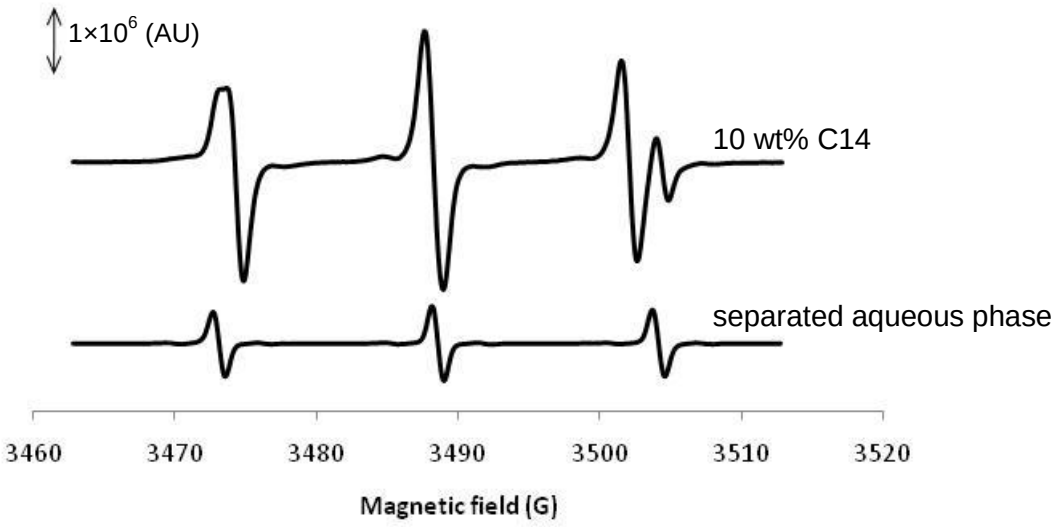


Figure 3.5. EPR spectra of PTMIO (200 μ*m*) in a 10 wt% tetradecane emulsion ($d_{32}$ = 0.2 μm) and in the aqueous phase after separation from the emulsion.

Having identified the two populations of PTMIO making up the EPR spectrum from an emulsion, the properties of the probe in the two environments were determined by first simulating the spectra (Figure 3.4a), then deconvoluting the simulated spectra into signals from the separate phases (Table 3.2). In these liquid oil emulsions the probe properties were the same for the 5 h and 24 h samples and so are considered together.

Table 3.2. Parameters describing the deconvoluted EPR spectra of PTMIO in emulsions. The different letters show significant difference of a parameter (i.e., in a column) between two samples for a given time, and different Roman numerals show significant difference for the same sample and parameter at different time ($\alpha = 0.05$).

| | | Probe fraction in | Properties of the probe in the aqueous environment | | | Properties of the probe in the lipid environment | | |
|---|---|---|---|---|---|---|---|---|
| | Sample ($d_{32}$) | aqueous phase (%) | $\tau_c(B) \times 10^{11}$ (sec) | $\tau_c(B)/\tau_c(C)$ | $a_N$ (G) | $\tau_c(B) \times 10^{11}$ (sec) | $\tau_c(B)/\tau_c(C)$ | $a_N$ (G) |
| 5 h | C14 (0.2 um) | $29.81 \pm 1.13^{a,I}$ | $5.09 \pm 0.43^{a,I}$ | $3.71 \pm 0.43^{ac,I}$ | $15.499 \pm 0.004^{a,I}$ | $2.21 \pm 0.20^{a,I}$ | $1.15 \pm 0.12^{a,I}$ | $13.854 \pm 0.003^{a,I}$ |
| | C14 (0.6 um) | $27.18 \pm 0.97^{b,I}$ | $3.73 \pm 0.22^{b,I}$ | $2.84 \pm 0.54^{ab,I}$ | $15.509 \pm 0.009^{ab,I}$ | $1.31 \pm 0.09^{bc,I}$ | $1.11 \pm 0.12^{a,I}$ | $13.841 \pm 0.005^{b,I}$ |
| | C14 (1.3 um) | $22.96 \pm 1.51^{c,I}$ | $2.66 \pm 0.36^{c,I}$ | $2.09 \pm 0.38^{b,I}$ | $15.516 \pm 0.003^{b,I}$ | $1.08 \pm 0.12^{b,I}$ | $1.04 \pm 0.15^{a,I}$ | $13.837 \pm 0.003^{b,I}$ |
| | C20 (0.2 um) | $35.64 \pm 0.73^{d,I}$ | $7.54 \pm 0.63^{d,I}$ | $5.36 \pm 1.14^{c,I}$ | $15.496 \pm 0.006^{a,I}$ | $2.64 \pm 0.19^{a,I}$ | $1.25 \pm 0.11^{a,I}$ | $13.853 \pm 0.003^{a,I}$ |
| | C20 (1.3 um) | $44.04 \pm 1.22^{e,I}$ | $3.55 \pm 0.40^{b,I}$ | $3.69 \pm 0.47^{ac,I}$ | $15.494 \pm 0.007^{a,I}$ | $1.96 \pm 0.51^{ac,I}$ | $1.31 \pm 0.35^{a,I}$ | $13.847 \pm 0.008^{ab,I}$ |
| 24 h | C14 (0.2 um) | $29.88 \pm 1.29^{a,I}$ | $5.42 \pm 0.66^{a,I}$ | $3.99 \pm 1.25^{a,I}$ | $15.502 \pm 0.005^{a,I}$ | $1.99 \pm 0.32^{a,I}$ | $1.08 \pm 0.19^{a,I}$ | $13.850 \pm 0.004^{a,I}$ |
| | C14 (0.6 um) | $27.06 \pm 1.03^{b,I}$ | $3.92 \pm 0.45^{b,I}$ | $2.93 \pm 0.41^{ab,I}$ | $15.510 \pm 0.003^{ab,I}$ | $1.23 \pm 0.11^{b,I}$ | $1.07 \pm 0.13^{a,I}$ | $13.838 \pm 0.002^{b,I}$ |
| | C14 (1.3 um) | $22.72 \pm 1.98^{c,I}$ | $2.54 \pm 0.36^{cd,I}$ | $2.16 \pm 0.40^{b,I}$ | $15.520 \pm 0.003^{b,I}$ | $1.02 \pm 0.10^{b,I}$ | $0.94 \pm 0.23^{a,I}$ | $13.834 \pm 0.003^{b,I}$ |
| | C20 (0.2 um) | 100 | $2.92 \pm 0.52^{bc,II}$ | $1.36 \pm 0.27^{c,II}$ | $15.474 \pm 0.006^{c,II}$ | NA | NA | NA |
| | C20 (1.3 um) | 100 | $1.98 \pm 0.15^{d,II}$ | $1.20 \pm 0.13^{c,II}$ | $15.471 \pm 0.002^{c,II}$ | NA | NA | NA |

The proportion of PTMIO in the aqueous environment was determined from the ratio of the intensity of the signal from the aqueous environment to that of the total signal (Table 3.2) as 30% and 23% for fine and coarse droplet emulsions respectively. Both of these values are much greater than for the bulk phase values (i.e., 1.7% of PTMIO in the Na-caseinate solution). The hyperfine splitting constants for PTMIO in the aqueous environment of emulsions decreased with decreasing particle size (Table 3.2), probably due to the increase in interfacial area. In a similar manner to analysis of the bulk phases, the rotational correlation times, $\tau_c(B)$, in the aqueous phase were higher than that in the lipid phase, and further increased with decreasing particle size (Table 3.2). Furthermore probe anisotropy (i.e., $\tau_c(B)/\tau_c(C)$) increased with decreasing particle size.

The increase in the proportion of probe in the aqueous environment with decreasing droplet size can be explained via two mechanisms. Firstly, fine droplets have a greater interfacial area. The probe has some affinity for caseinate so may accumulate at the surface where the protein is concentrated. This hypothesis is supported by our observations that in the presence of increased surface area the probe molecules have decreased mobility and increased anisotropy. Alternatively, the Laplace pressure increases with decreasing droplet size, and so the solubility of the lipophilic spin probe in the aqueous layer immediately surrounding the droplets would also increase. The extent of increase in solubility around the droplets can be calculated by the Kelvin equation (McClements, 2005):

$$S(r) = S(\infty)\exp\left(\frac{2\gamma V_m}{RTr}\right) \qquad [3.12]$$

where $V_m$ is the molar volume of the molecule of interest, $\gamma$ is the interfacial tension between lipid droplet surface and aqueous phase, $S(\infty)$ is the thermodynamic solubility of the solute in the continuous phase (i.e., no surface curvature), S(r) is the solubility of the solute when contained in a spherical droplet of radius r, T is temperature (in K), and R is the Boltzmann constant. It was calculated that decreasing droplet size from 1.3 μm to 0.2 μm increases the solubility of the hydrophilic solute around the droplets by 7%, and this value is in agreement with the change of the probe concentration in the aqueous phase with changing droplet size.

In a similar manner, the concentration of the lipophilic ingredients in the droplets increases with increasing droplet size. Moreover, a concentration gradient in the aqueous phase around a droplet between S(r) at the surface and S(∞) in the bulk is expected to occur (Figure 3.6).

The hyperfine splitting constants for PTMIO in the non-polar environment (i.e., lipid phase) of emulsions were similar to the splitting constant of the same molecule in bulk tetradecane (i.e., $a_N$ = 13.83 G) and increased with decreasing particle size (i.e., increase in the interfacial area) (Table 3.2). The rotational correlation times ($\tau_c$(B), Table 3.2) are consistent with those of similarly-sized nitroxide free-radicals reported previously (Ahlin et al., 2000a, 2003; Fairhurst et al., 1983; Nakagawa, 2009). In all cases, the molecular motion was rapid, and no meaningful anisotropy was observed for the probe in the liquid lipid phase.

The rotational correlation times for spin probe molecules in the lipid phase were higher for smaller droplets, probably due to the greater extent of interaction with the increased interfacial area in the fine particles. An alternative explanation would be the properties of the liquid oil change with changing droplet size. However, the greater internal pressure of fine droplets (i.e., pressure change on reducing the droplet size from 1.3 μm to 0.2 μm is about 0.35 MPa) is not high enough to cause sufficient change in the oil viscosity to impact probe mobility (i.e., less than 1% change) (Dickinson, 1977; Dymond and Young, 1980; Dymond et al., 1980; Kiran and Sen, 1992).

Based on the measurements in liquid oil emulsions, I conclude that PTMIO is predominantly present in the lipid phase where its mobility is somewhat affected by the presence of the droplet surface. A smaller fraction of the probe molecules is present in an aqueous environment where its properties depend on the particle size, suggesting some sort of interaction with the interface. A model for the distribution of PTMIO in C14 emulsions is presented in Figure 3.6 along with configuration of caseinate at the droplet interface. The organization of caseinate molecules on the droplet surface was sketched according to the description given by Leermakers et al. (1996), and assuming a monolayer coverage (2-3 mg / $m^2$) .The segments of caseinate was distributed as a dense (volume fraction is about 0.9) inner layer which is about 1 nm in thickness, and a diffuse outer layer (volume fraction is about 0.1)

which is about 4-5 nm in thickness, as measured by neutron scattering. However, dynamic light scattering measurements showed larger hydrodynamic layer thickness (about 10 nm) than the neutron scattering, since “hydrodynamic radius includes dangling segments at the very periphery of the adsorbed layer (i.e., long tails) where the local protein concentration is low” (Leermakers et al., 1996). I will consider the effects of crystallizing the droplets in the proceeding section.

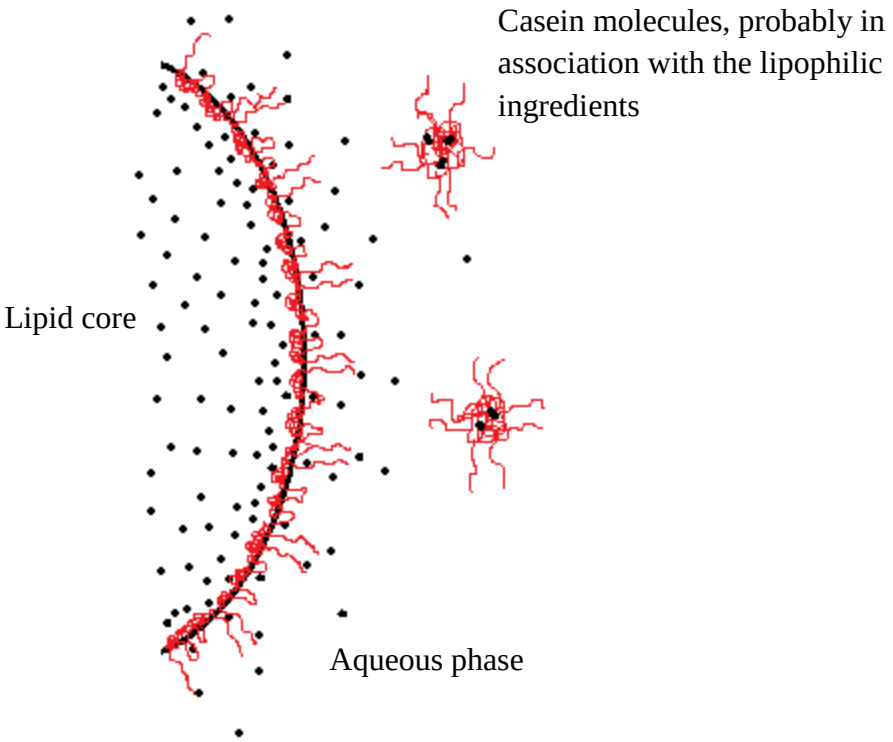


Figure 3.6. Hypothesized model for the distribution of PTMIO (~ 0.7 nm) across the C14 droplets stabilized with sodium-caseinate (the distribution of PTMIO is illustrated schematically as small black dots). The organization of caseinate molecules on the droplet surface was sketched according to the description given by Leermakers et al. (1996).

### 3.3.3 Probe behavior in SLN emulsions

The crystallization behavior of eicosane (m.p. 36.7 °C) in emulsions was investigated using microcalorimetry (Figure 3.7). The coarse ($d_{32}$ = 1.3 μm) eicosane droplets started to crystallize at ~24.0 °C (peak minimum 23.0 °C) and there was a second minor peak at 20.3 °C (Figure 3.7a). The fine ($d_{32}$ = 0.2 μm) eicosane droplets crystallized at a slightly lower temperature (23.4 °C onset, peak minimum 22.2 °C). The position of the minor secondary peak did not change with particle size (20.3 °C), but it was bigger for the fine droplets. The first, major exothermic peak can be attributed to the liquid-to-rotator transition, while the second, minor peak to a rotator-to-crystal transition (Gulseren and Coupland, 2008). The rotator phase is a metastable crystalline state observed in normal alkanes in which the molecules lack long-range order with respect to rotation about their long axes (Sirota, 1998; Sirota and Herhold, 1999). The presence of PTMIO did not affect the peak positions and crystallization behavior of eicosane droplets (Figure 3.7b).

Eicosane emulsions containing PTMIO were stored at 21.5 °C for either 5 or 24 h prior to EPR measurements, allowing the eicosane droplets to crystallize (similar results were seen for samples stored at 5 °C for 24 h) (Figure 3.8). There was no evidence of crystallization of the PMTIO itself, which would have been seen as a sharp decrease in the peak-to-peak height and loss in the signal intensity, as well as a distortion in line shape (Smith and Butler, 1976). However, the distribution of spin probe was affected by crystallization of the lipid.

a)

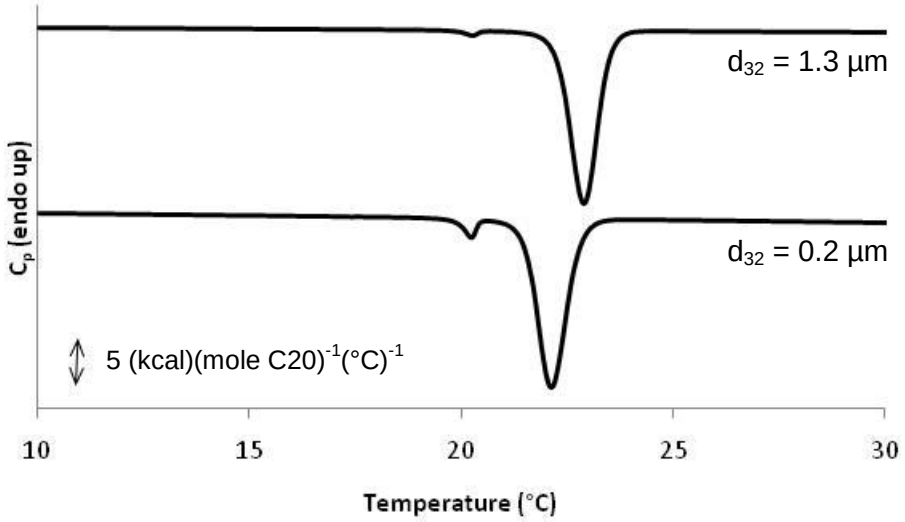


b)

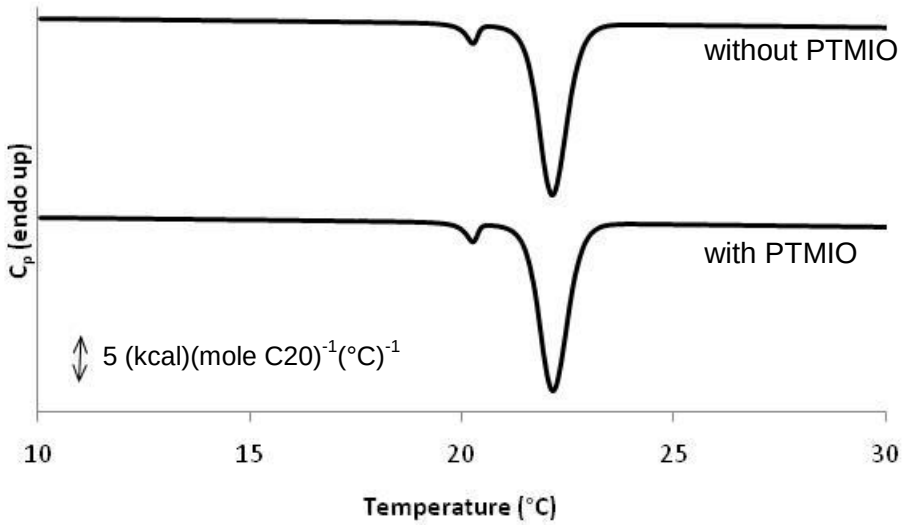


Figure 3.7. Cooling thermograms (at 12 °C / h) of (a) coarse ($d_{32}$ = 1.3µm) and fine ($d_{32}$ = 0.2 µm) eicosane emulsions; and (b) coarse ($d_{32}$ = 1.3µm) droplet eicosane emulsions with and without PTMIO.

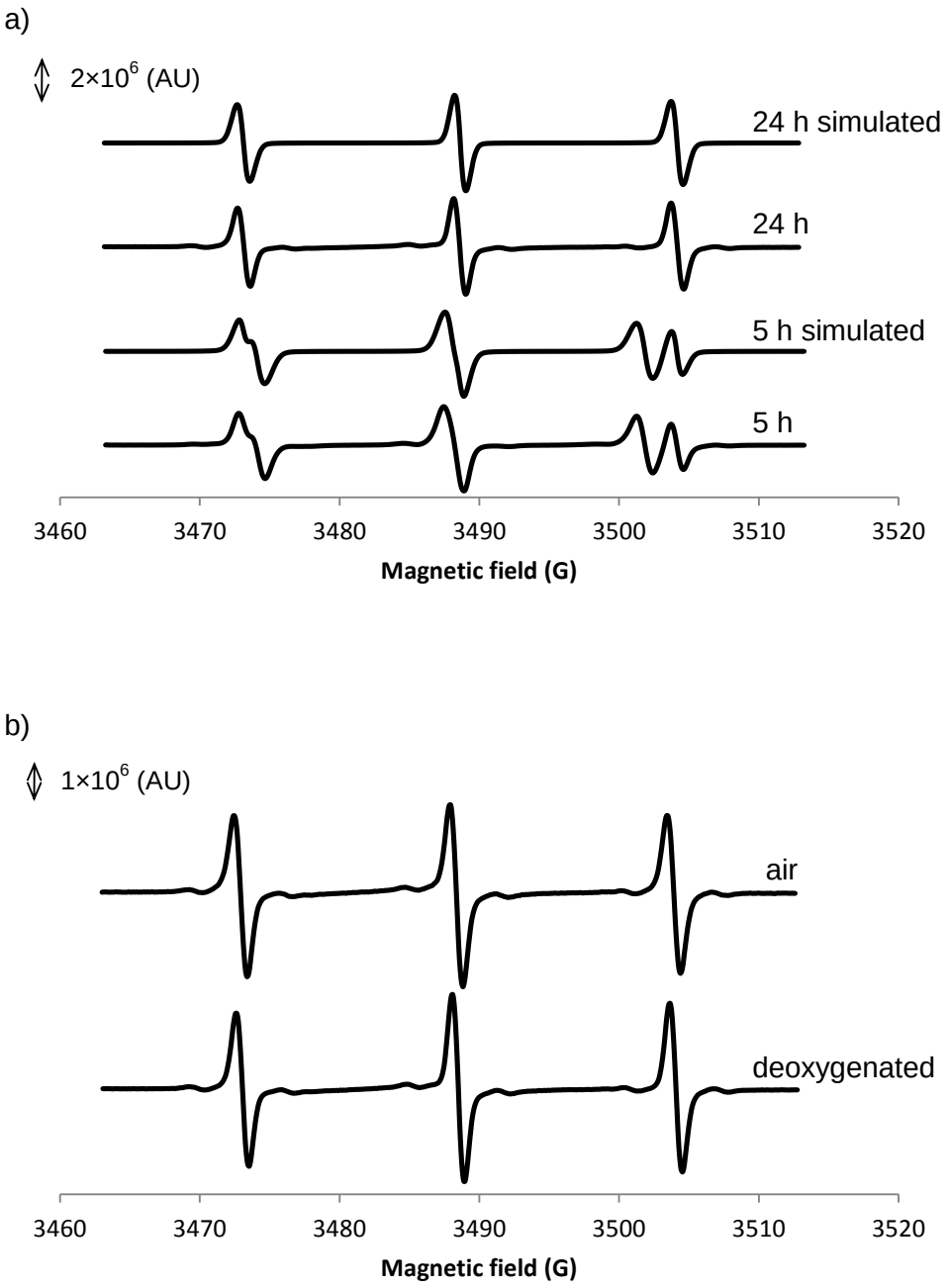


Figure 3.8. EPR spectra of PTMIO (200 μ*m*) in a10 wt% eicosane emulsion ($d_{32}$ = 1.3 μm). (a) After 5 h and 24 h storage at room temperature with simulated spectra, and (b) before and after deoxygenation of the 24 h stored sample.

There was still clear separation in the up-field hyperfine peak in eicosane droplets after 5 h storage (Figure 3.8a) similar to that seen for tetradecane droplets (Figure 3.4a) and consistent with some of the probe being present in the lipid environment and some in the aqueous environment. However, after 24 h of storage, a single high field hyperfine peak was observed that was consistent with the probe being present exclusively in the aqueous environment (i.e., similar peak position, peak properties unaffected by deoxygenation, Figure 3.8b). Moreover, after filtering out the crystalline droplets the intensity of the EPR signal from the aqueous filtrate was unchanged (Figure 3.9). The properties of the probes in the different environments were calculated by simulation of the spectra and deconvolution as described earlier (Tables 3.2). While there is no probe in the non-polar environment following 24 h storage, after 5 h storage 64% and 56% of the probe remains in the non-polar environment for fine and coarse droplet eicosane emulsions respectively (Table 3.2). This amount is less than the corresponding liquid droplets and indicates an intermediate state, which corresponds to partly crystalline droplets. While this observation is interesting, it is not a central focus of the present chapter and will be discussed further in Objective 2 (Chapter 4). Instead I will focus on our major observation; droplet crystallization excludes the spin probe from the droplets.

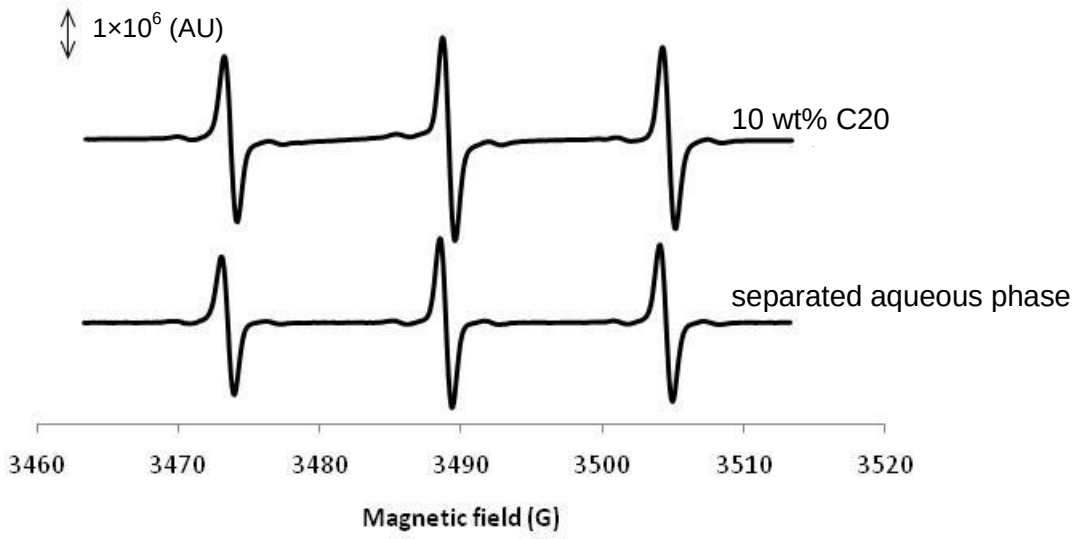


Figure 3.9. EPR spectra of PTMIO (200 μ*m*) in a10 wt% eicosane emulsion ($d_{32}$ = 0.2 μm) and in the aqueous phase after separation from the emulsion.

I can understand more about the changed environment of the probe by looking at the properties of the deconvoluted spectra. As there is no probe in the non-polar environment our discussion is focused exclusively on the signal from the polar environment. The hyperfine splitting constants of the probe in the aqueous environment did not change with droplet size in eicosane emulsions and are similar to values reported for the bulk aqueous phase. Droplet crystallization decreased the rotational correlation times and anisotropy compared to the values measured for the corresponding liquid droplets (Table 3.2). However, the rotational correlation times ($\tau_c$(B)) and probe anisotropy ($\tau_c$(B)/ $\tau_c$(C)) were still smaller for coarse eicosane emulsions than for fine eicosane emulsions (Table 3.2).

Presumably, droplet crystallization causes probe molecules to move out of the lipid environment into the aqueous environment where they are, on average, more affected by the presence of the surface due to an association between the probe and the aqueous portions of the interfacial protein. Ghosh et al. (2006, 2007) and Mikhaelev et al. (1989) previously showed that the crystallization of alkane droplets forced encapsulated lipophilic compounds out of the droplet core and to the droplet surface. Interestingly Jores et al. (2004) used electron microscopy to show the formation of liquid droplets on the surface of crystalline lipid particles (i.e., "nanospoons") that may correspond to the behavior seen in the present work. Ahlin et al. (2000b, 2003) argued that probe molecules could be trapped around the droplet surface but this finding may be specific to the aliphatic probes used and the presence of significant amounts of phospholipid. Arboleya et al. (2005) showed probe mobility decreased on droplet crystallization but provided no evidence for exclusion from the droplet. It may be the palm oil used in that study had enough residual liquid oil to solubilize the probe. Ghosh et al. (2007) showed the difference between liquid and solid mixed triacylglycerols was much less than the difference between solid and liquid pure alkanes and argued the presence of even a tiny fraction of liquid oil was sufficient to dominate the properties of the "SLN".

### 3.3.4 Chemical stability of PTMIO in emulsion based delivery systems

The EPR-active nitroxide spin probe can be reduced to its EPR-silent form by ascorbic acid but only if the spin probe is in a location where it can interact with aqueous species (Ahlin et al., 2003; Mikhalev, 1989). In the context of the analysis of the spectra discussed above, I propose that the probe molecules present in the aqueous environment (i.e., a high hyperfine splitting constant) will be vulnerable to chemical reduction. Thus, the reduction kinetics of the spin probe in the presence of an aqueous reducing agent can be used to provide supporting evidence of the location of the probe. The initial EPR signal intensity (i.e., before the addition of the iron/ascorbate blend) was higher in the coarse droplets than in the fine droplets (Figure 3.10). Presumably the higher pressure and temperature achieved during the preparation of the smaller droplets led to greater losses of the probe prior to the experiment. In all cases, the signal intensity decreased exponentially upon addition of the iron/ascorbate blend. The loss of the peak-to-peak height can be used to evaluate the change in the signal intensity as the line shape is not changing with reduction of the spin probe (as discussed later). An apparent first order rate constant ($k_{apparent}$) was calculated for each sample during the initial linear portion (i.e., up to $1/4^{th}$ of the initial peak-to-peak height) of the $\ln(I/I_0)$ vs. time plot (Table 3.3).

a)

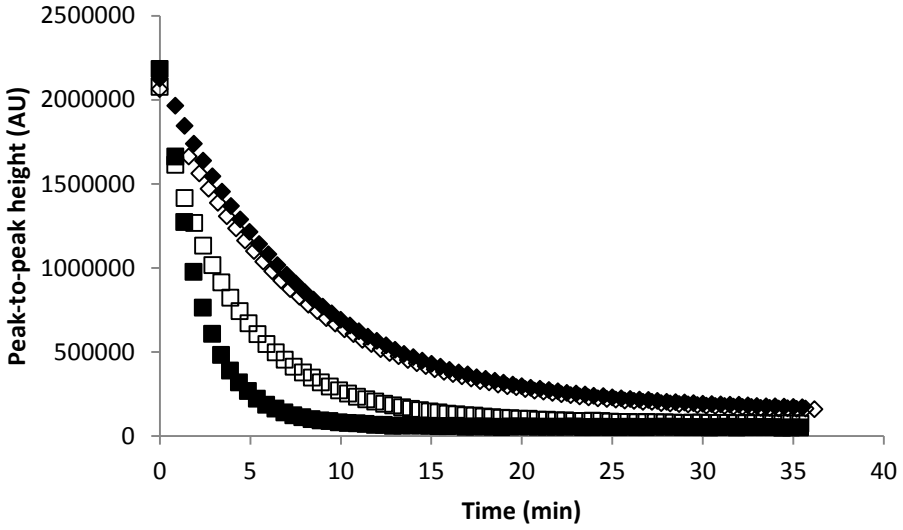


b)

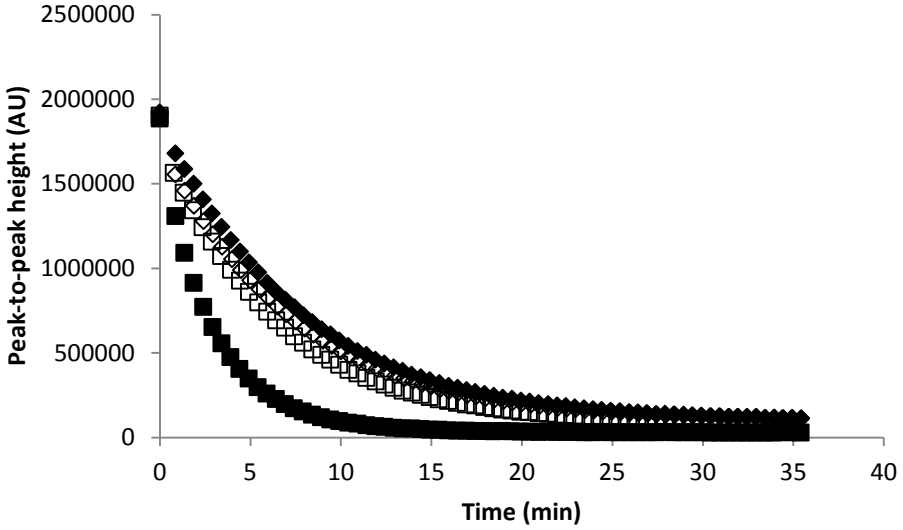


Figure 3.10. Degradation kinetics of PTMIO (200 μ*m* initial concentration) in (a) coarse ($d_{32}$ = 1.3 μm) and (b) fine ($d_{32}$ = 0.2 μm) tetradecane emulsions stored for ◊ 5 h and ♦ 24 h, and eicosane emulsions stored for □ 5 h and ■ 24 h following addition of iron/ascorbate blend.

Table 3.3. Apparent first order rate constants ($k_{apparent}$) ($s^{-1}$) for the degradation of PTMIO in emulsions and the calculated percentage of the probe in the aqueous environment (α). The different letters show significant difference of a parameter (i.e., in a column) between two samples for a given time, and different Roman numerals show significant difference for the same sample and parameter at different time (α = 0.05).

| | 5 h | | 24 h | |
|---|---|---|---|---|
| Sample ($d_{32}$) | $k_{apparent}$ ($s^{-1}$) | α (%) | $k_{apparent}$ ($s^{-1}$) | α (%) |
| C14 (0.2 um) | $0.122 \pm 0.004^{a,I}$ | $24.62 \pm 0.75^{a,I}$ | $0.118 \pm 0.002^{a,I}$ | $23.87 \pm 0.41^{a,I}$ |
| C14 (0.6 um) | $0.118 \pm 0.002^{a,I}$ | $23.80 \pm 0.45^{a,I}$ | $0.117 \pm 0.003^{ab,I}$ | $23.47 \pm 0.34^{ab,I}$ |
| C14 (1.3 um) | $0.111 \pm 0.002^{b,I}$ | $22.41 \pm 0.32^{b,I}$ | $0.111 \pm 0.002^{b,I}$ | $22.26 \pm 0.35^{b,I}$ |
| C20 (0.2 um) | $0.141 \pm 0.004^{c,I}$ | $28.37 \pm 0.90^{c,I}$ | $0.332 \pm 0.004^{c,II}$ | $66.84 \pm 1.04^{c,II}$ |
| C20 (1.3 um) | $0.195 \pm 0.012^{d,I}$ | $39.33 \pm 2.50^{d,I}$ | $0.497 \pm 0.005^{d,II}$ | 100 |

The degradation kinetics of PTMIO in liquid oil emulsions was the same after either 5 or 24 h storage (Table 3.3). This is to be expected, as the parameters describing the properties of the probe did not change over this time (Table 3.2). The degradation rates of PTMIO in solid lipid emulsions (24 h storage) were higher than the degradation rates in tetradecane emulsions (Figure 3.10, Table 3.3). This is expected, as the EPR spectra suggest the probe has been expelled from the lipid droplets into aqueous environment (Figure 3.8, Table 3.2). More surprisingly, the degradation rate was greater in the coarse eicosane emulsions ($k_{apparent}$ ~0.50 $s^{-1}$) than the degradation rate in the fine eicosane droplet emulsions ($k_{apparent}$ ~ 0.33 $s^{-1}$) after 24 h storage (Table 3.3), this despite the fact that the spectra of both coarse and fine emulsions show the probe is present exclusively in the aqueous environment (Table 3.2). There must be a role of the droplet surface in controlling reaction rate. In the next section, I develop a more quantitative model to analyze these effects.

As PTMIO has some aqueous solubility and ascorbate has virtually no lipid solubility, their reaction must occur in an aqueous environment. In this case, the rate of degradation could be limited either by the rate of chemical reaction or the rate of diffusion of the spin probe from lipid droplets to the aqueous phase (as ascorbate was present at molar excess, it is unlikely to be limiting). The kinetics of PTMIO diffusion during reduction were evaluated by monitoring

the changes in the shape of the EPR pattern during its reduction (Figure 3.11a). Although the signal intensity decreases with reaction time, the ratio of peaks corresponding to the aqueous and lipid phases is unchanged (Figure 3.11b). This suggests that the diffusion of probe from the lipid droplet to the aqueous environment (where it is reduced) is much faster than the rate of reduction. The rate of reduction therefore depends on the concentration of probe in the aqueous environment.

a)

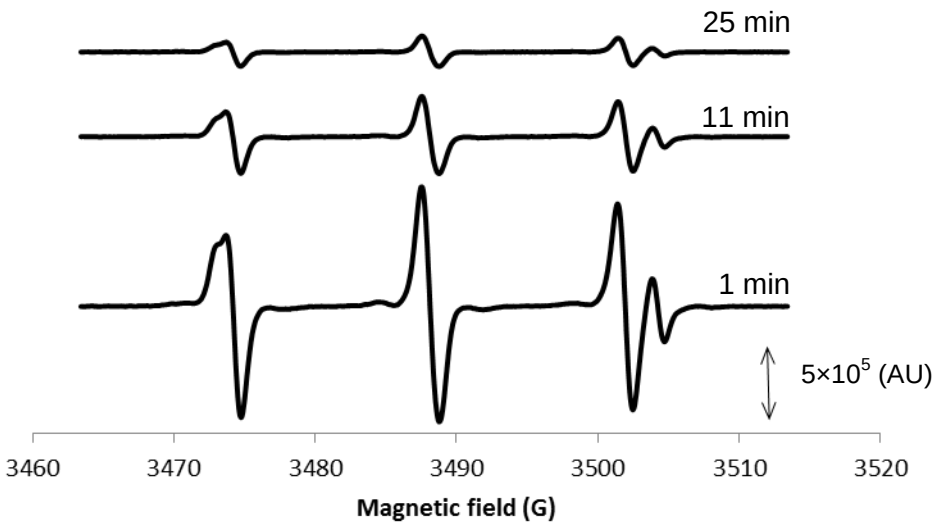


b)

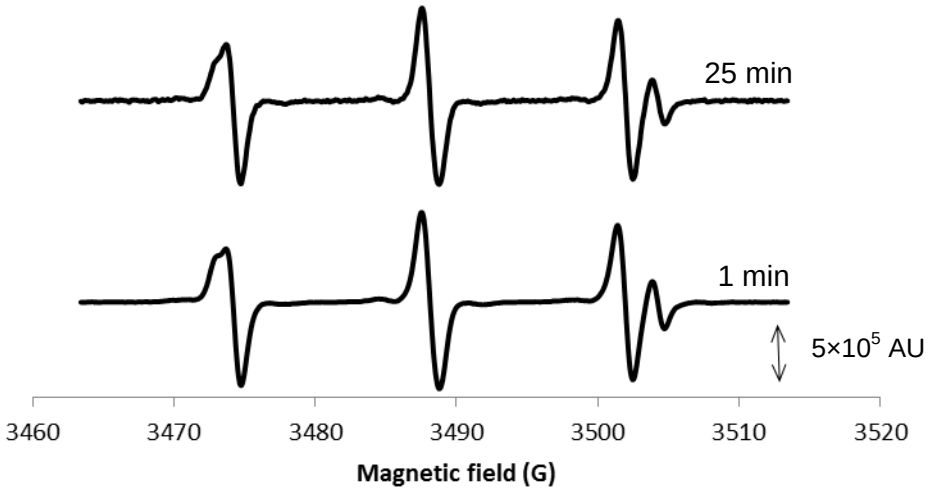


Figure 3.11. (a) The change in EPR spectra during degradation of PTMIO in a 10 wt% tetradecane emulsion ($d_{32}$ = 1.3 μm), and (b) EPR spectra at 25 min scaled so the center peak has the same intensity as that at 1 min.

As ascorbate is present to excess, we can assume the reaction is pseudo-first order with respect to PTMIO and the rate of reaction can be written as:

$$\frac{dC_T}{dt} = k(C_T\alpha) = (k\alpha)C_T \qquad [3.13]$$

$$\alpha = \frac{C_{aq}}{C_T} \qquad [3.14]$$

where $C_T$ is the total PTMIO concentration, t is time, k is reaction rate constant, $C_{aq}$ is the PTMIO concentration in the aqueous environment, and α is a measure of the measure of the proportion of the probe available for reaction. I tentatively hypothesize that α is equivalent to the partition coefficient calculated from deconvolution of the spectra.

Assuming probe concentration is proportional to peak-to-peak height, integration of Equation 3.13 gives:

$$\ln\frac{C_T}{C_{T0}} = \ln\frac{I}{I_0} = -(k\alpha)t \qquad [3.15]$$

where $C_{T0}$ is the initial PTMIO concentration, and I and $I_0$ are the peak-to-peak heights at time t and 0, respectively. The kα term is equivalent to the apparent rate constant ($k_{apparent}$, Table 3.3).

The fastest apparent rate constant was measured in eicosane droplets after 24 h storage. I therefore assumed for this sample all of the spin probe was in the aqueous environment and hence α = 1, and k = 0.497 $s^{-1}$. If I assume k is constant for all systems, I can then calculate α for the other samples. In general the estimates of reactive spin probe fraction (α) and partitioning calculated from the spectra were in good agreement. For example, the amount of reactive PTMIO (α) was found to be ~22 % for coarse tetradecane emulsions of total from chemical degradation rate analysis (Table 3.3), while a similar value (~23%) was calculated

from the spectra (Table 3.2). The agreement was weaker for fine emulsions, probably due to the probe in the aqueous phase being affected by the droplet surface (Table 3.2). The deviation between methods was greatest for the fine eicosane emulsion where the probe in the aqueous phase was highly affected by the droplet surface.

### 3.4 Conclusion

The EPR method used in the present work offers direct information on structure and function of a hydrophobic solute in EBDS. The distribution of the probe is inferred from analysis of the spectra and the chemical stability by measurement of reduction kinetics. A disadvantage of this method is that it only works for spin probes so there may be a challenge in applying the findings to real drugs or phytochemicals. An advantage is that it is completely non-destructive so the results are measurements of actual emulsions structure and properties. It is also interesting to note the strong effect of oxygen on lipid-phase signal. It may be possible to exploit this finding to study oxygen distribution in complex materials.

The model proposed for PTMIO distribution in solid and liquid droplets is given in Figure 3.12. In the liquid oil emulsion the bulk of the probe is in the droplets although a far greater proportion is present in the aqueous environment than would be expected from bulk partitioning experiments. This additional probe is affected by the presence of the surface and is presumably associated with the aqueous portions of the caseinate. Droplet solidification is unexpectedly slow, but results in complete exclusion of the probe from the non-polar environment and apparent accumulation at the droplet surface.

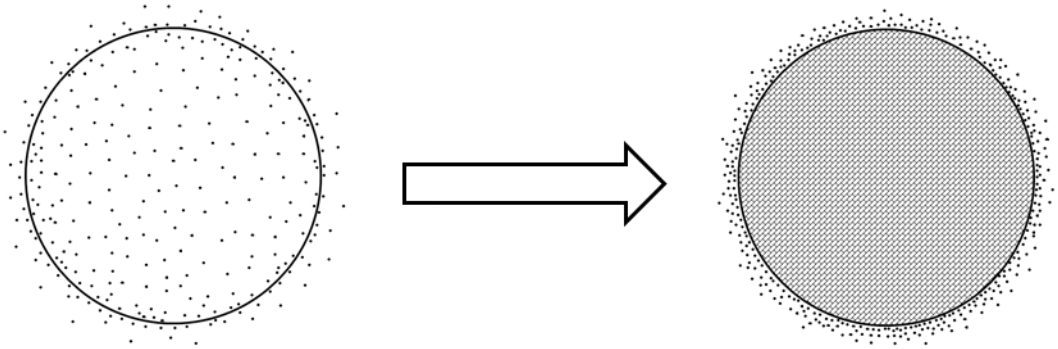


Figure 3.12. Proposed model for the distribution of the PTMIO in emulsions and solid lipid nanoparticles.

# Chapter 4

## 4. Effects of Liquid Oil Fraction and Storage on Distribution and Reactivity of a Hydrophobic Solute in Nanostructured Lipid Carriers (NLC)

### 4.1 Introduction

As discussed in Chapter 3, oil-in-water emulsions can be used as delivery systems for hydrophobic solutes to improve their chemical stability during storage or to modify their release profile at the time of use. In brief, an emulsion system can provide at least three environments for an added ingredient: the continuous aqueous phase, the lipid core of the droplets, and an amphiphilic surface layer. Lipophilic ingredients in the lipid droplets are protected from reaction with aqueous compounds (e.g., acids, transition metals) and their bioavailability may be enhanced (Acosta, 2009). Furthermore, the aqueous continuous phase allows EBDS to be readily miscible with a wide range of products.

The distribution characteristics and release profiles of ingredients can be controlled by modifying the composition and microstructure of EBDS. McClements et al. (2007) offered solid lipid nanoparticles (SLN) as one of five categories of EBDS (i.e., conventional emulsions, multiple emulsions, multilayer emulsions, filled hydrogel emulsions, SLN emulsions) suitable for delivery of lipophilic ingredients. In this work, I am concerned with SLN prepared by crystallizing the lipid droplets in fine emulsions.

Some early studies suggested that if solute molecules can be entrapped within the lipid crystal matrix of SLN, they would be protected from chemical degradation and their release rates controlled (Bunjes et al., 2001; Muhlen et al., 1998; Muller et al., 2000). However recent studies have shown that droplet crystallization can result in expulsion of lipophilic molecules from lipid droplets either into the aqueous phase or to the droplet surface. This model is consistent with the findings reported in Chapter 3 where I considered the differences between coarse and fine as well as liquid and solid emulsions. In liquid lipid emulsions, most of the hydrophobic molecules partitioned into the lipid droplets, and the distribution of the spin

probe was not affected by storage. On the other hand for SLN emulsions there was less probe in the droplets after 5 h and effectively none after 24 h. While the emphasis in Chapter 3 was on the behavior of probe in samples stored for 24 h, the focus of the present study will be the possible mechanisms for the differences on storage. I will also consider the effect of the presence of small amounts of liquid lipid in the SLN.

Emulsion droplets with mixed solid and liquid lipids are known as nano-structured lipid carriers, (NLC, Muller et al., 2002) and they have been suggested as a means to modify the crystalline structure of SLN and control the distribution of the lipophilic ingredients. For example, the entrapment efficiency for the drug clotrimazole was much higher in NLC formulated using blends of liquid (caprylic/capric acid triglyceride) and solids lipids (palmitic acid triglyceride) than that in SLN of pure solid lipid (Souto et al., 2004). Similar results have been reported by other workers (Jenning et al. 2000a,b; Jores et al., 2004). However, widely varying structural models were proposed for the distribution of the liquid lipid fraction as well as the lipophilic ingredient. For example, Jenning et al. (2000a, b) manufactured NLCs from binary mixtures of solid (behenic acid glycerides) and liquid (caprylic/capric acid glycerides) lipids and showed that a liquid lipid phase present at low concentrations (8-16%) was evenly distributed within the crystal matrix. In contrast, Jores et al. (2004) produced NLCs from similar lipids and observed irregular shapes and uneven distribution of the oil (i.e. on the surface of the solid portion). The EPR methods developed in Chapter 3 offer the possibility to directly measure the distribution and chemical reactivity of hydrophobic solutes in NLC and can provide a better physical model of their structure.

The objective of this work is to investigate the effect of addition of small amounts of tetradecane into eicosane SLN on distribution kinetics of a selected hydrophobic ingredient, PTMIO. Tetradecane was selected as it is a smaller molecule than eicosane, and so it is unlikely that it will be incorporated within the eicosane crystals. I hypothesize that the presence of liquid lipid will limit lipid crystallization and thus improve the retention of the spin probe within the droplet. I also consider the effects of sample storage on the properties of NLC.

## 4.2 Materials and Methods

### 4.2.1 Materials

The free radical spin probe 4-phenyl-2,2,5,5-tetramethyl-3-imidazoline-1-oxyl nitroxide (PTMIO, Figure 3.1a) was used as a model lipophilic ingredient (Enzo Life Sciences, Plymouth Meeting, PA, USA). Sodium caseinate (from bovine milk), n-eicosane, sodium L-ascorbate were obtained from the Sigma Chemical Company (St. Louis, MO, USA), n-tetradecane was obtained from Fisher Scientific (Pittsburgh, PA, USA), and ferric chloride 6-hydrate was obtained from Mallinckrodt Chemicals (Phillipsburg, NJ, USA). All other materials were reagent grade and were used as received.

### 4.2.2 Preparation of EBDS containing the lipophilic ingredient

Emulsions were prepared using the hot-homogenization technique described in Chapter 3. In brief, PTMIO was dissolved in hot (50 °C) blends of C14:C20, at weight ratios of 100:0 (100%C14), 10:90 (90%C20), and 1:100 (99%C20), and 0:100 (100%C20). An emulsion premix ($d_{32}$ ~40-50 μm) was prepared by mixing the lipid (10 wt%) with Na-caseinate solution (1 wt% in pH 7, 100 mM phosphate buffer) using a high-speed blender (Brinkmann Polytron, Brinkmann Instruments Inc., Westbury, NY). The emulsion premix was then passed through a microfluidizer (M-110Y Microfluidizer, Microfluidics, Newton, MA) at 65-70 °C (5 passes at 1200 bar). Final emulsions ($d_{32}$ ~0.2 μm) containing 200 μ*m* PTMIO were stored at either 21.5 ± 0.5 ºC (i.e., room temperature) or 5 ºC (i.e., refrigerator temperature). The particle size distribution of the emulsions was measured by static light scattering (Horiba LA-920, Irvine, CA). There was no change in particle size distribution over the course of the experiment.

4.2.3 EPR analysis

EPR spectra of emulsions were measured using a Bruker eScanR spectrometer (Bruker-Biospin, Billerica, MA) operating in X-band, as described in Chapter 3. In brief, all samples were deoxygenated by passing humidified nitrogen gas (3 sL/min) through the headspace of samples for about 90 min prior to EPR analysis (Figure 3.1b). Then aliquots of samples were loaded into a close-packed 19-bore quartz capillary measurement cell (AquaX, Bruker-Biospin, Billerica, MA) which had been previously flushed with $N_2$ gas, and EPR spectra was recorded (at 21.5 ± 0.5°C) using the following measurement parameters: microwave frequency, 9.775 GHz; modulation frequency, 86.0 kHz; microwave power, 18.97 mW; scan range, 50 G; modulation amplitude, 0.98; sweep time, 2.62 sec; time constant, 5.12 msec; conversion time, 5.12 msec. To study the chemical reduction of PTMIO, small volumes of sodium ascorbate solution and ferric chloride solution (final concentration 1 m*m* and 10 μ*m*, respectively) were added to the samples under a $N_2$ blanket and EPR spectra were recorded at intervals.

The experimental spectra were simulated using theWinSim2002 software (version 0.98, National Institute of Environmental Health Sciences, National Institutes of Health, USA) assuming 2 populations of PTMIO in environments with different polarities. The parameters describing the spectra (i.e., line widths, hyperfine splitting constants, g-values and shifts, and relative intensities, and Lorentzian-Gaussian line width ratio) of the probe in each phase were determined using a Simplex algorithm to provide a best fit. The correlation coefficient was greater than 0.995 for all simulations.

The significance of the parameters describing the EPR spectra was discussed in Chapter 3, and they are summarized as follows. The rotational correlation times (i.e., measurements of the inverse of probe mobility) and signal intensities (i.e., a measurement of the amount of spin probe in a given environment) from each phase were calculated from line widths (i.e., the distance between the maxima and minima of the first derivative absorption curve) and from a double integration of the signal from the corresponding phase, respectively. The g-factor (i.e., center peak position) and hyperfine splitting constants (i.e., positions of the hyperfine peaks)

are determined by the chemical nature of the radical and the polarity of its environment. The ratio of two rotational correlation times, $\tau_c(B)/\tau_c(C)$, can be used as a measure of probe anisotropy and is unity for isotropic motion.

### 4.2.4 DSC analysis

The crystallization and melting behavior of emulsion droplets were investigated by differential scanning calorimetry (VP-DSC, Microcal, Northampton, MA). The emulsion was diluted to 0.1 wt% lipid in phosphate buffer (pH 7, 0.1 m*m*) prior to analysis. Aliquots (0.513 mL) were loaded into the instrument, and then either cooled from 40 to 10 °C or heated from 10 to 40 °C at 12 °C/h. Heat flux was measured relative to water and any possible error resulting from Na-caseinate dissolved in aqueous phase was corrected by similar measurements using 1 wt% Na-caseinate solution. DSC thermograms are reported normalized to the molar concentration of eicosane present in each sample.

### 4.2.5 Statistics

The significance of difference between samples were evaluated using t-test for a pair-wise comparison of two samples at $\alpha = 0.05$.

## 4.3 Results and Discussion

### 4.3.1 Analysis of the EPR spectra

Emulsions containing 200 μ*m* were analyzed after 5 h and 24 h storage at room temperature (21.5 °C) and 24 h storage at a refrigerated temperature (5 °C) (Figure 4.1). All analyses were performed for deoxygenated samples since the presence of oxygen affects the EPR spectrum significantly, especially in non-polar environment (see discussion in Chapter 3). The EPR spectra of samples stored at room temperature are shown in Figures 4.1a and 4.1b, and EPR spectra of refrigerated samples are shown in Figure 4.1c. The spectra were similar to those seen in Chapter 3. The PTMIO retention in the lipid phase apparently increased with the

proportion of C14 in the droplets, but decreased with increasing storage time, notably at 5 °C. A more quantitative analysis was obtained by simulation and deconvolution of the spectra.

The properties of the spin probe in each environment were determined by deconvoluting the simulated spectra into separate EPR patterns for each of the two phases (Table 4.1). This approach to simulation is slightly different from that used in Chapter 3. In the present study the spectra of the 24 h stored C20 emulsions were simulated assuming two populations of probe, while in Chapter 3 the same sample was modeled assuming one population of the spin probe. The amount of non-aqueous probe identified by the two-population approach was very low (<0.5%, see below for further discussion) and did not affect the conclusions from Chapter 3. As the focus of this work is the structure of NLC, only the properties of the probe in the non-polar environment will be discussed. However, the properties of the aqueous part of the EPR signal were discussed in Chapter 3, and the data reported here for samples containing intermediate C14 concentrations followed similar trends.

In the liquid C14 emulsions (100%C14) the majority of the spin probe was in the lipid droplets (~70%) where it was highly mobile ($\tau_c$(B) ~0.02 ns), and the spectra were not affected by storage time (Table 4.1, Figure 4.2). In the lipid droplets containing C20 after 5 h storage, the amount of PTMIO decreased slightly with the proportion of C20, but the shape of the spectra (i.e., mobility, anisotropy, hyperfine splitting constant) remained unchanged. However after 24 h storage the amount of PTMIO in the lipid droplets containing C20 further decreased significantly, accompanied with a large increase in the rotational correlation times (as well as in the anisotropy term). The magnitude of the change on storage increased with the fraction of C20 in the droplets. However, $a_N$ did not change on storage with the exception of 100%C20, in which a very small spin probe population (< 0.5%) was characterized in an environment of intermediate polarity ($a_N$ ~14.3 G). Similar samples were also investigated at 5 °C.

As noted in Chapter 3, the EPR spectra of the 100%C14 and 100%C20 emulsions stored at refrigerated temperature for 24 h were the same as samples stored at room temperature for 24 h (Table 4.1, Figure 4.2). In emulsions of binary C14 and C20 mixtures, both the amount of

PTMIO in the droplets and $\tau_c$(B) of that fraction decreased with increasing proportion of C20, and was less for samples stored at lower temperatures. A small population of spin probe in an environment of intermediate polarity ($a_N$ ~14 G) was detected in both 99%C20 (3%, $a_N$ ~14.0 G) and 100%C20 (<0.5%, $a_N$ ~14.3 G) emulsions stored for 24 h at refrigerated temperature, similar to that seen in only the 100%C20 emulsion stored for 24 h at room temperature. The hyperfine splitting constant in the 90%C20 emulsion was similar to that in 100%C14 and unaffected by storage temperature.

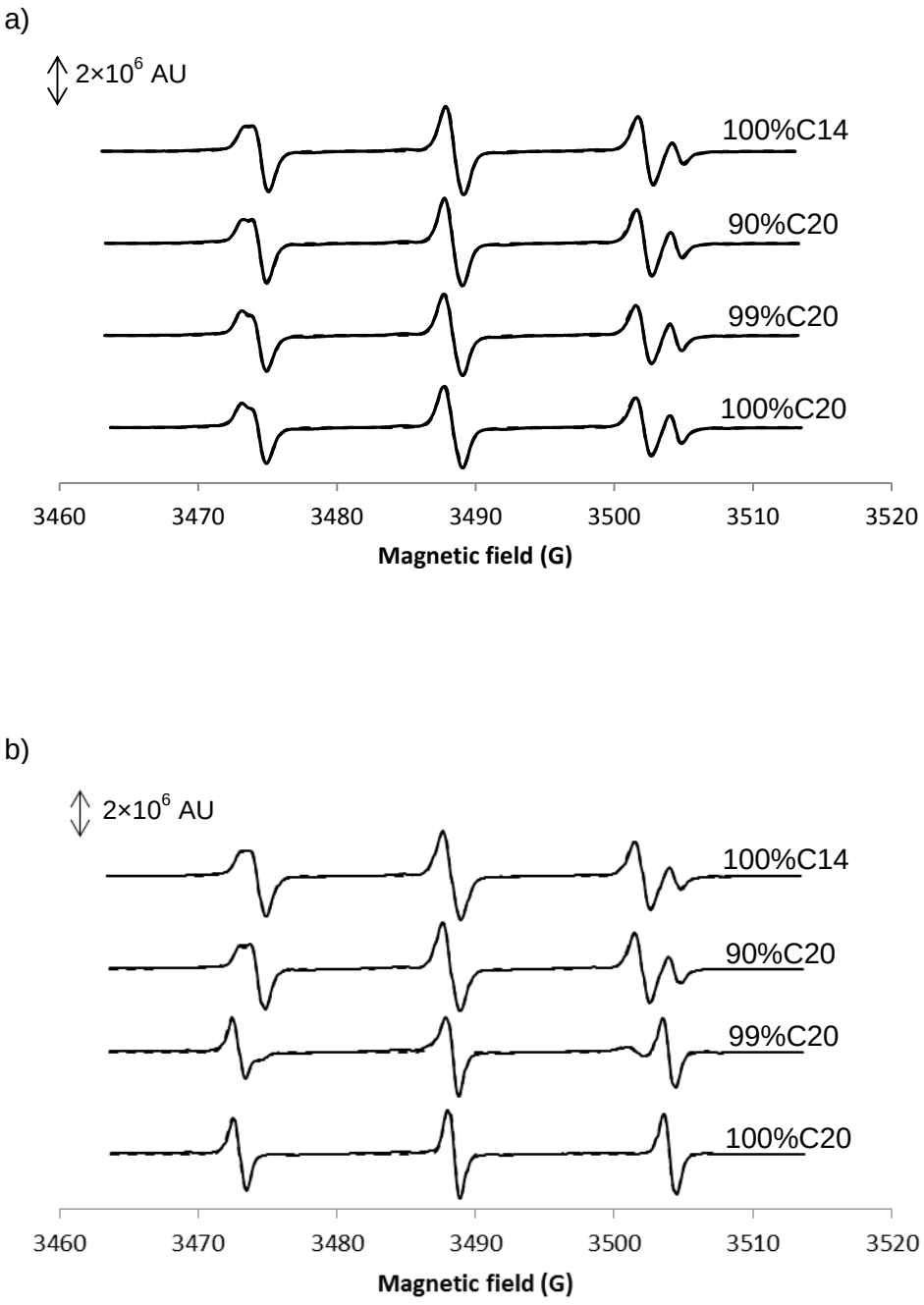


Figure 4.1. EPR patterns of PTMIO (200 μ*m*) in emulsions ($d_{32}$ = 0.2 μm) of 10 wt% eicosane (C20) and tetradecane (C14) mixtures after (a) 5 h storage at 21.5 °C, (b) 24 h storage at 21.5 °C, and (c) 24 h storage at 5 °C. The simulated spectra are shown as the broken line on top of the raw spectra shown as solid lines.

c)

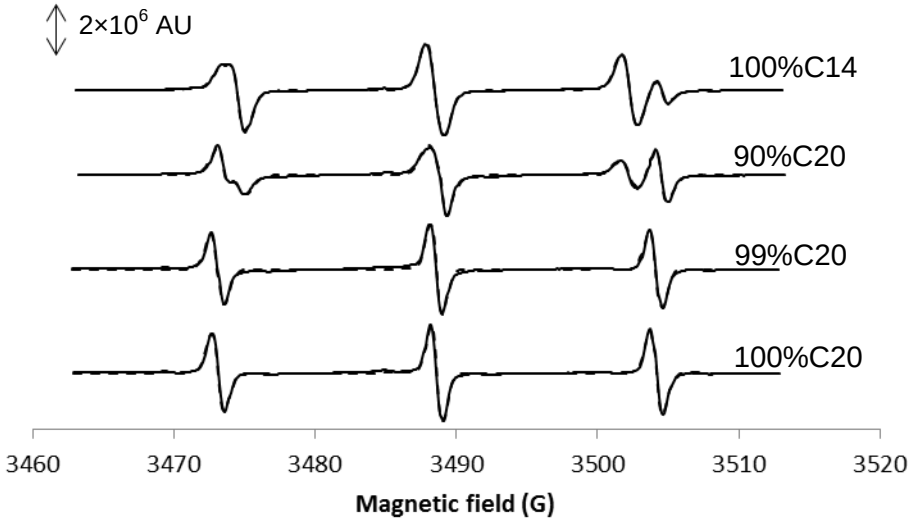


Figure 4.1. (Continued).

Table 4.1. Parameters describing the deconvoluted EPR spectra of PTMIO in emulsions. The different letters show significant difference of a parameter (i.e., in a column) between two samples for a given storage condition, and different Roman numerals show significant difference for the same sample and parameter at different time ($\alpha = 0.05$).

| | Sample | Aqueous fraction (%) | Properties of the probe in the aqueous environment | | | Properties of the probe in the lipid environment | | |
|---|---|---|---|---|---|---|---|---|
| | | | $\tau_c(B) \times 10^{11}$ (sec) | $\tau_c(B)/\tau_c(C)$ | $a_N$ (G) | $\tau_c(B) \times 10^{11}$ (sec) | $\tau_c(B)/\tau_c(C)$ | $a_N$ (G) |
| 5 h (21.5 °C) | 100%C14 | $29.81 \pm 1.13^{a,I}$ | $5.09 \pm 0.43^{a,I}$ | $3.71 \pm 0.43^{a,I}$ | $15.499 \pm 0.004^{a,I}$ | $2.21 \pm 0.20^{a,I}$ | $1.15 \pm 0.12^{a,I}$ | $13.854 \pm 0.003^{a,I}$ |
| | 90%C20 | $33.50 \pm 0.71^{b,I}$ | $5.76 \pm 0.31^{ab,I}$ | $5.03 \pm 0.62^{b,I}$ | $15.501 \pm 0.006^{a,I}$ | $2.47 \pm 0.43^{a,I}$ | $1.22 \pm 0.25^{a,I}$ | $13.854 \pm 0.005^{a,I}$ |
| | 99%C20 | $34.99 \pm 1.33^{bc,I}$ | $6.51 \pm 0.51^{bc,I}$ | $6.48 \pm 1.11^{b,I}$ | $15.498 \pm 0.006^{a,I}$ | $2.46 \pm 0.62^{a,I}$ | $1.21 \pm 0.30^{a,I}$ | $13.854 \pm 0.003^{a,I}$ |
| | 100%C20 | $35.64 \pm 0.73^{c,I}$ | $7.54 \pm 0.63^{c,I}$ | $5.36 \pm 1.14^{ab,I}$ | $15.496 \pm 0.006^{a,I}$ | $2.64 \pm 0.19^{a,I}$ | $1.25 \pm 0.11^{a,I}$ | $13.853 \pm 0.003^{a,I}$ |
| 24 h (21.5 °C) | 100%C14 | $29.88 \pm 1.69^{a,I}$ | $5.42 \pm 0.66^{a,I}$ | $3.99 \pm 1.25^{a,I}$ | $15.502 \pm 0.005^{a,I}$ | $1.99 \pm 0.32^{a,I}$ | $1.08 \pm 0.19^{a,I}$ | $13.850 \pm 0.004^{a,I}$ |
| | 90%C20 | $37.48 \pm 3.50^{b,II}$ | $4.91 \pm 0.35^{a,II}$ | $5.80 \pm 1.81^{a,I}$ | $15.503 \pm 0.011^{ab,I}$ | $2.05 \pm 0.43^{a,I}$ | $1.07 \pm 0.27^{a,I}$ | $13.855 \pm 0.004^{a,I}$ |
| | 99%C20 | $66.06 \pm 4.53^{c,II}$ | $3.04 \pm 0.09^{b,II}$ | $2.94 \pm 0.63^{a,II}$ | $15.486 \pm 0.007^{bc,I,II}$ | $14.53 \pm 0.91^{b,II}$ | $1.89 \pm 0.69^{a,I}$ | $13.851 \pm 0.011^{a,I}$ |
| | 100%C20 | > 99.5 | $2.73 \pm 0.46^{b,II}$ | $1.49 \pm 0.29^{b,II}$ | $15.473 \pm 0.006^{c,II}$ | $68.16 \pm 1.98^{c,II}$ | $3.43 \pm 0.14^{b,II}$ | $14.319 \pm 0.032^{b,II}$ |
| 24 h (5 °C) | 100%C14 | $29.86 \pm 0.98^{a,I}$ | $5.31 \pm 0.41^{a,I}$ | $3.88 \pm 0.58^{a,I}$ | $15.500 \pm 0.004^{a,I}$ | $2.17 \pm 0.30^{a,I}$ | $1.12 \pm 0.19^{a,I}$ | $13.850 \pm 0.006^{a,I}$ |
| | 90%C20 | $48.83 \pm 1.25^{b,III}$ | $2.94 \pm 0.34^{b,III}$ | $2.51 \pm 0.40^{b,II}$ | $15.490 \pm 0.005^{a,I}$ | $11.92 \pm 1.11^{b,II}$ | $2.60 \pm 0.25^{b,II}$ | $13.847 \pm 0.009^{a,I}$ |
| | 99%C20 | $97.10 \pm 0.39^{c,III}$ | $2.69 \pm 0.46^{b,II}$ | $1.49 \pm 0.31^{c,III}$ | $15.474 \pm 0.004^{b,II}$ | $65.67 \pm 2.47^{c,III}$ | $4.59 \pm 0.73^{c,II}$ | $13.962 \pm 0.031^{b,II}$ |
| | 100%C20 | > 99.5 | $2.55 \pm 0.36^{b,II}$ | $1.32 \pm 0.19^{c,II}$ | $15.473 \pm 0.005^{b,II}$ | $76.19 \pm 4.69^{d,II}$ | $17.06 \pm 2.57^{d,III}$ | $14.277 \pm 0.034^{c,II}$ |

a)

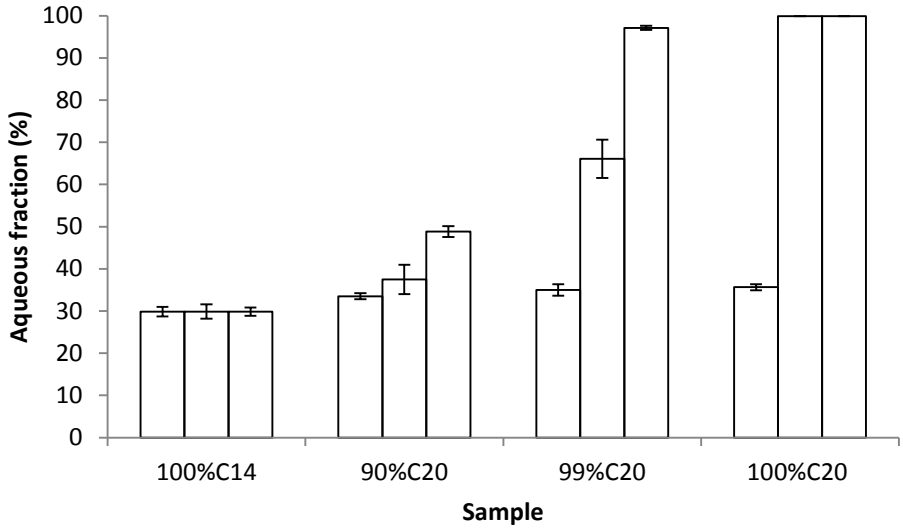


b)

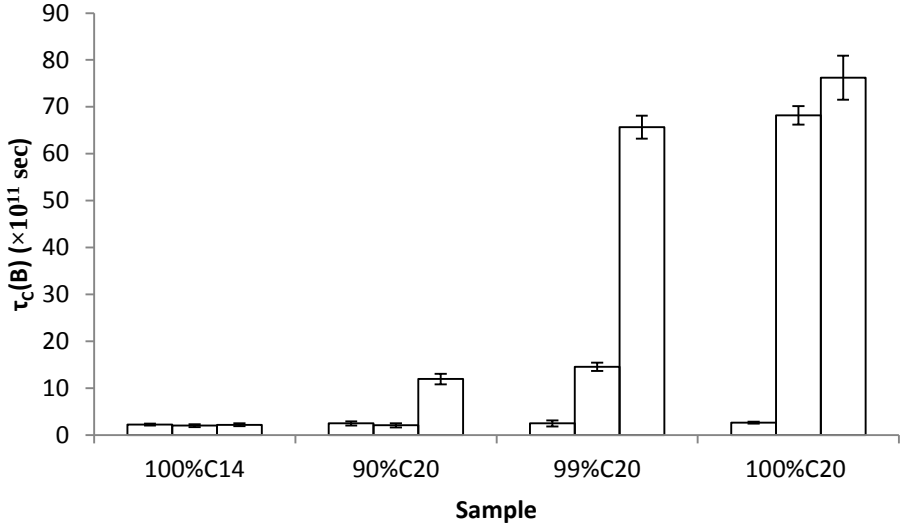


Figure 4.2. (a) Aqueous phase fraction (%) and (b) lipid phase rotational correlation time ($\tau_C$(B)) of PTMIO in emulsions of ($d_{32}$ = 0.2 μm) of 10 wt% eicosane (C20) and tetradecane (C14) mixtures as a function of storage time. In a sample: The first, second, and third bars show samples stored 5 h at 21.5 °C, 24 h at 21.5 °C, and 24 h at 5 °C, respectively. Error bars show standard deviation.

### 4.3.2 Physical model for NLC

As shown in Chapter 3, liquid lipid can dissolve large amounts of hydrophobic spin probe but droplet crystallization results in expulsion of the spin probe to the aqueous phase and the droplet surface. In order to modify this model to account for the effects of liquid oil and storage temperature on the properties of NLC I must consider three points: (i) Na-caseinate stabilized eicosane emulsions are believed to crystallize into a single crystal via homogeneous nucleation followed by a rapid crystal growth; i.e., there is no surface heterogeneous nucleation when Na-caseinate is used as an emulsifier (Coupland, 2002; Gulseren and Coupland, 2007; Palanuwech and Coupland, 2003; Ueno et al., 2003). (ii) EPR spectra showed that the probe neither precipitates nor forms a solid solution in the crystalline lipid matrix. (iii) Increases in $a_N$ and $\tau_c(B)$ with decreasing liquid lipid fraction suggest that the liquid fraction (carrying the spin probe) in the droplets is in a more polar environment and at the same time less mobile.

As droplet crystallization is not initiated at the surface (i.e., no surface heterogeneous nucleation) it must occur within the lipid core and progress towards the surface. Moreover, as the droplets are believed to be single crystals, there are no intercrystalline spaces (e.g., grain boundaries) to entrap the spin probe molecules and any uncrystallized material would be at the surface. Finally it is unlikely that either the spin probe or C14 would co-crystallize with C20 but may act as impurities and alter the progress of C20 crystallization. Based on these observations, I propose that the liquid lipid fraction is located surrounding the crystalline lipid core and in close proximity of the immobilized surface layer which hinders the mobility of the spin probe This model is consistent with the observed increase in $a_N$ and decrease in $\tau_c(B)$ of the spin probe in more crystalline samples (Table 4.1, Figure 4.2). However, the model does not explain the time-dependency seen in the C20 containing samples. Next, I will investigate the crystallization behavior of emulsions containing C20 to understand the mechanisms which might cause this time-dependency.

### 4.3.3 DSC analysis

The crystallization and melting behaviors of fine C20 droplets ($d_{32}$ = 0.2 μm) containing varying amounts of C14 (0, 1, and 10 wt%) were investigated using microcalorimetry (Figure 4.3). No phase transition was observed for pure tetradecane emulsions (100%C14), and so data from this sample are not reported. Cooling of 100%C20 droplets produced two exothermic peaks with the first minima at 22.2 °C and the second at 20.3 °C (Figure 4.3a). The first, major exothermic peak has been attributed to the liquid-to-rotator transition, while the second, minor peak to a rotator-to-crystal transition (Gulseren and Coupland, 2007, 2008). The rotator phase is a metastable crystalline state observed in normal alkanes in which the molecules lack long-range order with respect to rotation about their long axes (Sirota, 1998). Although Kraack et al. (2000) argued n-alkanes with chain lengths equal or smaller than 20 carbons directly nucleate into the stable triclinic crystal, Sirota and Herhold (1999) showed the presence of a meta-stable orthorhombic rotator phase intermediate in n-eicosane using synchrotron x-ray scattering measurements. While there have been no studies on the interactions of rotator-phase alkanes with hydrophobic small molecules, several researchers (Bunjes et al., 2000; Jenning et al., 2000c; Jenning and Gohla, 2001; Muller et al., 1998) have shown that TAG crystals in less-stable polymorphic forms are better able to bind small hydrophobic molecules than TAG crystals in stable polymorphic forms. If this trend persists in alkanes I would expect droplets in the rotator phase to incorporate more PTMIO than droplets in the crystal phase.

When 1 wt% of the C20 was replaced with C14 (99%C20), the cooling thermograms showed similar peaks slightly shifted to lower temperatures (~ -0.1 °C). Moreover, both the intensity ratio of first to second peak and the distance between these two peaks decreased slightly (Figure 4.3a). When 10 wt% of C20 was replaced with C14 (90%C20), a single crystallization peak was observed (minima at 19.6 °C) either because the liquid oil prevented the formation metastable rotator phase and the C20 nucleated directly into the stable triclinic crystal, or more probably both liquid-to-rotator and rotator-to-triclinic crystal transitions were happening simultaneously and were seen as a single exothermic peak. The latter mechanism is consistent

with the observation that even 1% C14 in C20 (99%C20) reduced the separation between two peaks and presumably more C14 would have a greater effect.

Two endothermic peaks were observed in the heating thermogram of 100%C20 emulsions (Figure 4.3b). The first, minor peak (maxima 24.9 °C) can be attributed to a crystal-to-rotator transition, and the second, major peak (maxima at 36.1 °C) to a rotator-to-liquid transition (Gulseren and Coupland, 2007, 2008). When a small fraction of C20 was replaced with C14 (99%C20 and 90%C20 samples), the major peak (i.e., rotator-to-liquid peak) broadened and its position shifted to a lower temperature, while minor peak (i.e., crystal-to rotator peak) was much less affected. The extent of broadening and shift in the peak position of the major peak was further increased with increasing C14 fraction in the droplets, probably due to the solubility of C20 crystals in liquid C14.

a)

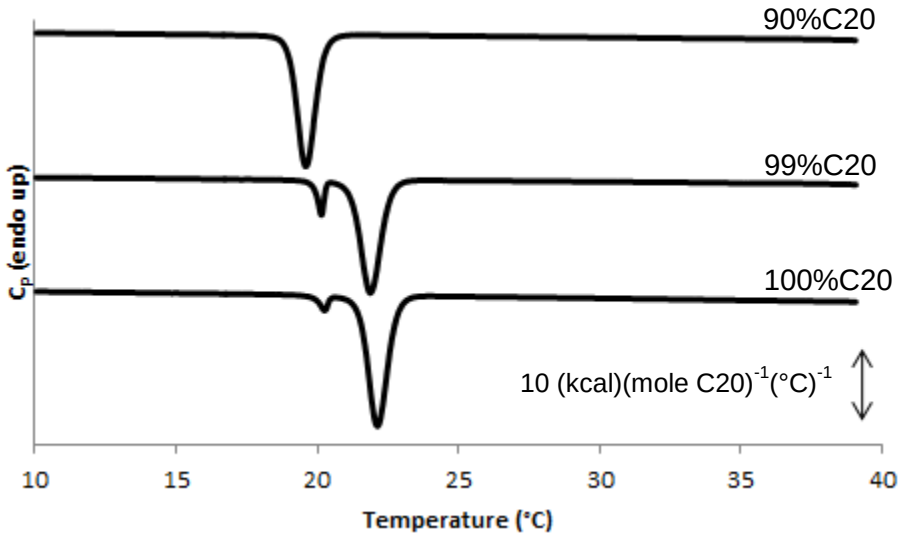


b)

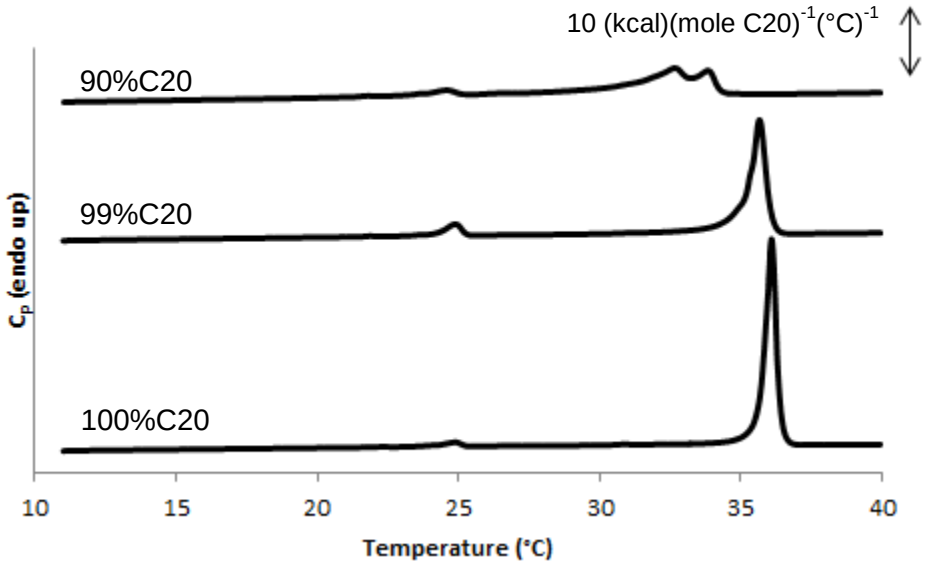


Figure 4.3. (a) Cooling and (b) heating thermograms (at 12 °C / h) of emulsions ($d_{32}$ = 0.2 μm) of eicosane (C20) and tetradecane (C14) mixtures of 100%C20, 99%C20, and 90%C20.

Analysis of the DSC data provides three possible reasons for the effects of storage time and temperature on the properties of the NLC.

(i) In fine emulsions the rate of crystallization is determined by the nucleation frequency. In this case room temperature (i.e., 21.5 ± 0.5 °C) was close to the maximum of the crystallization enthalpy of the major peak (22.2 °C) for 100%C20 emulsion. Thus, it is possible that after 5 h storage there are two populations of eicosane droplets (i.e., crystallized and not crystallized). Samples with higher proportions of C14 have lower nucleation temperatures, so will nucleate more slowly or, in the case of pure C14, not at all. Thus, for samples containing C20 stored at room temperature I would expect a fraction of liquid droplets that decreases with storage time and increases with the proportion of C14. On the other hand all samples (except 100%C14) stored at 5 °C would be fully nucleated at the time of measurement. Droplets containing more liquid oil are better able to retain PTMIO. It is notable that in refrigerated 90%C20 emulsions, the properties of the probe (i.e., $a_N$, $\tau_C(B)$) are very similar to the properties of probe in liquid oil.

(ii) In some samples, particularly those with lower proportions of C20, it is possible that a droplet may nucleate into a rotator phase but not immediately convert to the stable crystal phase. If the hypothesis regarding the interaction of the less-stable rotator phase crystals with hydrophobic small molecules were correct, we would expect samples remaining in the rotator phase to retain more PTMIO in the droplets. However the fact that in droplets retaining significant amounts of probe, the environment of that probe is similar to liquid oil suggests this mechanism may not be significant.

(iii) Increasing the proportion of C14 in the droplets can slow the growth of C20 crystals. After crystal nucleation occurs in a droplet, the crystals will grow quickly and any non-crystallizing material (i.e., PTMIO, C14, any impurities in the alkanes, hydrophobic portions of the caseinate interacting with the lipid) will be concentrated in the remaining liquid phase. As this phase becomes more concentrated, the crystallization of C20 from solution will slow and eventually stop. Samples with more C14 will tend to crystalize more slowly while

samples stored at lower temperatures will approach equilibrium more quickly. Once again, samples with more liquid oil will retain more PTMIO.

All three of these models are consistent with the crystalline fat content of droplets containing C20 increasing (i) with the fraction of C20 in the droplets and (ii) in the sequence 5 h at room temperature < 24 h at room temperature < 24 h at refrigerated temperature. Droplets with a higher crystalline fat content are less able to retain PTMIO. While model (ii) seems least probable, we cannot distinguish between models (i) and (iii) using the data available. If the relationship between probe location and probe reactivity persists for NLC, I should expect similar trends in reduction kinetics data.

### 4.3.4 Reduction kinetics

The EPR-active nitroxide spin probe can be reduced to its EPR-silent form with ascorbate but only if spin probe is in a location where it can interact with aqueous molecules (Ahlin et al., 2003). The reduction kinetics of the spin probe could be measured as the decrease of the peak-to-peak height in the EPR spectra because the line shape did not change during the reaction (data not reported). In all cases, the peak-to-peak height decreased exponentially upon addition of the iron/ascorbate blend (data for the refrigerated samples are shown as illustrative examples in Figure 4.4). Differences in the initial peak-to-peak heights between different samples were due to differences in peak shape and do not affect the analysis. It is notable that none of the samples show any anomalous crystallization behavior which might have provided evidence of unusual microstructure within the NLC.

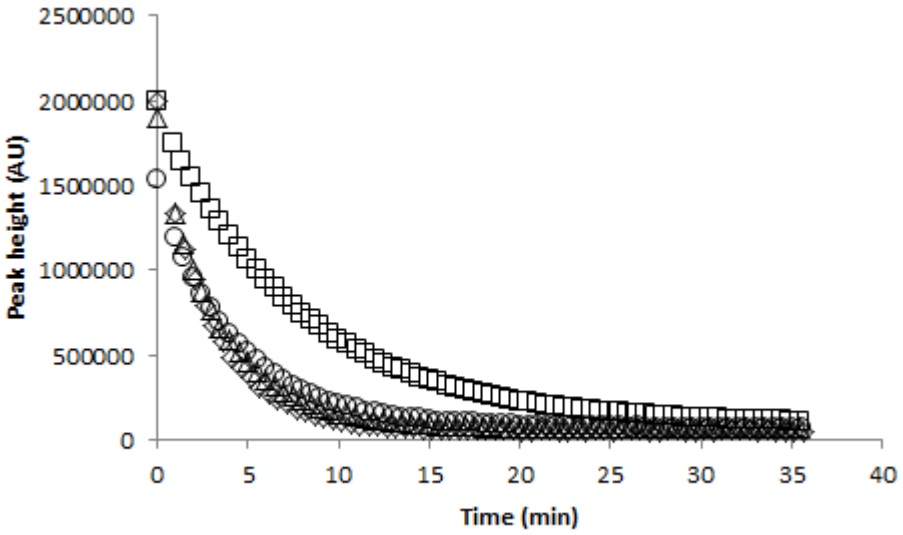


Figure 4.4. Degradation kinetics of PTMIO (200 µ*m* initial concentration) in emulsions ($d_{32}$ = 0.2 µm) of 10 wt% eicosane (C20) and tetradecane (C14) mixtures of 100 %C20(◊), 99%C20 (Δ), 90%C20 (○), and 100%C14 (□), respectively, following the addition of iron/ascorbate blend after 24 h of storage at 5 °C.

The reaction was modeled as a first order process and an apparent rate constant ($k_{apparent}$) was calculated from the initial linear portion (i.e., up to $1/4^{th}$ of the initial intensity) of the $\ln(I/I_0)$ vs. time plot (Table 4.2). As hypothesized, $k_{apparent}$ increased (i) with the fraction of C20 in the droplets and (ii) in the sequence 5 h at room temperature < 24 h at room temperature < 24 h at refrigerated temperature. The rate of reduction of PTMIO in the C14 samples was the slowest and was unaffected by storage. Consequently, it has been found that the chemical degradation analyses were in agreement with the proposed model for the distribution behavior of PTMIO in the emulsions as affected by storage time and temperature.

Table 4.2. Apparent first order rate constants ($k_{apparent}$) ($s^{-1}$) for the degradation of PTMIO in emulsions. The different letters show significant difference between two samples for a given storage condition (i.e., in a column), and different Roman numerals show significant difference for the same sample at different time ($\alpha = 0.05$).

| Sample | 5 h (21.5 °C) | 24 h (21.5 °C) | 24 h (5 °C) |
|---|---|---|---|
| 100%C14 | $0.122 \pm 0.004^{a,I}$ | $0.118 \pm 0.002^{a,I}$ | $0.119 \pm 0.003^{a,I}$ |
| 90%C20 | $0.134 \pm 0.003^{b,I}$ | $0.156 \pm 0.012^{b,II}$ | $0.197 \pm 0.007^{b,III}$ |
| 99%C20 | $0.140 \pm 0.003^{b,I}$ | $0.257 \pm 0.014^{c,II}$ | $0.272 \pm 0.006^{c,II}$ |
| 100%C20 | $0.141 \pm 0.004^{b,I}$ | $0.332 \pm 0.004^{d,II}$ | $0.328 \pm 0.003^{d,II}$ |

Similar observations were reported by other researchers. For example, the entrapment efficiency of solid lipid (palmitic acid triglyceride) emulsion for delivery of drug clotrimazole was improved when a liquid lipid (caprylic/capric acid triglyceride) was incorporated (Souto et al., 2004). In a similar manner, Ghosh et al. (2007) also inferred that some of the liquid lipophilic ingredients excluded from lipid droplets accumulated at the surface of the droplets and could even act as a solvent for the crystalline lipid resulting in the formation of a liquid layer on the surface of crystalline droplets.

In a related manner, Jores et al. (2003, 2004) produced emulsions of semi-crystalline droplets from binary mixtures of (behenic acid glycerides) and liquid (caprylic/capric acid glycerides) lipids. They similarly found that the retention of the lipophilic ingredient increased with

increasing liquid lipid fraction and the chemical stability was the highest in liquid droplet emulsions, and they concluded that the liquid oil was in between the crystallized droplet core and surfactant layer. Moreover, Jores et al. (2004) claimed that liquid fraction does not necessarily cover all the solid surfaces but can form individual droplets and attach to the edge of the needle-like β-form lipid crystals (named as "nano-spoons"). The needle like morphology can be attributed to β-form crystals (Bunjes et al., 2007), while selection of relevant surfactants can move the oil away from the crystallized particle as a separate droplet (Spicer and Hartel, 2005).

### 4.4 Conclusion

In Chapter 3, I proposed that the liquid oil in emulsions provides a reservoir for hydrophobic solute molecules while droplet crystallization leads to their expulsion to an aqueous environment at the droplet surface. In the present work, I used similar methods to modify that model to account for the presence of liquid oil within the droplets as well as effects of storage time and temperature. I argue that the liquid lipid fraction is located around the crystal core of the droplets. The amount of liquid lipid fraction depends on the composition of the droplets as well as storage time and temperature.

It is notable that even a small fraction of liquid oil can have a large effect on the properties of NLC. Very low levels of liquid oil in apparently solid fats are hard to measure using conventional NMR methods. In the mixed TAGs commonly used in studies of SLN and NLC (Ahlin et al., 2003; Jenning et al., 2000; Jenning and Gohla, 2001; Jores et al., 2004; Kristl et al., 2003) it seems likely that some undetermined amount of liquid oil persists and strongly affect the properties of the EBDS. The EPR technique can provide direct and non-invasive measurements of probe properties, such as mobility and the polarity of its environment. Finally, novel delivery systems for lipophilic ingredients can be developed by altering the solid fat content in SLNs (even at very small liquid lipid amounts) to control the ingredient concentration which is active.

# Chapter 5

## 5. **Effects of Surface Characteristics of Droplets of Liquid and Solid Droplet Emulsions on Distribution and Reactivity of a Hydrophobic Solute.**

### 5.1 Introduction

Emulsions can be used effectively and efficiently as delivery systems for lipophilic molecules. Emulsion based delivery systems (EBDS) can provide at least three distinct chemical environments where a selected ingredient can partition: the continuous aqueous phase, the lipid core of the droplets, and the amphiphilic surface layer. The distribution characteristics of a lipophilic ingredient in EBDS can determine their reactivity, and thus their chemical stability during storage or bioavailability post-consumption. EBDS can be modified to improve their performance as delivery systems; for example controlling the lipid composition and crystalline structure in the case of SLNs, or modifying the surface properties of the dispersed droplets can be used to control the distribution, release profiles, and reactivity of the selected ingredients (McClements et al., 2007).

The effect of lipid crystallization on the distribution of an EPR-active small molecule lipophilic ingredient (PTMIO) is reported in Chapter 3. It was found that the crystallization of eicosane droplets resulted in partitioning of all of the PTMIO into the aqueous phase where they interact with droplet surfaces. EBDS was also modified using binary liquid and solid lipid mixtures to improve the retention of PTMIO within the lipid droplets (Chapter 4). It was found that the retention of PTMIO increased and crystallization of C20 was retarded with increasing C14 concentrations within the droplets.

Another approach to modifying EBDS is by controlling the interfacial properties of the droplets. In general, crystallization in fine droplets is believed to proceed via homogeneous nucleation followed by very rapid crystal growth (Coupland, 2002). However, certain surfactants can promote (Ueno et al., 2003) or retard (Awad, 2004; Hodate et al., 1997) the crystal nucleation, as well as crystal growth. In the present chapter, the interfacial properties

of lipid droplets will be modified by replacing Na-caseinate with a soybean lecithin (70% phosphatidylcholine, PC) and bile salt blend in order to control the microstructure of the droplets, and to enhance the retention of the lipophilic ingredient.

The microstructure of SLN can be modified using lecithins with varying chemical compositions. For example, it has been shown that the crystallization temperatures of triglyceride droplets increase and the rate of polymorphic transition from α to β form decreases when lecithins consisting of saturated phospholipids are used in combination with bile salts as emulsifiers (Bunjes and Koch, 2005; Bunjes et al., 2007). It has been argued that the saturated alkyl chains of high melting lecithin can induce surface heterogeneous crystallization (i.e., formation of a shell of solidified phospholipid), which retards the rate of α to β polymorphic transition (Bunjes et al., 2007). However, it was also noted that the α-form crystals of similar triglycerides were the most stable when droplets were stabilized only with the bile salt (smaller than lecithin and incompatible with lipid crystals) as compared to when bile salts were blended with different lecithins (Bunjes et al., 2003). In another study, Helgason et al. (2009) claimed that the formation of a solid layer due to lecithin crystallization prior to crystallization of the droplet core can entrap β-carotene molecules within the solid droplets and, in turn, prevent their oxidation (Helgason et al., 2009). Although all of these studies reported consistent results, the exact mechanism by which lecithin influences the distribution of lipophilic ingredients in SLN has yet to be elucidated. It is essential to first understand lecithin's behavior as an emulsifier before a thorough analysis of how lecithin affects the distribution and reactivity of a lipophilic ingredient can be made.

PC (Figure 5.1a) has very low solubility in water (~$1\times10^{-10}$ M), and limited solubility in lipids (i.e., ~$1\times10^{-3}$ M in soybean oil) (Rydhag and Wilton, 1981). In the presence of an excess of water at temperatures above the chain melting temperature PC exists as a lamellar liquid crystalline phase in equilibrium with a very dilute aqueous solution of PC monomers (Friberg, 1971; Friberg et al., 1976; Friberg and Rydhag, 1971; Rydhag and Wilton, 1981). The dispersibility and swelling capacity of lecithins increases in the presence of charged lipids, and their swelling capacity determines their effectiveness as emulsifiers (Friberg and Rydhag, 1971; Rydhag and Wilton, 1981).

a)

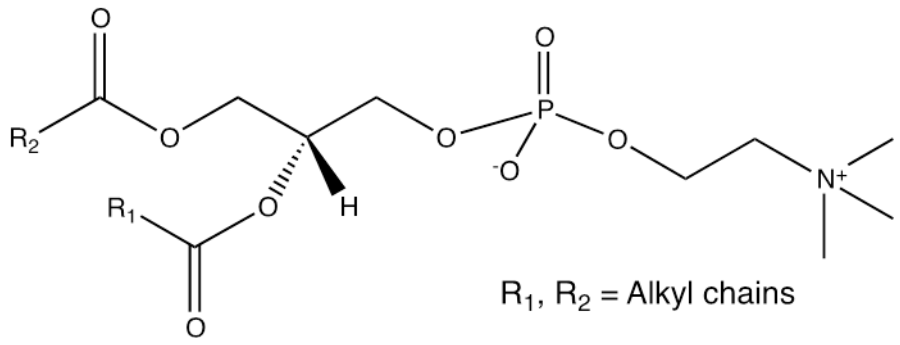


b)

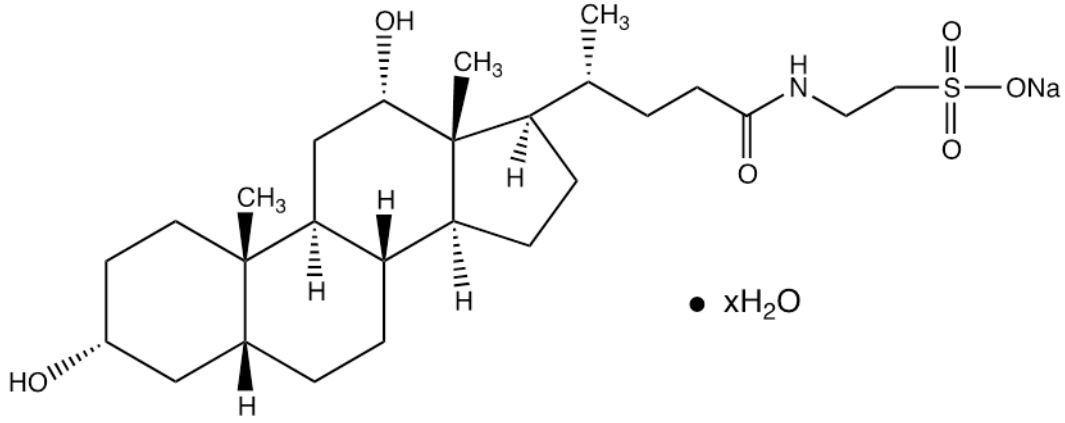


Figure 5.1. Molecular structure of (a) phosphatidylcholine and (b) sodium taurodeoxycholate hydrate.

Conventionally, oil is homogenized into an aqueous environment containing the emulsifier in order to prepare oil-in-water emulsions. In oil-in-water emulsions, all of the PC is believed to surround the droplets in the form of a lamellar liquid crystalline phase, and in equilibrium with negligible amounts of monomers in lipid and aqueous phases (Rydhag and Wilton, 1981). In addition, it has also been shown that multilayers of lamellar PC are required to stabilize emulsions (Friberg, 1971; Rydhag and Wilton, 1981). In general, PC is not a very effective emulsifier due to its highly lipophilic nature (Rydhag and Wilton, 1981).

In SLN research, lecithins are often used together with bile salts (e.g., sodium taurodeoxycholate, Figure 5.1b) as co-surfactants in order to improve their emulsification power. The diffusion rate of emulsifiers and their arrangement at the surface of the droplets, as affected by their chemical structure, determine their emulsification capacity. Although the exact mechanism is not thoroughly understood, it is known that the stability of emulsions increases and smaller droplet sizes can be achieved when lecithins are used in combination with bile salts as compared to lecithins alone (Sjostrom et al., 1993). Mun et al. (2007) showed that the magnitude of the surface charge on lecithin-stabilized lipid droplets increased when bile salts were used as co-surfactants (pH 7.0), indicating adsorption of the bile salt to the droplet surface along with the lecithin. Moreover, lecithin stabilized droplets were shown to have a greater net negative charge than the caseinate stabilized droplets. This more ionic nature might increase the water absorption capacity of lecithin at droplet surfaces and may further enhance the power of lecithins to stabilize the droplets. An alternative functionality of lecithins as emulsifiers were proposed when used in SLN formulations. It was argued that aqueous bile salts could diffuse rapidly to cover the newly formed lipid surface if crystallization results in a shape change (i.e., the diffusion and adsorption of bile salt to the droplet surface is believed to be faster than the rate of crystallization) (Bunjes et al., 2007; Unruh et al., 2002). Thus, droplet aggregation can be prevented as the hydrophobic attraction between exposed lipid surfaces is minimized.

A widely used approach for assessing the distribution of the lipophilic ingredient is by following changes in its degradation kinetics in response to a controlled chemical stress. Although this technique shows the change in reactivity of an ingredient, it is not always

directly correlated with the distribution of the ingredient. For example, Helgason et al. (2009) reported that β-carotene breakdown is much slower in lecithin stabilized liquid lipid emulsions than polysorbate stabilized emulsions. However, this finding cannot be directly correlated to the distribution profile of the β-carotene, not only because the charge on the surface of the droplets stabilized by two types of surfactants are different (Mun et al., 2007), but also because polysorbates are known to contain hydroperoxides (Nuchi et al., 2001). Lecithins and proteins (e.g., sodium caseinate) can also show antioxidant properties to varying extents (Elias et al., 2008; King et al., 1992).

EPR spectroscopy is a technique that allows direct and non-destructive measurement of ingredient properties in different environments of an emulsion. This is a potentially powerful tool that can be used to develop a better physical model of the structure of the EBDS and distribution characteristics of the lipophilic ingredient contained within. For example, Ahlin et al. (2000a, 2003) measured the EPR spectra of aliphatic spin probes in a phospholipid-stabilized glycerol tripalmitate emulsion above and below the melting point of the fat. Line broadening increased upon lipid crystallization, which is consistent with immobilization of the spin probe molecules. However, the probes used were aliphatic, and the changes observed may have been associated with a phase change in the phospholipid membrane. Ahlin et al. (2000b, 2003) also investigated the effect of chemical structure and lipophilicty of synthesized spin probes (i.e., methyl esters of palmitic acid with a doxyl nitroxide group introduced at varying positions on the alkyl chain) on their distribution and chemical stability in the presence of sodium ascorbate. They showed that the majority of the spin probe was distributed in the phospholipid layer, and the extent of penetration of the spin probes within the lipid core increased as the probe's nitroxide group moved to the carboxylic acid end, or as the molecule's alkyl chain length increased.

In the present study, I will compare the effects of PC+bile salt with caseinate as emulsifiers on the distribution characteristics of PTMIO in emulsions of C14 and C20. I hypothesize that PC molecules will modify the distribution of the probe in droplets because PTMIO can associate with the liquid crystalline lecithin layer surrounding the droplets. The probe population in the proximity of the lecithin layer is expected to have restricted mobility, which

can be observed as higher rotational correlation times. PC can also alter the crystallization behavior of C20 droplets, as its hydrocarbon tails are expected to interact with C20 molecules. I hypothesize that the PC layer can limit the increase in the aqueous probe population with crystallization of C20 in droplets. Finally, the liquid crystalline lecithin layer may not limit the probe reactivity because of the very small diffusion pathway. The findings are used to develop a mechanistic model to describe the effect of lecithin on the distribution of a lipophilic ingredient in emulsions consisting of liquid or solid lipids.

## 5.2 Materials and Methods

### 5.2.1 Materials

The spin probe 4-phenyl-2,2,5,5-tetramethyl-3-imidazoline-1-oxyl nitroxide (PTMIO, Figure 3.1a) was used as a model lipophilic ingredient (Enzo Life Sciences, Plymouth Meeting, PA, USA). Sodium caseinate (from bovine milk), n-eicosane, sodium L-ascorbate, and taurodeoxycholic acid sodium were obtained from the Sigma Chemical Company (St. Louis, MO, USA), n-tetradecane was obtained from Fisher Scientific (Pittsburgh, PA, USA), and ferric chloride 6-hydrate was obtained from Mallinckrodt Chemicals (Phillipsburg, NJ, USA). All other materials were reagent grade and were used as received. Fat-free soybean lecithin, Alcolec PC75 (PC75), was a gift from American Lecithin Company (Oxford, CT), and its composition is shown in Table 5.1.

Table 5.1. Chemical composition of Alcolec PC 75. (Data provided by manufacturer).

| | |
|---|---|
| Phospholipids | Phosphatidylcholine (> 68%) |
| | Phosphatidylethanolamine (< 10%) |
| Non-polar lipids | Triglycerides (< 5%) |
| | D,L-α-Tocopherol (0.1-0.2%) |
| Fatty acid composition | Palmitic acid (17-20%) |
| | Stearic acid (2-5%) |
| | Oleic acid (8-12%) |
| | Linoleic acid (58-65%) |
| | Linolenic acid (4-6%) |

### 5.2.2 Preparation of EBDS containing the lipophilic ingredient

The emulsions were prepared as described previously in Chapters 3 and 4. Briefly, emulsifier solutions were prepared in phosphate buffer (pH 7, 100 mM). Na-caseinate (1 wt%) was dissolved in the phosphate buffer overnight at room temperature, and heated to 50 °C for 2-3 h prior to preparation of emulsions. PC75 + bile salt (2.4 wt% + 0.6 wt%) was first dispersed in phosphate buffer for about 1 h at room temperature, and subsequently heated to 50 °C for about 2-3 h prior to preparation of emulsions.

PTMIO was dissolved in hot (50 °C) C14 or C20. An emulsion premix ($d_{32}$ ~40-50 μm) was prepared by mixing the lipid (10 wt%) with the Na-caseinate or PC75 + bile salt solution using a high-speed blender (Brinkmann Polytron, Brinkmann Instruments Inc., Westbury, NY). The emulsion premix was then passed through a microfluidizer (M-110Y Microfluidizer, Microfluidics, Newton, MA) at 70-75 °C (5 passes at 1200 bar). Final emulsions containing 200 μ*m* PTMIO were stored at 5 ºC (i.e., refrigerator temperature) for 24 h. The particle size distribution of the emulsions was measured by static light scattering (Horiba LA-920, Irvine, CA).

### 5.2.3 EPR analysis

EPR spectra of emulsions were measured using a Bruker eScanR EPR spectrometer (Bruker-Biospin, Billerica, MA) operating in X-band, as described in Chapters 3 and 4. In brief, all emulsions were deoxygenated by passing humidified nitrogen gas (3 sL/min) through the headspace of samples for approximately 90 min prior to EPR analysis (Figure 3.1b). Aliquots of samples were then loaded into a 19-bore quartz capillary measurement cell (AquaX, Bruker-Biospin, Billerica, MA), which had been flushed with $N_2$ gas. EPR spectra were recorded at 21.5 ± 0.5°C. In order to study the chemical reduction of PTMIO, small volumes of sodium ascorbate solution and ferric chloride solution (final concentration 1 m*m* and 10 μ*m*, respectively) were added to the samples under a $N_2$ blanket and the EPR spectra were recorded at regular time intervals.

EPR measurements in bulk lipids were carried out in a similar manner, except for the following modifications. Nitrogen gas used to deoxygenate bulk lipid samples was not dehumidified, and samples were loaded into borosilicate glass capillary tubes (VWR, Cat. No. 53432-783) instead of a 19-bore quartz measurement cell.

The experimental spectra were simulated using theWinSim2002 software (version 0.98, National Institute of Environmental Health Sciences, National Institutes of Health, USA), as described in Chapters 3 and 4.

### 5.2.4 DSC analysis

The crystallization behavior of emulsion droplets was investigated by differential scanning calorimetry (VP-DSC, Microcal, Northampton, MA). The emulsion was diluted in phosphate buffer to achieve 0.1 wt% lipid prior to analysis. Aliquots (0.513 mL) were loaded into the instrument and cooled from 40 to 10°C at 12 °C/h. Heat flux was measured relative to water and reported as normalized to the molar concentration of eicosane.

### 5.2.5 Statistics

Results were evaluated for statistical significance using t-test for a pair-wise comparison of two samples at $\alpha = 0.05$.

## 5.3 Results and Discussion

### 5.3.1 Probe behavior in bulk lipid

The EPR spectra of PTMIO (0.2 m*m*) were measured in bulk C14 or C20 containing PC75 (2.4 wt%), and compared similar spectra in pure C14 and C20 (Figure 5.2, Table 5.2). All EPR measurements were taken after the samples were deoxygenated in glass capillary tubes.

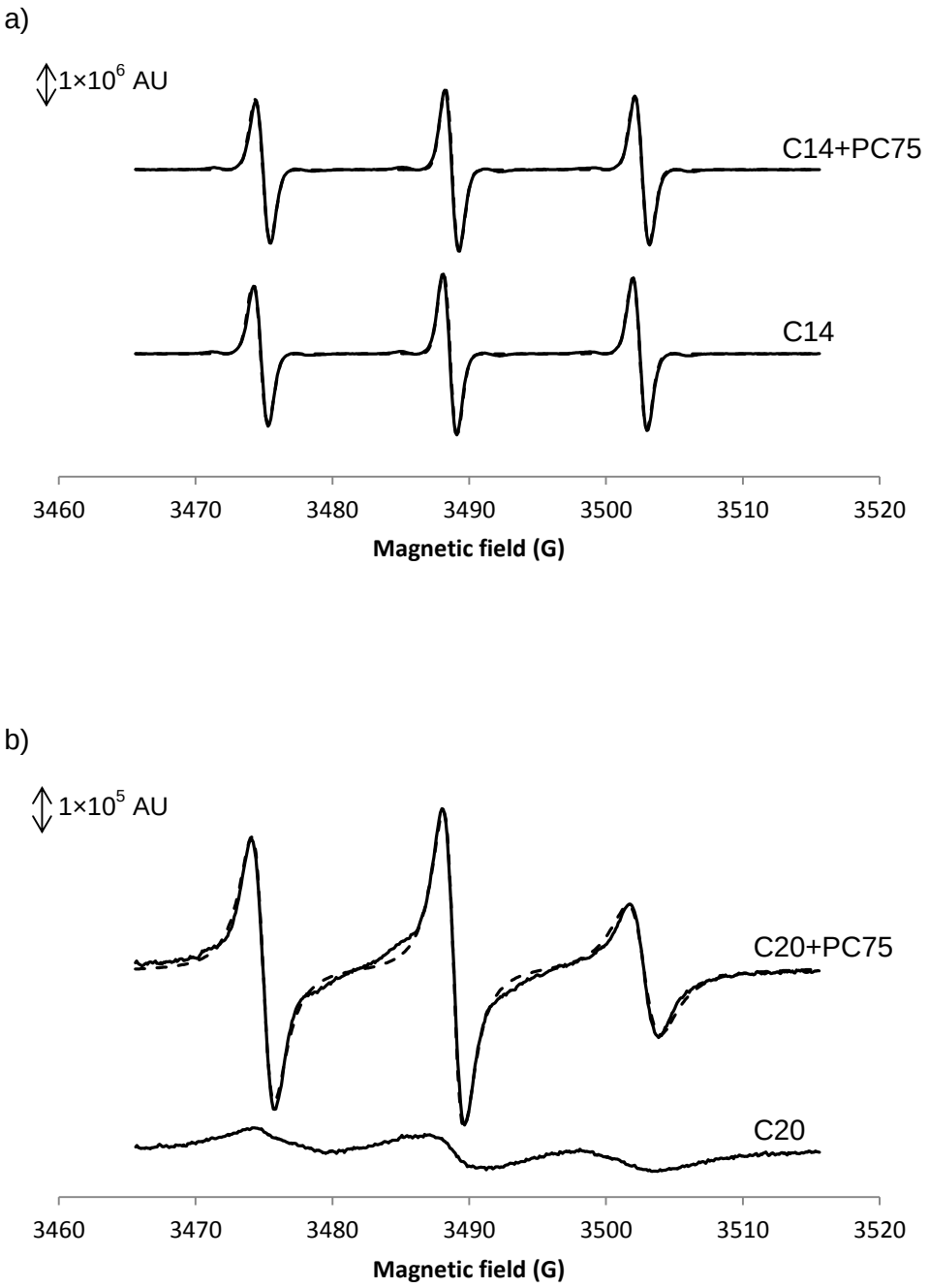


Figure 5.2. EPR pattern (at 21.5 ± 0.5 ° C) of PTMIO (200 μ*m*) in bulk (a) tetradecane, and (b) eicosane with or without PC75 (2.4 wt%); and (c) EPR pattern of PTMIO crystal only. The simulated spectra are shown as broken lines on top of the raw spectra shown as solid lines.

c)

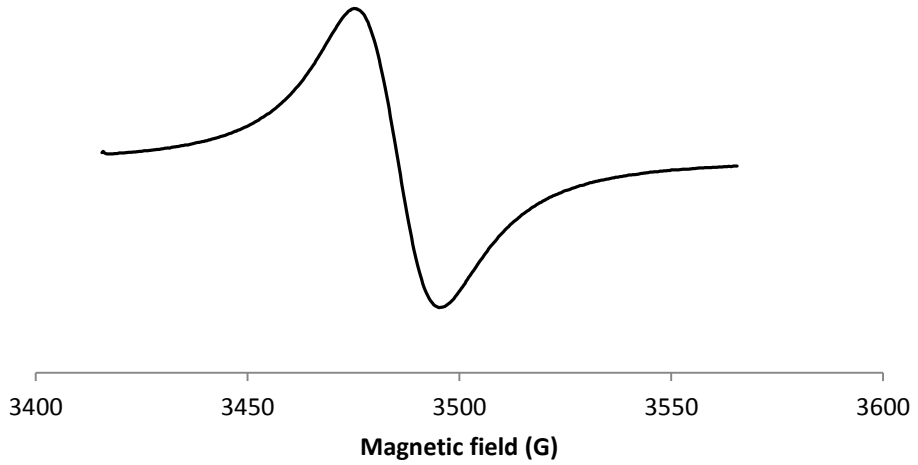


Figure 5.2. (Continued).

Table 5.2. Parameters of the simulated EPR spectra of PTMIO (200 μ*m*) in pure C14 and lecithin in C14 solution (2.4 wt%). The different letters show significant difference of a parameter (i.e., in a column) between two samples ($\alpha = 0.05$).

| Sample | $\tau_c(B) \times 10^{11}$ (sec) | $\tau(B)/\tau(C)$ | $a_N$ (G) |
|---|---|---|---|
| c14 no lecithin | $1.42 \pm 0.19^a$ | $1.1 \pm 0.18^a$ | $13.828 \pm 0.003^a$ |
| c14 lecithin | $0.73 \pm 0.09^b$ | $0.90 \pm 0.11^a$ | $13.838 \pm 0.004^b$ |
| c20 lecithin | $74.46 \pm 0.84^c$ | $4.14 \pm 0.08^b$ | $13.909 \pm 0.005^c$ |

The shape of the spectra of PTMIO in C14 were apparently similar to those in C14 containing PC75 (Figure 5.2a). However, when the properties of the spectra in each system were evaluated from the simulated spectra, there were significant differences (Table 5.2). The rotational correlation time ($\tau_c$(B)) of PTMIO in C14+PC75 solutions was smaller than that of pure C14 ($p<0.05$). This was expected as it is known that the addition of lecithin can decrease the viscosity of lipids, thereby resulting in an increase in the mobility of the spin probe (i.e., smaller $\tau_c$(B)). Moreover, there was a small increase in $a_N$ indicating an increase in the polarity of the probe's environment. In accordance with this observation, Shchipunov (1997) reported that non-polar solvents are localized about the alkyl chains of lecithins, which can lead to the formation of reverse micelles. The probe anisotropy was not affected by the presence of lecithin as these molecules move freely in both environments. This suggests that there is no preferential binding of the probe to PC75, therefore any anisotropic effects, measured as $\tau_c(B)/\tau_c(B)$, were averaged to unity.

The EPR spectra of PTMIO in bulk C20 were different from those obtained in C14, and were also affected by the presence of lecithin (2.4 wt%) (Figure 5.2b). Although a triplet signal was seen, the absorption lines at the three nuclei spin states merged into each other causing a decrease in the signal intensity due to Heisenberg spin exchange. This suggests that when pure C20 was crystallized, PTMIO did not precipitate out as a single crystal but probably formed a solid solution within the C20 crystal matrix. The EPR spectrum of crystalline PMTIO alone is a broad single peak (Figure 5.2c), which is due to extensive overlapping of the free electron-bearing orbitals and resulting Heisenberg spin exchange, and was different than the spectrum recorded for the C20-PTMIO mixture. In the presence of lecithin (2.4 wt%) in C20, PTMIO did not precipitate and retained some measurable mobility (as seen from well-separated three absorption curves), although this mobility was considerably more restricted than the comparable C14 system. In addition, the total intensity (i.e., calculated by double integration) of EPR spectra in C20 was similar to that measured in C14, so there is no significant intensity loss due to spin exchange. In the light of these observations, it is believed that PC75 molecules form self-assembled structures (e.g., reverse micelles) when dispersed in both solid and liquid alkanes, which can interact with the spin probe and further prevent their precipitation in the crystalline lipid (i.e., they retain some measurable mobility). Similar EPR

spectra were obtained by quickly submerging glass capillaries containing liquid C20 solutions into liquid nitrogen before warming up to room temperature for measurement (data not shown). This provides evidence that the C20 was fully crystalline in both cases, and that the rate of crystallization does not affect EPR patterns (i.e., formation of solid solution).

More detailed information about C20+PC75 samples can be obtained from the simulated spectrum, however pure C20 could not be simulated due to precipitation of the probe (Table 5.2). The $\tau_c$(B) increased by approximately two orders of magnitude upon crystallization of the lipid. Although the anisotropy term increased upon crystallization of C20, it was not affected to the same degree as $\tau_c$(B), indicating that lecithin reverse micelles do not preferentially bind PTMIO (i.e., the restriction to the mobility in one molecular axis is similar to that in others).

### 5.3.2 Probe behavior in liquid lipid emulsions

The area-averaged droplet size ($d_{32}$) of PC75+bile salt-stabilized C14 emulsions were slightly smaller (0.17 ± 0.01 μm) than those C14 emulsions stabilized by sodium caseinate (0.20 ± 0.01 μm). Similarly, Sjostrom et al. (1993) showed that oil-in-water emulsions prepared using lecithin and bile salt mixtures as emulsifiers had consistently smaller droplet sizes compared to a range of other emulsifiers (e.g., pure lecithins and sorbitan esters). The mean droplet size of test emulsions remained unchanged upon storage for over 30 days at room temperature.

Interestingly C20 emulsions using a saturated PC (i.e., chain melting temperature higher than the melting temperature of the solid lipid, Phospholipon 80 H, American Lecithin Company, Oxford, CT) creamed a few hours after preparation and could not be used. This is in contrast to the work of (Helgason et al., 2009) which reported limited stability (less than 3 weeks) for SLN and nanoemulsions prepared with this formulation.

Emulsions containing PTMIO (200 μ*m*) were stored under refrigeration temperatures (~ 5°C) for 24 h, and then returned to room temperature (21.5 ± 0.5 °C) for EPR analyses. Similar

results were obtained for EPR measurements 8 h after emulsion preparation (i.e., samples stored at 5°C for 5 h and returned to room temperature for analyses) (data not reported). The deconvoluted EPR spectra and parameters of the separated phases of caseinate-stabilized emulsions are shown in Figure 5.3 and Table 5.3, respectively. The properties of the EPR spectra, as well as the distribution profile of PTMIO in caseinate-stabilized C14 and C20 emulsions, were discussed in Chapters 3 and 4. In brief, it was found that the majority of PTMIO partitions to the liquid lipid droplets, however crystallization of the lipid excludes the probe from droplets into the aqueous phase. Although it has been shown that the probe distribution in either phase was affected by protein at the droplet surface, a separate probe population immobilized at this region could not be characterized.

The EPR spectra obtained for PC75+bile salt-stabilized C14 emulsions were similar to those of caseinate-stabilized C14 emulsions (Figure 5.3). A quantitative comparison was performed using the parameters of the individual populations following deconvolution of the spectra (Table 5.4). Although two distinct populations of probe could be discerned in the caseinate-stabilized emulsions, three distinct populations of PTMIO were observed in PC75+bile salt-stabilized emulsions: a high mobility aqueous population (i.e., small $\tau_C$(B); $a_N$ ~ 15.45 G), a high mobility lipid population (i.e., small $\tau_C$(B); $a_N$ ~ 13.92 G), and a low mobility interfacial population (i.e., high $\tau_C$(B); $a_N$ ~ 14.16 G). This finding is consistent with the physical model proposed earlier.

Indeed, when an F-test is performed (using MS Excel 2010) between 2 center and 3 center simulations of PC75+bile salt-stabilized C14 emulsions at -1 position (i.e., between 3496 G and 3506 G), they were significantly different ($\alpha = 0.05$). Moreover, the marginal effect of using 3 centers over 2 centers for simulations to predict the raw spectrum can be evaluated from (Kutner et al., 2005):

$$F^* = \frac{(SSR_{c3|c2})/(p-q)}{(SSE_{c3})/(n-p)} \qquad [5.1]$$

$$SSR_{c3|c2} = SSR_{c3} - SSR_{c2} \qquad [5.2]$$

where $SSR_{c3|c2}$ is sequential sum of squares regression for the addition of 1-center, $SSR_{c3}$ and $SSR_{c2}$ are sum of squares regression for 3-center and 2-center simulations, respectively, $SSE_{c3}$ is the sum of squares error for 3-center simulation, p is the number of centers in 3-center model, q is the number of centers in 2-center model, and n is the number of observations. For the PC75+bile salt-stabilized C14 emulsions F* was calculated as 13.34, which is higher than $F_{critical}$ (2.7 at $\alpha = 0.05$), showing that the 3-center simulation is significantly better than 2-center simulation.

In contrast, no significant difference was found between simulations of the EPR spectra of the caseinate-stabilized C14 emulsions using 3 centers and 2 centers ($\alpha = 0.05$). Indeed, when 3 centers were used for simulations, two non-polar centers converged to a single spectrum (i.e., hyperfine splitting constants and rotational correlation times were found to be similar, $\alpha = 0.05$).

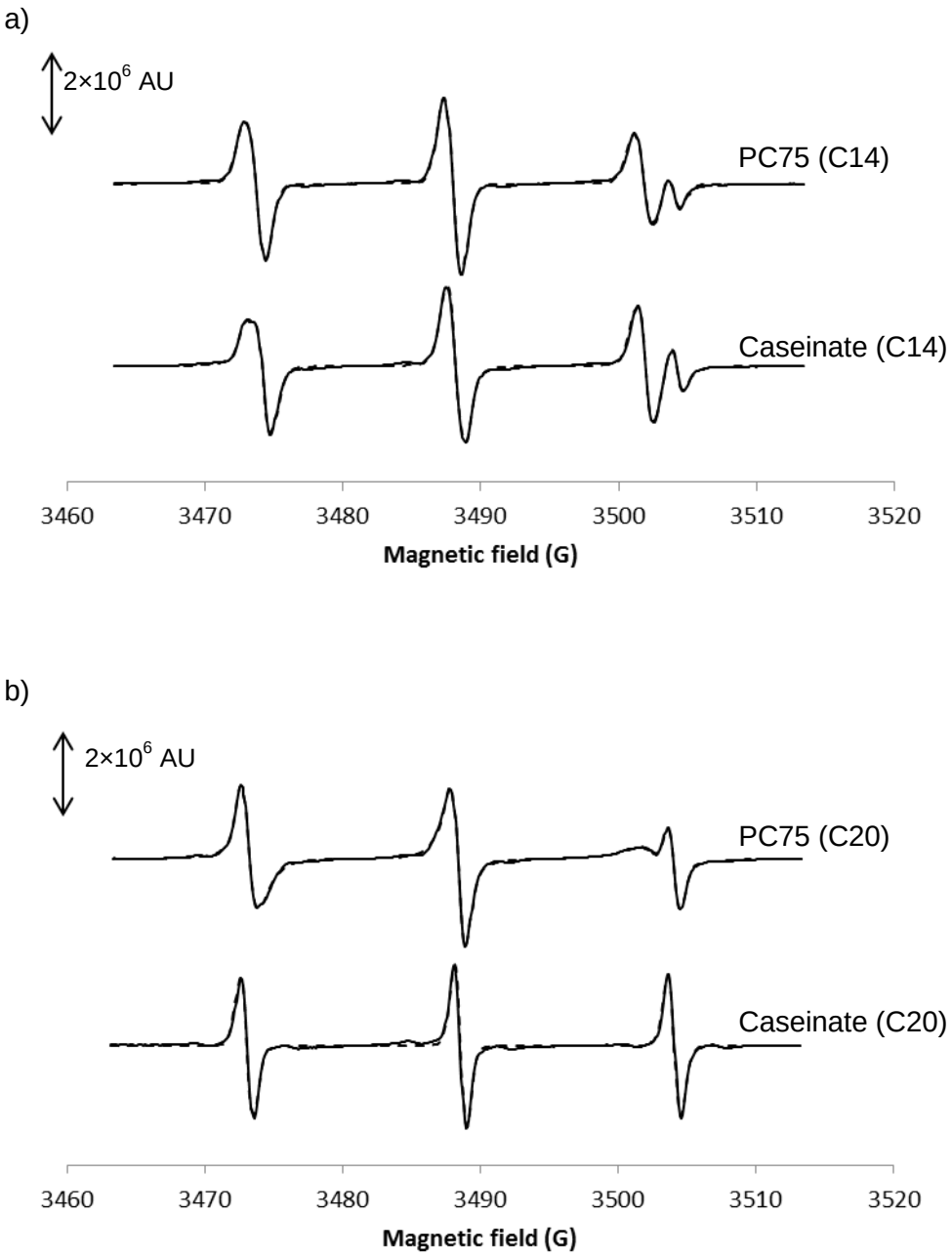


Figure 5.3. EPR pattern (at 21.5 ± 0.5 ° C) of PTMIO (200 μ*m*) in 10 wt% (a) tetradecane and (b) eicosane emulsions stabilized with PC75 and Na-caseinate after 24 h storage (at ~5 °C). The simulated spectra are shown as broken lines on top of the raw spectra shown as solid lines.

Table 5.3. Parameters describing the deconvoluted EPR spectra of PTMIO in Na-caseinate stabilized C14 and C20 emulsions: a) aqueous phase, b) lipid phase. The different letters show significant difference of a parameter (i.e., in a column) between two samples ($\alpha = 0.05$).

a) aqueous phase

| Sample | Fraction (%) | $\tau_c(B) \times 10^{11}$ (sec) | $\tau(B)/\tau(C)$ | $a_N$ (G) |
|---|---|---|---|---|
| C14 | 30.43 ± 1.05 | $5.68 \pm 0.33^a$ | $4.04 \pm 0.45^a$ | $15.498 \pm 0.004^a$ |
| C20 | > 99.5 | $2.48 \pm 0.24^b$ | $1.33 \pm 0.14^b$ | $15.475 \pm 0.003^b$ |

b) lipid phase

| Sample | Fraction (%) | $\tau_c(B) \times 10^{11}$ (sec) | $\tau(B)/\tau(C)$ | $a_N$ (G) |
|---|---|---|---|---|
| C14 | 69.57 ± 1.14 | $2.29 \pm 0.19^a$ | $1.15 \pm 0.14^a$ | $13.848 \pm 0.003^a$ |
| C20 | <0.5 | $78.91 \pm 3.47^b$ | $17.09 \pm 1.21^b$ | $14.249 \pm 0.046^b$ |

Table 5.4. Parameters describing the deconvoluted EPR spectra of PTMIO in PC75+bile salt stabilized C14 and C20 emulsions: a) aqueous phase, b) lipid phase, c) interface. The different letters show significant difference of a parameter (i.e., in a column) between two samples ($\alpha = 0.05$).

a) aqueous phase

| Sample | Fraction (%) | $\tau_c(B) \times 10^{11}$ (sec) | $\tau(B)/\tau(C)$ | $a_N$ (G) |
|---|---|---|---|---|
| C14 | $18.63 \pm 0.56^a$ | $6.72 \pm 1.15^a$ | $2.70 \pm 0.89^a$ | $15.446 \pm 0.018^a$ |
| C20 | $23.44 \pm 1.19^b$ | $2.96 \pm 0.09^b$ | $1.70 \pm 0.34^a$ | $15.453 \pm 0.022^a$ |

b) lipid phase

| Sample | Fraction (%) | $\tau_c(B) \times 10^{11}$ (sec) | $\tau(B)/\tau(C)$ | $a_N$ (G) |
|---|---|---|---|---|
| C14 | 61.11 ± 1.01 | 1.02 ± 0.15 | 0.96 ± 0.20 | 13.924 ± 0.011 |
| C20 | NA | NA | NA | NA |

c) interfacial

| Sample | Fraction (%) | $\tau_c(B) \times 10^{11}$ (sec) | $\tau(B)/\tau(C)$ | $a_N$ (G) |
|---|---|---|---|---|
| C14 | $20.25 \pm 0.86^a$ | $42.35 \pm 2.77^a$ | $4.77 \pm 0.85^a$ | $14.159 \pm 0.047^a$ |
| C20 | $76.56 \pm 0.98^b$ | $118.42 \pm 1.55^b$ | $4.30 \pm 0.52^b$ | $14.515 \pm 0.016^b$ |

### 5.3.3 Physical model for PC75+bile salt-stabilized C14 emulsion as compared to that of caseinate-stabilized

A physical model can be developed by combining what is already known about PC functionality in emulsions with the findings from the analyses of the EPR spectra. The majority of the probe is present within the liquid lipid core, while there are significant amounts of probe within the interfacial and aqueous environments (Figure 5.4). PC75 is believed to surround the droplets as a multilayer, and the thickness of this layer is expected to exceed 10 nm (Rydhag and Wilton, 1981). PC75 can only stabilize emulsions when it swells by absorbing large amounts of water (up to 50%) to form a liquid crystalline structure (Rydhag and Wilton, 1981). Furthermore, this layer is capable of dissolving some of the lipid (Friberg, 1971; Friberg and Rydhag, 1971; Shchipunov, 1997). Consequently, the probe at the PC75 layer is expected to be surrounded by largely immobilized lecithin molecules, as well as lipid and water molecules.

An immobilized probe population at the interfacial layer of caseinate stabilized emulsions could not be characterized, most likely due to the properties of caseinate surrounding the droplets, which can be approximated as a train-loop-tail model (Figure 3.6). The segments of caseinate were distributed as a dense (volume fraction ~ 0.9) inner layer of about 1 nm in thickness, and a diffuse outer layer (volume fraction ~ 0.1) of about 4-5 nm in thickness, as measured by neutron scattering (Leermakers et al., 1996). However, dangling segments around the adsorbed layer (i.e., tails) can extend up to 10 nm with a very diffuse distribution density. Consequently, although the distribution of probe in lipid and aqueous phases were modified by this caseinate arrangement at the surface, a separate surface population could not be characterized. I will consider the effects of crystallization in PC75+bile salt stabilized droplets in the proceeding section.

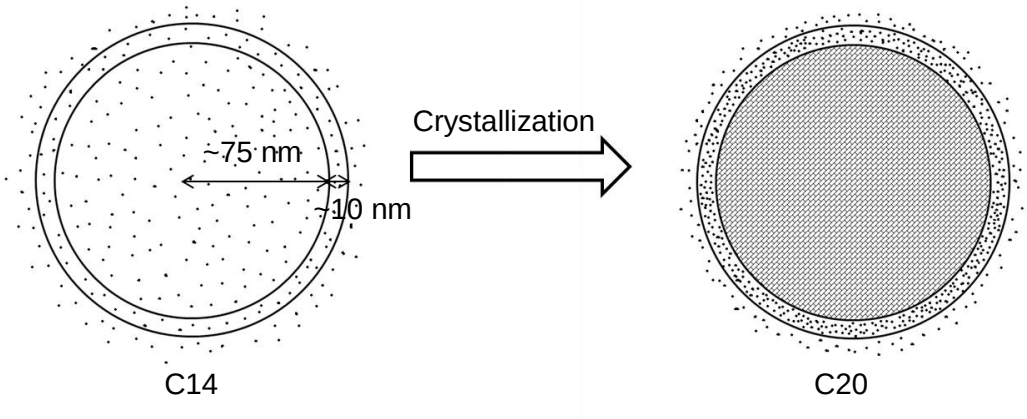


Figure 5.4. Proposed model for the distribution of the PTMIO in PC75+bile salt stabilized emulsions and solid lipid nanoparticles.

### 5.3.4 Probe behavior in solid lipid emulsions

The crystallization behavior of eicosane (m.p. 36.7 °C) in emulsions was investigated using microcalorimetry. Caseinate-stabilized eicosane droplets started to crystallize at 23.4 °C (peak minimum 22.2 °C), with a second minor peak at 20.3 °C (Figure 5.5a). The first major exothermic peak is due to crystallization of eicosane into a non-triclinic crystal form, most likely a metastable rotator phase, while the second minor peak was indicative of a solid-solid transition of eicosane into a triclinic crystal. The crystallization behavior of PC75+bile salt-stabilized C20 emulsions was more complex than caseinate-stabilized C20 emulsions. The main crystallization event in PC75+bile salt C20 emulsions started at a higher temperature (23.9 °C) than caseinate-stabilized C20 emulsions, with a slightly lower peak minimum (21.9 °C), and a broader peak. The higher onset temperature of crystallization suggests that C20 crystallization was affected by the hydrocarbon chain of the PC75, probably via the palmitic and stearic acid moieties. This is in agreement with reports by Bunjes and Unruh (2007), who showed that lecithins can affect the crystallization properties of C20 and modify the microstructure of crystalline matrix in the droplets (Bunjes and Unruh, 2007). Other workers have shown that interfacial caseinate has no such affect on emulsified alkane crystallization (Gulseren and Coupland, 2007; Palanuwech and Coupland, 2003; Ueno et al., 2003).

A separate crystallization event was observed during the cooling of PC75+bile salt-stabilized C20 emulsions near the melting point of C20. There was no such enthalpic transition observed in PC75 dispersion in water either with or without bile salt, or in PC75 solution in C14. Bunjes and Koch (2005) reported similar “precrystallization” events in emulsions of different solid TAGs stabilized with various lecithins, and attributed them to crystallization of the droplet surface. In some cases, the precrystallization event seen by Bunjes and Koch (2005) was comparable to the transition temperature seen in bulk lecithin dispersion (lipid free) while in several other cases it occurred at considerably higher temperature. The results seen in the present work correspond to the latter case reported by Bunjes and Koch (2005), and presumably due to the involvement of C20 in the crystallization of the lecithin crystallization (probably with the palmitic and stearic acid fractions of PC75).

The heating thermograms of C20 emulsions stabilized with caseinate and lecithin are shown in Figure 5.5b. Two endothermic peaks were observed in the heating thermogram of 100%C20 emulsions (Figure 5.5b). The first, minor peak (maxima 24.9 °C) can be attributed to a solid-solid transition (most likely crystal-to-rotator), and the second, major peak (maxima at 36.1 °C) to a solid-liquid transition (most likely rotator-to-liquid), as discussed in Chapters 3 and 4. The melting thermogram of the PC75+bile salt-stabilized C20 emulsion was broader and more complex than that of caseinate-stabilized C20 emulsions. In parallel with cooling thermograms, this finding suggests that there are at least two populations of C20 with different crystalline structure due to C20-lecithin interactions which alters the course of crystallization of C20.

a)

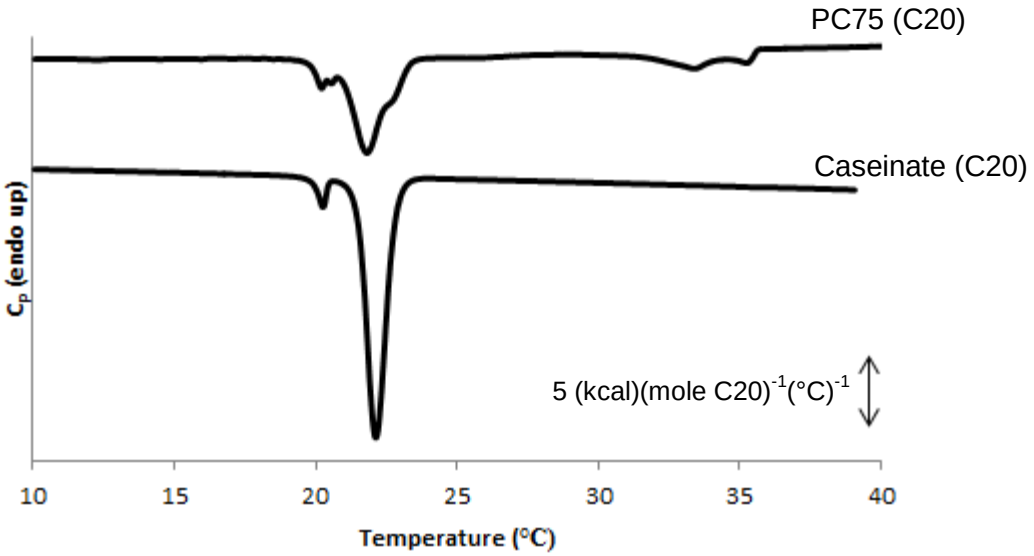


b)

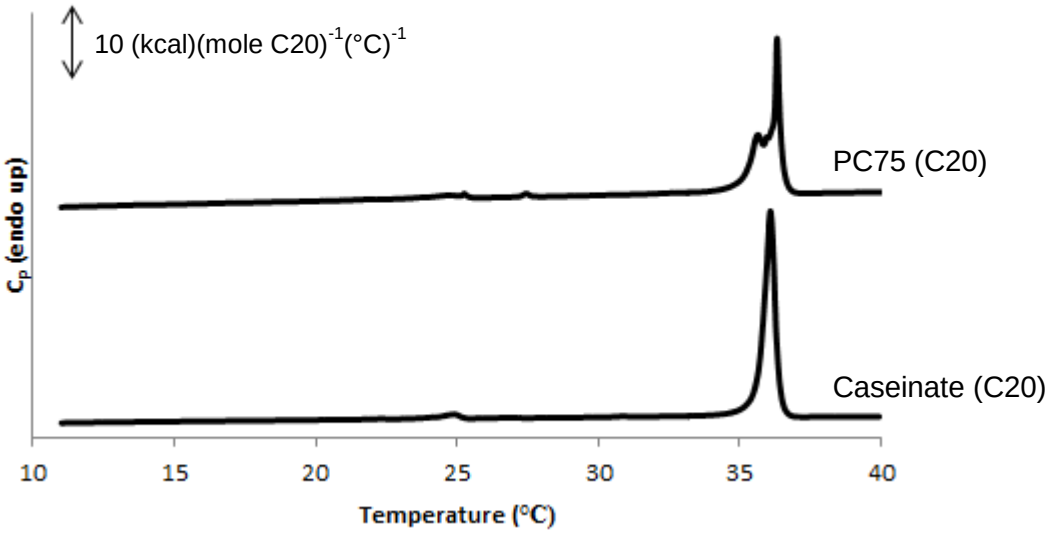


Figure 5.5. (a) Cooling and (b) heating thermograms (at 12 °C / h) of Na-caseinate (1 wt%) or PC75+bile salt (2.4 wt% + 0.6 wt%) stabilized eicosane emulsions.

As discussed in Chapters 3 and 4, PTMIO is only present in the aqueous environment in caseinate-stabilized C20 emulsions, as evidenced by a single hyperfine splitting with properties indicative of PTMIO in the aqueous phase. However, in the EPR spectrum of PC75+bile salt-stabilized C20 emulsions, an immobilized probe population in a non-polar environment was observed. This observation based on the presence of a broad signal with a hyperfine splitting constant smaller than that of PTMIO in the aqueous environment (Figure 5.3b). Moreover, the solid fat contents of caseinate and PC75+bile salt-stabilized C20 emulsions were found to be similar to each other as measured by NMR (data not reported), suggesting that the difference in EPR spectra of two emulsifiers was not due to the presence of uncrystalline C20. A quantitative analysis for the probe properties in these systems was performed based on simulated and deconvoluted EPR spectra.

Two populations of PTMIO were found based on simulation of the spectra of PC75+bile salt-stabilized C20 emulsions (i.e., when the EPR spectra were simulated using three populations of probe, the two non-polar centers converged to a single spectrum) (Table 5.4). The majority of the probe (76.6 %) had a polarity ($a_N$) between that of the probe in the aqueous and lipid phases so is presumably present at the interface.

The $\tau_c$(B) of PTMIO at the interface of C20 droplets was significantly higher than $\tau_c$(B) of PTMIO measured in bulk C20+PC75 solution ($p<0.05$). This difference could be explained as the close-packed liquid crystalline structure of PC75 molecules surrounding the droplets is different than the reverse micelle like structure with a negative curvature of PC75 molecules in bulk oil. Further evidence of lecithin-C20 interactions at droplet surface is seen in the shift of the crystallization peak, as well as the appearance of a precrystallization event, in the cooling thermogram of PC75+bile salt-stabilized C20 emulsion as compared to that of caseinate-stabilized. The different arrangement of the lecithin molecules may also be responsible for the much slower mobility of the probe at the droplet surface of PC75+bile salt-stabilized C20 emulsions as compared to that in PC75+bile salt-stabilized C14 emulsions or the probe mobility in bulk C20 containing PC75. Similar lecithin behavior in SLNs was reported by others. For example, Ahlin et al. (2000, 2003) measured the EPR spectra of aliphatic nitroxide spin probes in a phospholipid-stabilized glycerol tripalmitate emulsion held

above and below the melting point of the fat. Line broadening of the associated EPR spectrum was seen to increase upon lipid crystallization, which is consistent with immobilization of the spin probes. However, the probes used were aliphatic, and the changes observed may have been associated with a phase change in the phospholipid membrane.

The anisotropy terms of the emulsion were not significantly different ($p<0.05$) to those observed in the bulk system, indicating that the probe was associated with PC75's hydrocarbon chains in a similar way to bulk C20+PC75 solutions (Tables 5.2 and 5.4).

### 5.3.5 Updated physical model for PC75+bile salt-stabilized solid lipid emulsions

In the light of these observations, the physical model proposed for liquid droplets can be modified to account for PC75+bile salt-stabilized C20 emulsions. Crystallization of the lipid core excludes probe molecules, forcing them into the lamellar liquid crystalline phase that surrounds the droplets. This causes significant ($p<0.05$) but small increases in the aqueous probe concentration (Figure 5.4). The model for the distribution profile of PTMIO was tested by following the reduction kinetics of the probe, assuming that the probe's location and its chemical reactivity are correlated.

Changes in the peak-to-peak heights of the EPR signals were measured upon addition of the iron/ascorbate blend to the aqueous phase, in a similar manner as shown in Chapters 3 and 4. The reaction was modeled as a first order process and an apparent rate constant ($k_{apparent}$) was calculated from the initial linear portion (i.e., up to $1/4^{th}$ of the initial intensity) of the $\ln(I/I_0)$ vs. time plot (Table 5.5), as described previously (Chapters 3 and 4).

The difference in the apparent rate constants for emulsions stabilized with different emulsifiers cannot solely be accounted for the differences in their aqueous probe concentrations. This is because not only is the surface charge of the droplets different between the emulsions (Mun et al., 2007), but PC75 and sodium caseinate are known to exhibit different antioxidant properties (Elias et al., 2008; King et al., 1992) that could protect the PTMIO from the ascorbyl radicals.

Table 5.5 Apparent first order rate constants ($k_{apparent}$) ($s^{-1}$) for the degradation of PTMIO in emulsions. The different letters show significant difference of a parameter (i.e., in a column) between two samples ($\alpha = 0.05$).

| Sample | $k_{apparent}$ ($s^{-1}$) |
|---|---|
| C14 (caseinate) | $0.114 \pm 0.003^{a}$ |
| C20 (caseinate) | $0.330 \pm 0.004^{b}$ |
| C14 (PC75) | $0.129 \pm 0.008^{c}$ |
| C20 (PC75) | $0.381 \pm 0.010^{d}$ |

As noted in Chapters 3 and 4, in caseinate-stabilized emulsions, $k_{apparent}$ was greater for C20 droplets than for C14 droplets due to exclusion of the probe molecules from the droplets to the aqueous phase (Table 5.5).

Although the aqueous probe population was only slightly higher in PC75+bile salt-stabilized C20 emulsions compared to PC75+bile salt -stabilized C14 emulsions (~25% greater, Table 5.4), $k_{apparent}$ was much higher (~300% greater, Table 5.5). This is presumably because the population of probe in the interfacial layer (~77% of the total) was highly vulnerable to reduction by iron-ascorbate. This is reasonable as the diffusion path in the PC layer is so small (ca. ~10 nm) and contains a considerable amount of water adsorbed in this lecithin layer, which can also carry iron/ascorbate capable of reducing the probe.

**5.4 Conclusion**

The distribution behavior of PTMIO in EBDS was modified by controlling the interfacial properties of the droplets. In C14 emulsions stabilized with either PC75+bile salt or caseinate, two highly mobile probe populations were found: the majority of the probe was in the lipid core while less was found in the aqueous environment. In addition, a third probe population was characterized at the immobilized liquid crystalline interfacial layer in C14 emulsions stabilized by PC75+bile salt, which was not seen in emulsions stabilized by caseinate (the proposed model is given in Figure 5.4).

Crystallization of droplets excluded PTMIO molecules from lipid core. In C20 emulsions stabilized by caseinate, all of the probe was located in the aqueous environment around the droplets. In contrast, in PC75+bile salt-stabilized C20 emulsions, the fraction of the probe in the aqueous phase remained unchanged; however, the majority of the probe was located at the immobilized interfacial layer (Figure 5.4, Table 5.4). Moreover, the mobility of the probe in the interfacial layer was affected by the droplet crystallization, suggesting that the PC75's alkyl chains altered the crystallization behavior of C20.

For both emulsifier systems, the fraction of the probe available to react with aqueous phase iron/ascorbate increased significantly as a result of droplet crystallization. Although similar observations were reported in the literature, the exact location of the solute could not be determined because of the limitations of the indirect techniques.

Lecithin layer can carry large amounts of a small hydrophobic solute following the droplet crystallization. Although in the present work the immobilized lecithin layer was not sufficient to limit the reactivity of the probe in solid droplet emulsion as much as liquid droplets do, the distribution profile and the reactivity of a similar ingredient could further be modified by controlling the thickness of the surface layer via lipid/emulsifier ratio.

# Chapter 6

## 6. Conclusions and Recommendations for the Future Work

There is a broad need to encapsulate certain lipophilic ingredients (e.g., drugs, bioactive molecules) which are poorly bioavailable or prone to chemical loss on storage. Conventional oil-in-water emulsions have been used successfully for delivery of drugs in pharmaceutical products and bioactive compounds in foods. Various efforts have been made to improve their effectiveness and efficiency; for example, advances in homogenization technology allowed production of nano-scale droplets, which were associated with increased bioavailability of hydrophobic bioactive ingredients and improved physical stability of emulsions against gravitational separation. In addition, early work on EBDS suggested the use of crystalline emulsion droplets to limit and control the diffusion of ingredients from droplets into the aqueous environment where they are active. However, to my knowledge, there has been no study reporting improved behavior in solid droplets compared to liquid. Although several researchers considered different approaches to improve the entrapment characteristics of SLN, these have not been systematically investigated and there are still questions remaining thoroughly unanswered, partly because of the limitations in the available characterization techniques. The outstanding research questions for use of emulsions as delivery systems include: if solid droplets are better than liquid, if fine droplets are better than coarse, or how modifications in solid fat content or interfacial properties of the droplets affect the distribution and reactivity of a selected ingredient.

The main goal of this study was to investigate how changes in EBDS structure (i.e., droplet size, crystallinity, surface properties) modify the physical distribution and reactivity of a hydrophobic solute. The results of this work can be used and further be developed to elucidate rules and establish guidelines to select the most appropriate EBDS for a particular kind of lipophilic ingredient and use in industrial applications and products. Within this framework, I approached the research questions via three specific objectives: (1) effects of droplet size and crystallinity, (2) effects of liquid oil fraction and storage, (3) effects of surface composition.

EPR measurements are non-destructive and can characterize the properties of a solute *in situ* in a given EBDS. However, this technique requires the use of an EPR-active molecule (i.e., spin probe, in this case the hydrophobic molecule PTMIO), as a model for the properties of the real ingredient (e.g., bioactive molecules, drugs). EPR measurements are not limited by the samples optical properties or physical characteristics (e.g., viscoelasticity), so they can be used to investigate the probe behavior in real foods during storage or even after consumption either *in vitro* or *in vivo*. Moreover, EPR is about 3 orders of magnitude more sensitive than NMR (i.e., nuclear magneton is $10^3$ times higher than electron Bohr magneton) (Borbat et al., 2001).

I developed an EPR technique to analyze the spin probe distribution in EBDS, and then proposed a model describing the distribution of PTMIO in each system. In this work, model systems were used to find answers to research questions. Although the results of the present work show how a specific small molecule hydrophobic ingredient behaves with changing EBDS structure, other ingredients will not behave in exactly the same way. For example, larger molecules with aliphatic hydrocarbon chains in their structure are expected to be present mostly at the surface of the droplets. The chemical structure of the spin probe could be designed by synthesizing them as an analog of a real ingredient, which can allow a more realistic estimation of distribution of the actual ingredient. The phase behavior of a solute could also be different in TAG emulsions than alkane emulsions. Indeed, I also found that in caseinate-stabilized Miglyol 812 (caprylic/capric acid TAG, l Germany GmbH, Witten, Germany) emulsions the aqueous probe population was less than half of that in C14 emulsions (data not shown). This was interesting as compared to work of Ghosh et al. (2007), who did not observe that much difference in headspace-oil partitioning of a volatile hydrophobic solute between alkane and vegetable oil emulsions. The higher solubility of alkanes around the droplets can also result in variations in the mass transfer process as compared to emulsions of bigger TAGs (this is shown in a separate study in our lab, and not reported here). Moreover, the distribution behavior of the probe in SLNs of TAGs may also be different to that seen in crystalline alkanes due to less perfect crystalline microstructure and the multicomponent lipid fractions.

It is also interesting to note the strong effect of oxygen on lipid-phase signal. It may be possible to exploit this finding to study oxygen distribution in complex materials, or study oxygen related reactions (e.g., lipid oxidation).

In Objective 1, the effects of droplet size and crystallization on the distribution of PTMIO were investigated. Although some early studies suggested entrapment of a hydrophobic solute in SLN could allow improved control over their release profile and reactivity, there has been no published study showing that SLNs are superior to liquid droplets as delivery systems. Indeed, these findings based on indirect techniques and did not consider the solute characteristics (e.g., its mobility and interactions with neighboring molecules) in detail. Moreover there is no study, which directly and quantitatively considers both the distribution of a hydrophobic solute and its reactivity and compares solid vs. liquid and coarse vs. fine droplets. In the liquid oil emulsions two distinctly separated PTMIO populations were characterized: the lipid phase where the majority of the probe was present, and the aqueous phase. The aqueous probe population was more than an order of magnitude higher than that seen in bulk phases, probably due to increasing surface area and Laplace pressure. In parallel to this, the decreasing droplet size increased the aqueous probe fraction and decreased the mobility of probe, suggesting that the probe is in association with interfacial protein. Droplet solidification was unexpectedly slow, but resulted in complete exclusion of the probe from the lipid phase into the aqueous region around the droplets. The results from the chemical degradation analyses generally supported those from deconvolution of the EPR spectra, however there were some surface effects not adequately described by the model.

In Objective 2, the effects of small amounts of liquid lipid in SLN on the properties and functionality of PTMIO were investigated as a function of storage time and temperature. Although some researchers studied nanostructured lipid carriers (NLC) formed from mixtures of liquid and solid lipids, there were conflicting reports on the distribution liquid lipid fraction. Moreover, the effects of small amounts of liquid lipid on solute distribution characteristics and its functionality have not been evaluated quantitatively. Even a small fraction of liquid oil can greatly enhance the solute retention in NLC and affect its reactivity. Because very low levels of liquid oil in apparently solid fats are hard to measure using NMR

methods, the presence of some undetermined amount of liquid oil in SLNs can cause error in conclusions drawn for a particular situation. This phenomenon could be the reason for inconsistent reports in several of the previous studies, which used TAGs as the lipid phase.

The liquid lipid fraction was argued to be surrounding the crystalline lipid core and in close proximity of the immobilized surface layer, which hinders the mobility of the spin probe. Moreover, the crystallization of C20 was retarded with increasing C14 proportion in the droplets, thus affecting the distribution of PTMIO in EBDS. This time-dependency of C20 containing emulsions was attributed to three probable mechanisms as: (i) difference in nucleation frequency, (ii) the rate of rotator-to-solid transition, and (iii) solvent effects of C14 slowing down the crystal growth. A careful manipulation of liquid:solid lipid ratios of droplets could be used to design novel delivery systems with controllable reactive solute population in the aqueous phase over the course of intended use.

In Objective 3, the effects of surface properties of droplets in the distribution and reactivity of PTMIO were investigated. Most of the successful SLN formulations have used lecithins to stabilize the EBDS. Furthermore, changing the hydrocarbon chains in lecithin structure allowed control over crystalline microstructure of SLN. Existing reports on lecithin-stabilized EBDS considered mostly the extent of probe retention within the droplet in a qualitative manner, but the effects of the interfacial lecithin layer itself as a separate domain remains largely unknown. In C14 emulsions stabilized with PC75+bile salt, three populations of PTMIO were seen: lipid core containing the majority of the probe and aqueous phase with high mobility, and immobilized surface layer with low mobility. In C14 emulsions stabilized by caseinate, two distinct populations of PTMIO were seen: lipid phase and aqueous phase with high mobility. Although crystallization of droplet excluded PTMIO from droplet core in either case, the majority of the probe was located in the surface layer of PC75+bile salt-stabilized C20 emulsions while all of the probe was in aqueous phase of caseinate-stabilized C20 emulsions.

The results of the present work can further be developed in the future by investigating the effect of thickness of lecithin layer or its mobility on the distribution and reactivity of the probe. The thickness of the surface layer can be increased by decreasing the lipid/lecithin ratio, which might limit the probe reactivity beyond a critical point. The hydrocarbon composition of lecithins and their arrangement at the droplet surface could further affect the probe behavior in EBDS, and their effects on crystallization history of droplets and distribution of the probe in EBDS are worth investigating. Moreover, the effects of bile salt on the arrangement of lecithin molecules on the droplet surface are still largely unknown, and needs further investigation. Finally, the present work considered delivery systems based on oil-in-water emulsions, but the efficiency and effectiveness of other EBDS such as multiple emulsions, hydrogels, or micro-emulsions (surfactant micelles) could also be investigated with the developed EPR technique.

## REFERENCES

Acosta E. 2009. Bioavailability of nanoparticles in nutrient and nutraceutical delivery. Current Opinion in Colloid and Interface Science, 14(1): 3-15.

Ahlin P, Julijana K, Slavko P, Janez S, Marjeta S. 2003. The effect of lipophilicity of spin-labeled compounds on their distribution in solid lipid nanoparticle dispersions studied by electron paramagnetic resonance. Journal of Pharmaceutical Sciences, 92(1): 58-66.

Ahlin P, Sentjurc M, Strancar J, Kristl J. 2000a. Location of lipophilic substances and ageing of solid lipid nanoparticles studied by EPR. S.T.P. Pharma Sciences, 10(2): 125-132.

Ahlin P, Kristl J, Sentjurc M, Strancar J, Pecar S. 2000b. Influence of spin probe structure on its distribution in SLN dispersions. International Journal of Pharmaceutics, 196: 241-244.

Amar I, Aserin A, Garti N. 2003. Solubilization patterns of lutein and lutein esters in food grade nonionic microemulsions. Journal of Agricultural and Food Chemistry, 51(16): 4775-4781.

Anton N, Benoit JP, Saulnier P. 2008. Design and production of nanoparticles formulated from nano-emulsion templates – A review. Journal of Controlled Release, 128: 185-199.

Arboleya JC, Sutcliffe LH, Wilde PJ, Fairhurst SA. 2005. Density and microviscosity studies of palm oil/water emulsions. Journal of Agricultural and Food Chemistry, 53(11): 4448-4453.

Awad TS. 2004. Ultrasonic studies of the crystallization behavior of two palm fats O/W emulsions and its modification. Food Research International, 37: 579-586.

Awad TS, Sato K. 2002.Acceleration of crystallisation of palm kernel oil in oil-in-water emulsion by hydrophobic emulsifier additives. Colloids and Surfaces B-Biointerfaces, 25(1): 45-53.

Awad TS, Helgason T, Kristbergsson K, Decker EA, Weiss J, McClements DJ. 2008. Effect of cooling and heating rates on polymorphic transformations and gelation of tripalmitin solid lipid nanoparticle (SLN) suspensions. Food Biophysics, 3: 155-162.

Berliner LJ. 1976. Appendix. In: Berliner LJ, editor. Spin Labeling. Theory and Applications. New York: Academic Press, Inc. p 562-582.

Bonacucina G, Cespi M, Misici-Falzi M, Palmieri GF. 2009. Collodial soft matter as drug delivery system. Journal of Pharmaceutical Sciences, 98(1): 1-42.

Boon CS, Xu Z, Yue X, McClements DJ, Weiss J, Decker EA. 2008. Factors affecting lycopene oxidation in oil-in-water emulsions. Journal of Agricultural and Food Chemistry, 56(4): 1408-1414.

Borbat PP, Costa-Filho AJ, Earle KA, Moscicki JK, Freed JH. 2001. Electron spin resonance in studies of membranes and proteins. Science, 291: 266-269.

Bunjes H, Drechsler M, Koch MHJ, Westesen K. 2001. Incorporation of the model drug Ubidecarenone into solid lipid nanoparticles. Pharmaceutical Research,18(3): 287-293.

Bunjes H, Koch MHJ, Westesen K. 2000. Effect of particle size on colloidal solid triglycerides. Langmuir, 16: 5234-5241.

Bunjes H, Koch MHJ, Westesen K. 2002. Effects of surfactants on the crystallization and polymorphism of lipid nanoparticles. Progress in Colloid and Polymer Science, 121: 7-10.

Bunjes H, Koch MHJ, Westesen K. 2003. Influence of emulsifiers on the crystallization of solid lipid nanoparticles. Journal of Pharmaceutical Sciences, 92(7): 1509-1520.

Bunjes H, Koch MHJ. 2005. Saturated phospholipids promote crystallization but slow down polymorphic transitions in triglyceride nanoparticles. Journal of Controlled Release, 107: 229-243.

Bunjes H, Steiniger F, Richter W. 2007. Visualizing the structure of triglyceride nanoparticles in different crystal modification. Langmuir, 23(7): 4005-4012.

Bunjes H, Unruh T. 2007. Characterization of lipid nanoparticles by differential scanning calorimetry, x-ray and neutron scattering.Advanced Drug Delivery Reviews, 59: 379-402.

Bunjes H, Westesen K, Koch MHJ. 1996. Crystallization tendency and polymorphic transitions in triglyceride nanoparticles. International Journal of Pharmaceutics, 129: 159-173.

Bunjes H, Westesen K. 2001. Influences of colloidal state on physical properties of solid fats. In: Garti N, Sato K, editors. Crystallization Processes in Fats and Lipid Systems. New York: Marcel Dekker, Inc. p 457-484.

Chaiyasit W, Silvestre MP, McClements DJ, Decker EA. 2000. Ability of surfactant hydrophobic tail group size to alter lipid oxidation in oil-in-water emulsions. Journal of Agricultural and Food Chemistry, 48(8): 3077-3080.

Chee CP, Gallaher JJ, Djordjevic D, Faraji H, McClements DJ, Decker EA, Hollender R, Peterson DG, Roberts RF, Coupland JN. 2005. Chemical and sensory analysis of strawberry flavoured yogurt supplemented with an algae oil emulsion. Journal of Dairy Research, 72(3): 311-316.

Chee CP, Djordjevic D, Faraji H, Decker EA, Hollender R, McClements DJ, Peterson DG, Roberts RF, Coupland JN. 2007. Sensory properties of vanilla and strawberry flavored ice cream supplemented with omega-3 fatty acids. Milchwissenschaft, 62(1): 66-69.

Claesson PM, Blomberg E, Poptoshev E. 2004. Surface forces and emulsion stability. In: Friberg SE, Larsson K, Sjoblom J, editors. Food Emulsion.4th Ed. New York: Marcel Dekker, Inc. p 257-297.

Coupland JN. 2002. Crystallization in emulsions. Current Opinion in Colloid and Interface Science, 7: 445-450.

Craig SR, Hastie GP, Roberts KJ, Gerson AR, Sherwood JN, Tack RD. 1998. Investigation into the structures of binary-, tertiary- and quinternary- mixtures of n-alkanes and real diesel waxes using high resolution synchrotron X-ray powder diffraction. Journal of Materials Chemistry, 8(4): 859-869.

Dalgleish DG, Srinivasan M, Singh M. 1995. Surface properties of oil-in-water emulsion droplets containing casein and Tween-60. Journal of Agricultural and Food Chemistry,43: 2351-2355.

Deo N, Somasundaran P. 2002. Electron spin resonance study of phosphatidyl choline vesicles using 5-doxyl stearic acid. Colloids and Surfaces B: Biointerfaces, 25: 225-232.

Diakova G, Bryant RG. 2006. The aqueous reference for ESR oximetry. Journal of Magnetic Resonance, 178: 329-333.

Dickinson E. 1992. An Introduction to Food Colloids. New York: Oxford University Press.

Dickinson E. 1977. Pressure dependence of shear viscosity in n-alkane + dimethylsiloxane mixtures. Journal of Physical Chemistry, 81(22): 2108-2113.

Donnelly JL, Decker EA, McClements DJ. 1998. Iron-catalyzed oxidation of Menhaden oil as affected by emulsifiers. Journal of Food Science 63(6): 997-1000.

Dymond JH, Oye HA. 1994. Viscosity of selected liquid n-alkanes. Journal of Physical and Chemical Reference Data, 23(1): 41-53.

Dymond JH, Young KJ. 1980. Transport properties of nonelectrolyte liquid mixtures-I. Viscosity coefficients for n-alkane mixtures at saturation pressure from 283-378 K. International Journal of Thermophysics, 1(4): 331-344

Dymond JH, Young KJ, Isdale JD. 1980. Transport properties of nonelectrolyte liquid mixtures-I. Viscosity coefficients for the n-hexane + n-hexadecane system at temperature from 25 to 100 °C at pressures up to the freezing pressure or 500 MPa. International Journal of Thermophysics, 1(4): 345-373.

Edgcomb MR, Sirimanne S, Wilkinson BJ, Drouin P, Morse II, PD. 2000. Electron paramagnetic resonance studies of the membrane fluidity of the foodborne pathogenic psychrotroph *Listeria monocytogens*. Biochimica et Biophysica Acta, 1453: 31-42.

Elias RJ, Kellerby SS, Decker EA. 2008. Antioxidant activity of proteins and peptides. Critical Reviews in Food Science and Nutrition, 48: 430-441.

Fairhurst SA, Pilkington RS, Sutcliffe LH. 1983. Rotational correlation times and radii of dithiazol-2-yl and dithiazolidin-2-yl free radicals. Journal of the Chemical Society, Fraday Transactions 1, 79: 439-452.

Freed JH. 1976. Theory of slowly tumbling ESR spectra for nitroxides. In: Berliner LJ, editor. Spin Labeling. Theory and Applications. New York: Academic Press, Inc. p 53-132.

Friberg S. 1971. Liquid crystalline phases in emulsions. Journal of Colloid and Interface Science, 37(2): 291-295.

Friberg S, Jansson PO, Cederberg E. 1976. Surfactant association structure and emulsion stability. Journal of Colloid and Interface Science, 55(3): 614-623.

Friberg S, Rydhag L. 1971. Solubilization of triglycerides by hydrophobic interaction: Liquid crystalline phases. Journal of the American Oil Chemists' Society, 48(3): 113-115.

Garside J. 1985. Industrial crystallization from solution. Chemical Engineering Science, 40(1): 3-26.

Gerson F, Huber W. 2003. Electron Spin Resonance Spectroscopy of Organic Radicals. Darmstadt: Wiley-VCH.

Ghosh S, Peterson DG, Coupland JN. 2006. Effects of droplet crystallization and melting on the aroma release properties of a model oil-in-water emulsion. Journal of Agricultural and Food Chemistry, 54(5): 1829-1837.

Ghosh S, Peterson DG, Coupland JN. 2007. Aroma release from solid droplet emulsions: Effect of lipid type. Journal of the American Oil Chemists' Society, 84: 1001-1014.

Gulseren I, Coupland JN. 2007. The effect of emulsifier type and droplet size on phase transitions in emulsified even-numbered n-alkanes. Journal of the American Oil Chemists' Society, 84(7): 621-629.

Gulseren I, Coupland JN. 2008. Surface melting in alkane emulsion droplets as affected by surfactant type. Journal of the American Oil Chemists' Society, 85(5): 413-419.

Haumann BF. 1994. Tools: Hydrogenation, interesterification. INFORM, 5: 668-674.

Helgason T, Awad TS, Kristbergsson K, McClements DJ, Weiss J. 2008. Influence of polymorphic transformations on gelation of tripalmitin solid lipid nanoparticle suspensions. Journal of the American Oil Chemists' Society, 85: 501-511.

Helgason T, Awad TS, Kristbergsson K, Decker EA, McClements DJ, Weiss J. 2009. Impact of surfactant properties on oxidative stability of β-carotene encapsulated within solid lipid nanoparticles. Journal of Agricultural and Food Chemistry, 57: 8033-8040.

Higami M, Ueno S, Segawa T, Iwanami K, Sato K. 2003. Simultaneous synchrotron radiation X-ray diffraction - DSC analysis of melting and crystallization behavior of trilauroylglycerol in nanoparticles of oil-in-water emulsion. Journal of the American Oil Chemists' Society, 80(8): 731-739.

Himawan C, Starov VM, Stapley AGF. 2006. Thermodynamic and kinetic aspects of fat crystallization. Advances in Colloid and Interface Science, 122: 3-33.

Hu M, McClements DJ, Decker EA. 2003. Impact of whey protein emulsifiers on the oxidative stability of salmon oil-in-water emulsions. Journal of Agricultural and Food Chemistry 51(5): 1435-1439.

Illing A, Unruh T, Koch MHJ. 2004. Investigation on particle self-assembly in solid lipid-based colloidal drug carrier systems. Pharmaceutical Research, 21(4): 592-597.

Jani P, Halbert GW, Langridge J, Florence AT. 1990. Nanoparticle uptake by the rat gastrointestinal mucosa: quantitation and particle size dependency. Journal of Pharmacy and Pharmacology, 42: 821-826.

Jenning V, Gohla SH. 2001. Encapsulation of retinoids in solid lipid nanoparticles (SLN). Journal of Microencapsulation, 18(2): 149-158.

Jenning V, Thunemann AF, Gohla SH. 2000a. Characterization of a novel solid lipid nanoparticle carrier system based on binary mixtures of liquid and solid lipids. International Journal of Pharmaceutics, 199: 167-177.

Jenning V, Mader K, Gohla SH. 2000b. Solid lipid nanoparticles (SLN) based on binary mixtures of liquid and solid lipids: a H-NMR study. International Journal of Pharmaceutics, 205: 15-21.

Jenning V, Schafer-Korting M, Gohla S. 2000c. Vitamin A-loaded solid lipid nanoparticles for topical use: drug release properties. Journal of Controlled Release, 66: 115-126.

Jores K, Mehnert W, Drechsler M, Bunjes H, Johann C, Mader K. 2004. Investigations on the structure of solid lipid nanoparticles (SLN) and oil-loaded solid lipid nanoparticles by photon correlation spectroscopy, field-flow fractionation and transmission electron microscopy. Journal of Controlled Release, 95: 217-227.

Jores K, Mehnert W, Mader K. 2003. Physicochemical investigations on solid lipid nanoparticles and on oil-loaded solid lipid nanoparticles: A nuclear magnetic resonance and electron spin resonance study. Pharmaceutical Research, 20(8): 1274-1283.

Hodate Y, Ueno S, Yano J, Katsuragi T, Tezuka Y, Tagawa T, Yoshimoto N, Sato K. 1997 . Ultrasonic velocity measurements of crystallization rates of palm oil in oil-water emulsions. Colloids and Surfaces A: Physicochemical and Engineering Aspects, 128: 217-224.

Kaneko N, Horie T, Ueno S, Yano J, Katsuragi T, Sato K. 1999. Impurity effects on crystallization rates of n-hexadecane in oil-in-water emulsions. Journal of Crystal Growth, 197: 263-270.

King MF, Boyd LC, Sheldon BW. 1992. Antioxidant properties of individual phospholipids in a salmon oil model system. Journal of the American Oil Chemists' Society, 69(6): 545-551.

Kiokias S, Dimakou C, Oreopoulou V. 2007. Effect of heat treatment and droplet size on the oxidative stability of whey protein emulsions. Food Chemistry, 105(1): 94-100.

Kiran E, Sen YL. 1992. High-pressure viscosity and density of n-alkanes. International Journal of Thermophysics, 13(3): 411-442.

Klinkesorn U, Sophanodora P, Chinachoti P, Decker EA, McClements DJ. 2005. Encapsulation of emulsified tuna oil in two-layered interfacial membranes prepared using electrostatic layer-by-layer deposition. Food Hydrocolloids, 19(6): 1044-1053.

Kraack H, Sirota EB, Deutsch M. 2000. Measurements of homogeneous nucleation in normal-alkanes. Journal of Chemical Physics, 112(15): 6873-6885.

Kreuter J. 1991. Peroral administration of nanoparticles. Advance Drug Delivery Reviews, 7: 71–86.

Kristl J, Volk B, Gasperlin M, Sentjurc M, Jurkovic P. 2003. Effect of colloidal carriers on ascorbyl palmitate stability. European Journal of Pharmaceutical Sciences, 19, 181-189.

Kutner MH, Nachtsheim CJ, Neter J, Li W. 2005. Applied Linear Statistical Models. 5$^{th}$ Ed. Boston: McGraw-Hill Irwin.

Lee S, Decker EA, Faustman C, Mancini RA. 2005. The effects of antioxidant combinations on color and lipid oxidation in n-3 oil fortified ground beef patties. Meat Science, 70(4): 683-689.

Lee S, Faustman C, Djordjevic D,Faraji H, Decker EA. 2006a. Effect of antioxidants on stabilization of meat products fortified with n-3 fatty acids. Meat Science, 72(1): 18-24.

Lee S, Hernandez P, Djordjevic D, Faraji H, Hollender R, Faustman C, Decker EA.2006b. Effect of antioxidants and cooking on stability of n-3 fatty acids in fortified meat products. Journal of Food Science, 71(3): C233-238.

Leermakers FAM, Atkinson PJ, Dickinson E, Horne DS. 1996. Self-consistent-field modeling of adsorbed β-casein: Effects of pH and ionic strength on surface coverage and density profile. Journal of Colloid and Interface Science, 178: 681-693.

Let MB, Jacobsen C, Sorensen ADM, Meyer AS. 2007. Homogenization conditions affect the oxidative stability of fish oil enriched milk emulsions: Lipid oxidation. Journal of Agricultural and Food Chemistry, 55(5): 1773-1780.

Losso JN, Khachatryan A, Ogawa M, Godber JS, Shih F. 2005. Random centroid optimization of phosphatidylglycerol stabilized lutein-enriched oil-in-water emulsions at acidic pH. Food Chemistry, 92(4): 737-744.

Luykx DMAM, Peters RJB, Van Ruth SM, Bouwmeester H. 2008. A review of analytical methods for the identification and characterization of nano delivery systems in food. Journal of Agricultural and Food Chemistry, 56: 8231-8247.

McClements DJ. 2005. Food Emulsions: Principles, Practice, and Techniques. 2nd ed. Boca Raton: CRC Press.

McClements DJ, Decker EA. 2000. Lipid oxidation in oil-in-water emulsions: Impact of molecular environment on chemical reactions in heterogeneous food systems. Journal of Food Science, 65(8): 1270-1282.

McClements DJ, Decker E, Weiss J. 2007. Emulsion-based delivery systems for lipophilic bioactive components. Journal of Food Science, 72(8): 109-124.

McClements DJ, Decker EA, Park Y, Weiss J. 2009. Structural design principles for delivery of bioactive components in nutraceutical and functional foods. Critical Reviews in Food Science and Nutrition, 49: 577-606.

Mehnert W, Mader K. 2001. Solid lipid nanoparticles: production, characterization and applications. Advanced Drug Delivery Reviews, 47: 165-196.

Mei L, Decker EA, McClements DJ. 1998a. Evidence of iron association with emulsion droplets and its impact on lipid oxidation. Journal of Agricultural and Food Chemistry, 46: 5072-5077.

Mei L, McClements DJ, Wu J, Decker EA. 1998b. Iron-catalyzed lipid oxidation in emulsion as affected by surfactant, pH and NaCl. Food Chemistry, 61(3): 307-312.

Mikhalev OI, Karpov IN, Kazarova EB, Alfimov MV. (1989). The effect of crystallization of the dispersion phase in emulsions on the rate of interfacial reactions. Chemical Physics Letters, 164(1): 96-100.

Muhlen A, Schwarz C, Mehnert W. 1998. Solid lipid nanoparticles (SLN) for controlled drug delivery – Drug release and release mechanisms. European Journal of Pharmaceutics and Biopharmaceutics, 45: 149-155.

Muller RH, Mader K, Gohla S. 2000. Solid lipid nanoparticles (SLN) for controlled drug delivery – a review of the state of the art. European Journal of Pharmaceutics and Biopharmaceutics, 50: 161-177.

Muller RH, Radtke M, Wissing SA. 2002. Nanostructures lipid matrices for improved microencapsulation of drugs. International Journal of Pharmaceutics, 242: 121-128.

Mun S, Decker EA, McClements DJ. 2007. Influence of emulsifier type on *in vitro* digestibility of lipid droplets by pancreatic lipase. Food Research International, 40: 770-781.

Nakagawa K. 2009. EPR investigations of spin-probe dynamics in aqueous dispersions of a nonionic amphiphilic compound. Journal of the American Oil Chemists' Society, 86:1-17.

Nakazawa R, Shima M, Adachi S. 2008. Effect of oil-droplet size on the oxidation of microencapsulated methyl linoleate. Journal of Oleo Science, 57(4): 225-232.

Nordio PL. 1976. General magnetic resonance theory. In: Berliner LJ, editor. Spin Labeling. Theory and Applications. New York: Academic Press, Inc. p 5-52.

Nuchi CD, McClements DJ, Decker EA. 2001. Impact of Tween 20 hydroperoxides and iron oxidation of methyl linoleate and salmon oil dispersions. Journal of Agricultural and Food Chemistry, 49: 4912-4916.

Owenius R, Engstrom M, Lindgren M, Huber M. 2001. Journal of Physical Chemistry A, 105: 10967-10977.

Palanuwech J, Coupland JN. 2003. Effect of surfactant type on the stability of oil-in-water emulsions to dispersed phase crystallization. Colloids and Surfaces A: Physicochemical and Engineering Aspects, 223(1-3): 251-262.

Popp CA, Hyde JS. 1981. Effects of oxygen on EPR spectra of nitroxide spin-label probes of model membranes. Journal of Magnetic Resonance, 43: 249-258.

Povey MJW. 2001. Crystallization of oil-in water emulsions. In: Garti N, Sato K, editors. Crystallization Processes in Fats and Lipid Systems. New York: Marcel Dekker Inc. p 251-288.

Reineccius G. 2006. Flavor Chemistry and Technology. Boca Raton: CRC Press.

Ribeiro HS, Rico LG, Badolato GG, Schubert H. 2005. Production of O/W emulsions containing astaxanthin by repeated Premix membrane emulsification. Journal of Food Science, 70(2): E117-123.

Ribeiro HS, Guerrero JMM, Briviba K, Rechkemmer G, Schuchmann HP, Schubert H. 2006. Cellular uptake of carotenoid-loaded oil-in-water emulsions in colon carcinoma cells in vitro. Journal of Agricultural and Food Chemistry, 54(25): 9366-9369.

Richelle M, Bortlik K, Liardet S, Hager C, Lambelet P, Baur M, Applegate LA, Offord EA. 2002. A food-based formulation provides lycopene with the same bioavailability to humans as that from tomato paste. The Journal of Nutrition, 132: 404-408.

Rosenblatt KM, Bunjes H. 2009. Poly(vinyl alcohol) as Emulsifier Stabilizes Solid Triglyceride Drug Carrier Nanoparticles in the alpha-Modification. Molecular Pharmaceutics, 6(1): 105-120.

Rothwell JA, Day AJ, Morgan MRA. 2005. Experimental determination of octanol-water partition coefficients of quercetin and related flavors. Journal of Agricultural and Food Chemistry, 53: 4355-4360.

Rydhag L, Wilton I. 1981. The function of phospholipids of soybean lecithin in emulsions. Journal of the American Oil Chemists' Society, 58(8): 830-837.

Santipanichwong R, Suphantharika M. 2007. Carotenoids as colorants in reduced-fat mayonnaise containing spent brewer's yeast beta-glucan as a fat replacer. Food Hydrocolloids, 21(4): 565-574.

Sato K. 1999. Solidification and phase transformation behavior of food fats – a review. Fett/Lipid, 12: 467-474.

Sato K. 2001. Crystallization behavior of fats and lipids – a review. Chemical Engineering Science, 56: 2255-2265.

Shchipunov YA. 1997. Self-organising structures of lecithin. Russian Chemical Reviews, 66(4): 301-322.

Semo E, Kesselman E, Danino D, Livney Y. 2007. Casein micelles as a nano-capsular vehicle for neutraceuticals. Food hydrocolloids, 21: 936-942.

Sharma R. 2005.Market trends and opportunities for functional dairy beverages. Australian Journal of Dairy Technology, 60(2): 195-198.

Shinohara Y, Takamizawa T, Ueno S, Sato K, Kobayashi I, Nakajima M, Amemiya Y. 2008. Microbeam X-ray diffraction analysis of interfacial heterogeneous nucleation of n-hexadecane inside oil-in-water emulsion droplets. Crystal Growth & Design, 8(9): 3123-3126.

Silvestre MPC, Chaiyasit W, Brannan RG, McClements DJ, Decker EA. 2000. Ability of surfactant head group size to alter lipid and antioxidant oxidation in oil-in-water emulsions. Journal of Agricultural and Food Chemistry, 48:2057-2061.

Sirota EB. 1998. Supercooling, nucleation, rotator phases, and surface crystallization of n-Alkane melts. Langmuir, 14: 3133-3136.

Sirota EB, Herhold AB. 1999. Transient phase-induced nucleation. Science, 283: 529-532.

Sjostrom B, Bergenstahl B, Kronberg B. 1993. A method for the preparation of submicron particles of sparingly water-soluble drugs by precipitation in oil-in-water emulsions. II: Influence of the emulsifier, the solvent, and the drug substance. Journal of Pharmaceutical Sciences, 82(6): 584-589.

Smith ICP, Butler KW. 1976. Oriented lipid systems as model membranes. In: Berliner LJ, editor. Spin Labeling. Theory and Applications. New York: Academic Press, Inc. p 411-451.

Solans S, Izquierdo P, Nolla J, Azemar N, Garcia-Celma MJ. 2005. Nano-emulsions. Current Opinion in Colloid and Interface Science, 10: 102-110.

Souto EB, Wissing SA, Barbosa CM, Muller RH. 2004. Development of a controlled release formulation based on SLN and NLC for topical clotrimazole delivery. International Journal of Pharmaceutics, 278: 71-77.

Spicer PT, Hartel RW. 2005. Crystal comets: Dewetting during emulsion droplet crystallization. Australian Journal of Chemistry, 58: 655-659.

Swartz HM, Clarkson RB. 1998. The measurement of oxygen *in vivo* using EPR techniques. Physics in Medicine and Biology, 43: 1957-1975.

Takeuchi M, Ueno S, Floter E, Sato K. 2002a. Binary phase behavior of 1,3-Distearoyl-2-oleoyl-sn-glycerol (SOS) and 1,3-Distearoyl-2-linoleoyl-sn-glycerol (SLS). Journal of the American Oil Chemists' Society, 79(7): 627-632.

Takeuchi M, Ueno S, Sato K. 2002b. Crystallization kinetics of polymorphic forms of a molecular compound constructed by SOS (1,3-distearoyl-2-oleoyl-sn-glycerol) and SSO (1,2-distearoyl-3-oleoyl-rac-glycerol). Food Research International, 35: 919-926.

Tyssandier V, Lyan B, Borel P. 2001. Main factors governing the transfer of carotenoids from emulsion lipid droplets to micelles. BiochimicaetBiophysicaActa (BBA) - Molecular and Cell Biology of Lipids, 1533(3): 285-292.

Ueno S, Hamada Y, Sato K. 2003. Controlling polymorphic crystallization of n-alkane crystals in emulsion droplets through interfacial heterogeneous nucleation. Crystal Growth and Design, 3(6): 935-939.

Unruh T, Westesen K, Bosecke P, Linder P, Koch MHJ. 2002. Self-assembly of triglyceride nanocrystals in suspension. Langmuir, 18: 1796-1800.

Vanapalli SA, Coupland JN. 2004. Orthokinetic stability of food emulsions. In: Friberg SE, Larsson K, Sjoblom J, editors. Food Emulsion.4th Ed. New York: Marcel Dekker, Inc. p 327-351.

Velikov KP, Pelan E. 2008. Colloidal delivery systems for micronutrients and nutraceuticals. Soft Matter, 4: 1964-1980.

Yannai S. 2004. Dictionary of Food Compounds. Boca Raton: Chapman & Hall / CRC Press.

Wagner LA, Warthesen JJ. 1995. Stability of spray-dried encapsulated carrot carotenes. Journal of Food Science, 60(5): 1048-1053.

Weil JA, Bolton JR. 2007. Electron Paramagnetic Resonance: Elementary Theory and Practical Applications. 2nd Ed. Hoboken: John Wiley and Sons, Inc.

Weiss J, Coupland JN, McClements DJ. 1996. Solubilization of hydrocarbon emulsion droplets suspended in nonionic surfactant micelle solutions. Journal of Physical Chemistry, 100: 1066-1071.

Weiss J, McClements DJ, Kristbergsson K, Helgason T, Awad T. 2008. Solid lipid nanoparticles as delivery systems for bioactive food components. Food Biophysics, 3: 146-154.

Westesen K, Siekmann B. 1997. Investigation of the gel formation of phospholipid stabilized solid lipid nanoparticles. International Journal of Pharmaceutics, 151: 35-45.

Wu XZ, Sirota EB, Sinha SK, Ocko BM, Deutsh M. 1993. Surface crystallization of liquid normal-alkanes. Physical Review Letters, 70(7): 958-961.

# APPENDIX

## A.1. Principles of Electron Paramagnetic Resonance Spectroscopy (EPR)

The following description EPR theory is developed from the work of Weil and Bolton (2007), and Gerson and Huber (2003).

The principle of EPR spectroscopy relies on the interaction of unpaired electrons of paramagnetic species (i.e., electrons with non-zero spin angular momenta) with the magnetic component of microwave radiation known as the Zeeman effect. The spin of unpaired (free) electrons gives them measurable magnetic moments. In the absence of an external magnetic field, the electrons' magnetic moment will orient randomly. However, when an external magnetic field is applied, the moment of the electron orients either parallel or anti-parallel with the field into low-energy and high-energy levels, respectively. Irradiation at microwave frequencies can drive the electrons between low- and high-energy states which results in the absorption of electromagnetic energy. The transition between two energy levels due to absorption of electromagnetic energy follows Planck's law:

$$\Delta E = E_+ - E_- = h\nu \qquad [A.1]$$

where $E_+$ and $E_-$ are the energy of the two Zeeman levels, h is Plank's constant, and ν is the frequency of the applied microwave radiation. The energy shift between two states can also be defined a function of magnetic field strength:

$$\Delta E = h\nu = gM_B B_0 \qquad [A.2]$$

where g is the g-factor of the sample, $M_B$ is the Bohr magneton (magnetic moment of the electron), and $B_0$ is the external magnetic field. In practice, EPR measurements are made by adjusting the magnetic field energy instead of the applied microwave frequency. When the magnetic field strength is tuned (i.e., constant frequency), at some point the energy level difference between two spin states (i.e., low and high Zeeman levels) will be equal to the

magnetic field strength. At this point, the maximum energy absorption will occur (i.e. field of resonance) which is characterized by the g-factor of the sample.

The total magnetic moment of an electron (J) is defined by two quantum numbers: spin angular momentum (S) and orbital angular momentum (L). For systems containing light atoms (e.g., free radicals, samples with s-type orbitals), the contribution of orbital angular momentum to the total magnetic moment is effectively zero and spin angular momentum (S) becomes the only contributor to the total magnetic moment.

Nuclei with spin influence the magnetic field that the unpaired electrons experience (i.e., hyperfine interactions). As the magnetic moment of the nuclei adds or subtracts to the externally applied magnetic field, hyperfine interactions cause a split of the absorption line centered about the g-factor. For example, a nitroxide free-radical contains one unpaired electron (S = 1/2) and a nucleus with an effective spin quantum number of I = 1 (i.e., I is the $^{14}N$ nuclear spin) allowing three EPR transitions, and results in an EPR spectra as three absorption lines (at the nuclei spin states of $M_I$ = -1, 0, +1): two hyperfine peaks centered about the g-factor (Figure A.1). The position of the hyperfine peaks are determined by the hyperfine splitting constant, which is to show how much the nucleus magnetic moment shifts the external magnetic energy responsible for the resonance condition (position of the g-value):

$$B_k = (h\nu) / (gM_B) + (g_e/g)a_0 \qquad (M_I = +1) \qquad [A.3]$$

$$B_k = (h\nu) / (gM_B) \qquad (M_I = 0) \qquad [A.4]$$

$$B_m = (h\nu) / (gM_B) - (g_e/g)a_0 \qquad (M_I = -1) \qquad [A.5]$$

where $a_0 = A_0 / g_eM_B$ is the hyperfine splitting constant (in Gauss or Tesla), $A_0$ is isotropic hyperfine coupling constant, and the factor $g/g_e$ is the chemical shift correction (The effective magnetic field B, is the vectorial sum of external magnetic field and any possible local magnetic fields, which might be permanent or be induced by the external magnetic field. The variable factor $g_e$ is used to correct the deviation in g-factor due to a local magnetic field).

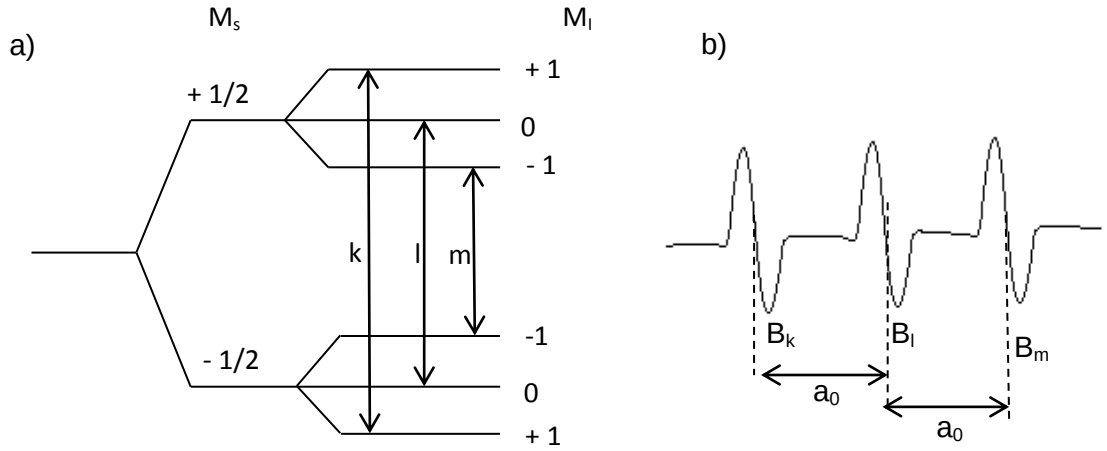


Figure A.1. (a) Energy levels and allowed EPR transitions at constant frequency for an atom with S = 1/2 and I = 1; and (b) sketched EPR-spectrum. The absorption peaks are conventionally given as the first derivative of the absorption spectra (the figure was reproduced from Weil and Bolton, 2007).

The extent of EPR interactions (e.g., Zeeman interactions, hyperfine coupling) is affected by the chemical nature of the nuclei of radicals and the physicochemical properties of the environment surrounding them (e.g., polarity, viscosity). The line shape of the EPR spectra is determined by the relaxation times of the unpaired electrons, and carries valuable information about molecular mobility of the EPR-active molecules, as well as the nature of chemical bonds they are associated with. Line-width can be explained in terms of the Heisenberg uncertainty principle, and life-time of a spin-state in a frequency dependent manner. Spin-relaxation is complex, and a thorough explanation relies on changes in the Boltzmann distribution of spin temperature of two Zeeman states. However, in a much more simplified way, the life time of a spin-state is given by:

$$\frac{1}{\Delta t} \cong \left(\frac{1}{T_1}\right) + \left(\frac{1}{T_2}\right) \qquad [A.6]$$

where Δt is the life time of a spin-state, $T_1$ is the spin-lattice relaxation time (i.e., energy exchange between the spin state and its surroundings), $T_2$ is the spin-spin relaxation time (i.e., interactions within the spin-state). For organic radicals, $T_1$ is often much larger than $T_2$, hence:

$$\frac{1}{\Delta t} \cong \left( \frac{1}{T_2} \right) \qquad [A.7]$$

The deconvolution of the line-shape can be used to analyze the properties of the EPR-active molecules in a given environment. The broadening of the spectral lines can be classified as homogenous (Lorentzian) or inhomogeneous (Gaussian) broadening. Although there can be several factors causing non-homogenous line-broadening (such as inhomogeneous external magnetic field, unresolved hyperfine structure due to high number of hyperfine components from a nuclei, or dipolar interactions with other fixed paramagnetic centers), it is often via Heisenberg spin exchange (or electron spin exchange) where spin-bearing orbitals can overlap causing line-broadening. Thus the line shape can be defined as the sum of absorption of Lorentzian shape and spin-exchange induced dispersion. The line shape of such EPR spectra can be analyzed via simulation algorithms based on perturbation theory in quantum mechanics. In the next section the parameters of the EPR spectra used in my analyses are summarized.

## A.2. Summary of the Parameters Used in the Analyses of EPR Spectra

a)

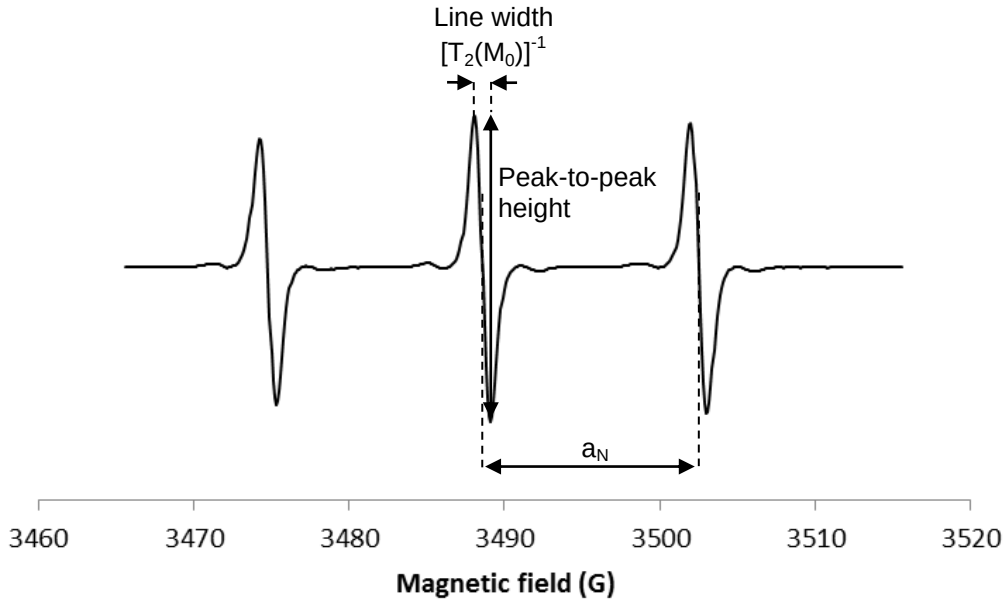


b)

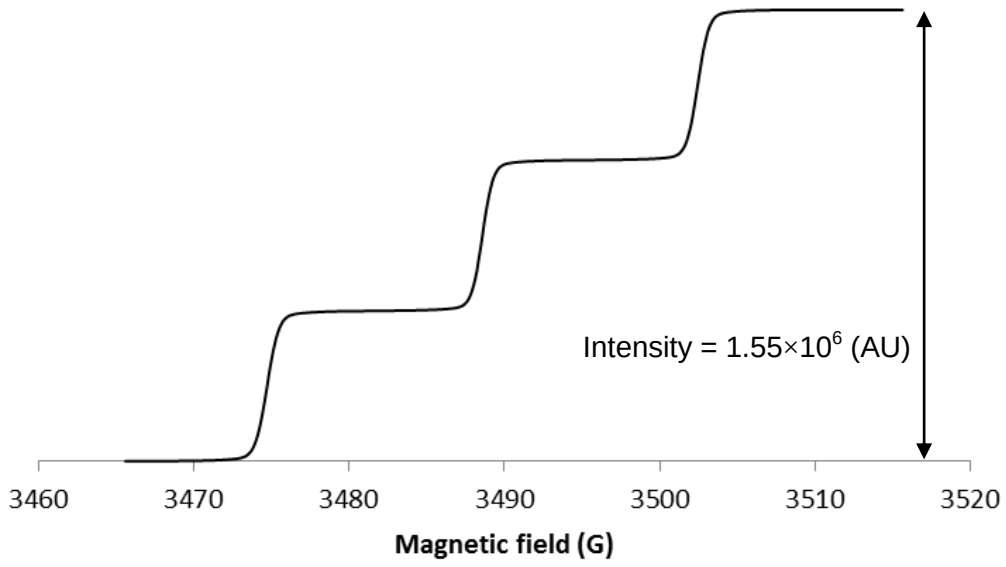


Figure A.2. (a) EPR spectra of PTMIO (200μm) in tetradecane, and (b) double integration of the same spectra used to calculate the intensity.

Table A. Summary of the EPR parameters used in the analyses.

| **Parameter** | **Calculated from** | **Indicates** |
|---|---|---|
| Peak-to-peak height | Difference between minima and maxima of the absorption curve | Used in chemical stability analysis |
| Intensity | Double integration of the simulated spectra | Amount of spin-probe in different environments |
| Hyperfine splitting constant ($a_N$) | Separation of the hyperfine peak from center peak | Polarity of the environment (~13.8 G in lipid; ~15.5 in aqueous) |
| Rotational correlation time ($\tau_c(B)$, $\tau_c(C)$) | Line widths | Mobility of the spin-probe (smaller rotational correlation time indicates higher mobility) |
| Extent of anisotropy ($\tau_c(B)/\tau_c(C)$) | From difference in the rotational correlation times | Ordering of spin-probe, restricted motion on one of the axes |

# Curriculum Vitae

Umut Yucel

## EDUCATION

• PhD in Food Science, The Pennsylvania State University, USA. (Fall 2011)
• MS in Food Science, The Pennsylvania State University, USA (Spring 2010)
• MS in Food Engineering, Middle East Technical University, Turkey (Fall 2006)
• BS in Food Engineering, Middle East Technical University, Turkey (Spring 2004)

## SELECTED PUBLICATIONS

Poster Presentations:

- Yucel U, Coupland JN (2009). Ultrasonic measurements of crystal dispersions. Conference of Food Engineering, Columbus, OH (April 5-8, 2009).
- Yucel U, Elias RJ, Coupland JN (2011). Effect of droplet size and crystallinity on the efficiency of emulsions as delivery systems. 2011 IFT Annual Meeting, New Orleans, LA (June 11-14, 2011).

Oral presentations:

- Yucel U, Coupland JN (2011). Ultrasonic characterization of dispersions of sugar in vegetable oil. 102$^{nd}$ AOCS Annual Meeting, Cincinnati, OH (May 1-4, 2011).

Research Papers:

- Vardhanabhuti B, Yucel U, Coupland JN, Foegeding EA. (2009). Interaction between β-lactoglobulin and dextran sulfate at near neutral pH and their effect on thermal stability. Food Hydrocolloids, 23 (6), 1511-1520.
- Yucel U, Alpas H, Bayindirli A (2010). Evaluation of high pressure pretreatment for enhancing the drying rates of carrot, apple, and green bean. Journal of Food Engineering, 98, 266-272.
- Yucel U, Coupland JN (2010). Ultrasonic characterization of lactose dissolution. Journal of Food Engineering, 98, 28-33.
- Yucel U, Coupland JN (2010). Ultrasonic attenuation measurements of the mixing, agglomeration, and sedimentation of sucrose crystals suspended in oil. Journal of American Oil Chemists Society, 88(1), 33-38
- A book chapter in press: Yucel U, Elias RJ, Coupland JN. Emulsions, nanoemulsions and solid lipid nanoparticles as delivery systems in foods. In Bioprocessing and Bio-Based Product Development (Ed. by Dunford, N), Wiley-Blackwell Food Science Books.
- Samtlebe M, Yucel U, Weiss J, Coupland JN (2011). Stability of solid lipid nanoparticles in the presence of liquid oil emulsions. Journal of the American Oil Chemists' Society, in press.
- Yucel U, Elias RJ, Coupland JN (2011). Solute distribution and stability in emulsion-based delivery systems. 1: Droplet size and crystallinity. Submitted to Crystal Growth and Design.
- Yucel U, Elias RJ, Coupland JN (2011). Solute distribution and stability in emulsion-based delivery systems. 2: Solid fat content and storage conditions. Submitted to Crystal Growth and Design.
- Yucel U, Elias RJ, Coupland JN. Evaluation of the effects of phosphatidylcholine and caseinate as surfactants on the distribution of a lipophilic ingredient. Under preparation for Soft Matter.